Schweizerische Eidgenossenschaft
Confédération suisse
Confederazione Svizzera
Confederaziun svizra

Eidgenössisches Departement für
Umwelt, Verkehr, Energie und Kommunikation UVEK

Bundesamt für Energie BFE

Schlussbericht September 2014

Alteration and petrology in a fossil hydrothermal system at Geitafell central volcano, Iceland

Master Thesis

Auftraggeber:

Bundesamt für Energie BFE
Forschungsprogramm Geothermie
CH-3003 Bern
www.bfe.admin.ch

Auftragnehmer:

Institute of Geochemistry and Petrology
Department of Earth Science
ETH Zurich, 8092 Zurich, Switzerland
http://www.geopetro.ethz.ch

Autoren:

David Baumann, ETHZ, davbauma@alumni.ethz.ch
Co-Autoren: Thomas Driesner, Dr. Björn Hannes Mattsson, IGP, ETH Zurich

BFE-Bereichsleiter: Gunter Siddiqi
BFE-Programmleiter: Rudolf Minder
BFE-Vertragsnummer: SI/500913-01

Eidgenössische Technische Hochschule Zürich
Swiss Federal Institute of Technology Zurich

DERDW
Departement Erdwissenschaften

Alteration and petrology in a fossil hydrothermal system at Geitafell central volcano, Iceland

Master Thesis

David Baumann, Department of Earth Science, ETH Zurich, Switzerland
davbauma@alumni.ethz.ch

Zurich, September 2014

Examiner:
Dr. Thomas Driesner, IGP, ETH Zurich

Co-Examiner:
Dr. Björn Hannes Mattsson, IGP, ETH Zurich

Institute of Geochemistry and Petrology, Department of Earth Science, ETH Zurich

Panoramic view of Hoffell and Geitafell area from south. The glacier in the center is Hoffelsjökull.

Abstract

At *Geitafell* in SE Iceland a fossil hydrothermal system related to a Tertiary central volcano is exposed due to glacial erosion. The gabbroic magma chamber and several generations of dykes and cone sheets are hosted by tholeiitic basalt lava flows. All rock types are overprinted by regional zeolite alteration as well as zones of high temperature alteration.

Mapping of late stage magmatic features and hydrothermal veining on outcrop scale was used to get insight into processes within the roots of the high enthalpy hydrothermal system. Abundance of veins and haloes represent intensity of hydrothermal alteration. Combining hydrothermal mineral overgrowth sequence with homogenization temperatures of fluid inclusions, a temporal evolution of fluid temperatures is reconstructed in two localities. Bulk rock XRF analysis of intrusive rocks is used to understand magmatic evolution during intrusive events. Variability in alteration of flow basalt bulk composition was analyzed.

Several batches of magma intruded the basaltic host rock at *Geitafell* and crystallized to Fe-Ti rich gabbros. During crystallization *Pegmatoidal Gabbro* was formed by fluid saturation. Evolved magmas were expelled from a crystal mush producing silicic dykelets of variable composition. Motion of larger volumes of silicic rock with dacitic composition also brecciates gabbro and host rock. Zones with vesiculated silicic rocks provide enhanced permeability. High temperature hydrothermal alteration along intrusive contacts as well as mineralization in vesicles is abundant even in silicic rocks where hydrothermal reaction is weak compared to mafic intrusives and basalts.

In host basalt, preserved mineral sequences and fluid inclusions of meteoric water show a pro- and retrograde evolution of temperatures. Minerals include low temperature amorphous silica and chlorite followed by garnet formation at 220° and quartz at peak temperatures of about 370°. Subsequently, temperatures decreased to regional calcite-zeolite alteration level. Infill sequences also document multiple changes in temperature. In the gabbroic magma chamber peak alteration is represented by actinolite veining which is controlled by magmatic structures, while with lower temperatures of alteration brittle veins become more important as fluid path. Abundance of hydrothermal veins representing lower temperatures increases due to the propagating cracking front.

Re-heating of the hydrothermal system is recorded by fluid inclusions within *Intrusive Breccia* in the margin of the solidified magma chamber. Homogenization temperatures increase during quartz precipitation from 250° to 350° where rhyolitic magma cooled previously from at least 700°. Supercritical temperatures in the hydrothermal system may only be reached in these inclusions by entrapment at elevated pressures and with an ice cover of more than 500 m.

Table of contents

Mineral Abbrevations

Act	Actinolite	Dio	Diopside	Mag	Magnetite
Alb	Albite	En	Enstatite	Myrm	Myrmekite
An	Anorthite	Epi	Epidote	Opx	Orthopyroxene
And	Andradite	Fs	Ferrosilite	Orth	Orthoclase
Aug	Augite	Grs	Grossular	Plag	Plagioclase
Byw	Bywtonite	Gt	Garnet	Px	Pyroxene
Cc	Calcite	Hed	Hedenbergite	Py	Pyrite
Chl	Chlorite	Hem	Hematite	Qtz	Quartz
Cpx	Clinopyroxene	Ilm	Ilmenite	Tt	Titanite
Cpy	Chalcopyrite	Kfsp	K-Feldspar	Zeo	Zeolite

1 Introduction

With the aim of increasing our understanding about the root zone in natural geothermal fluid systems I studied a fossil geothermal system in *Geitafell*, SE Iceland. This system is assumed to have produced high enthalpy supercritical fluids during its active period, similar as Krafla today (Troyer, 2007). To gain insights rocks from a magma chamber which represents the magmatic heat source as well as host rocks of the magma chamber with overprint of a hydrothermal system are investigated. Main emphasis was on intrusive magmatic features, hydrothermal alteration and veining to understand what processes took place during and after the intrusion of the magmas.

1.1 Natural hydrothermal systems

Hydrothermal systems become more and more important for electrical energy production. In 2010 a total of 48.493 MW geothermal energy used for heating were installed worldwide. (Lund et al., 2011). For electrical energy, the installed capacity was 10'898 MW in 2010 which was increasing by about 400 MW/year since 2005 (Bertani, 2012).

Natural hydrothermal systems are found in areas of elevated crustal heat flow, permeable rocks and sufficient fluid recharge. Compared to enhanced geothermal systems these have a stable fluid circulation over a certain time period and often surface features like hot springs. Natural hydrothermal systems have been classified in different types based on the presence of liquid water and vapor phase, volcanism or on temperatures measured in the uppermost kilometer. Low and high temperature systems correspond to temperatures below 150° C and above 200° C respectively (Bödvarsson, 1961; Friðleifsson, 1979). During recent times the terms "high" and "low temperature" are partly replaced by the terms high and low enthalpy. This accommodates for the increasing importance as source for renewable electrical energy.

High enthalpy geothermal systems incorporate the potential for much higher energy recovery compared to drill holes in other systems (Björnsson et al., 1982) as enthalpy in the fluids is much higher (Figure 1-1). The scientific understanding of sub-surface processes in these magmatically driven, natural geothermal systems still needs improvement. Understanding is even more complicated as every system has its own characteristics. However, most systems share some common features (Arnórsson, 1995; Arnórsson et al., 2007).

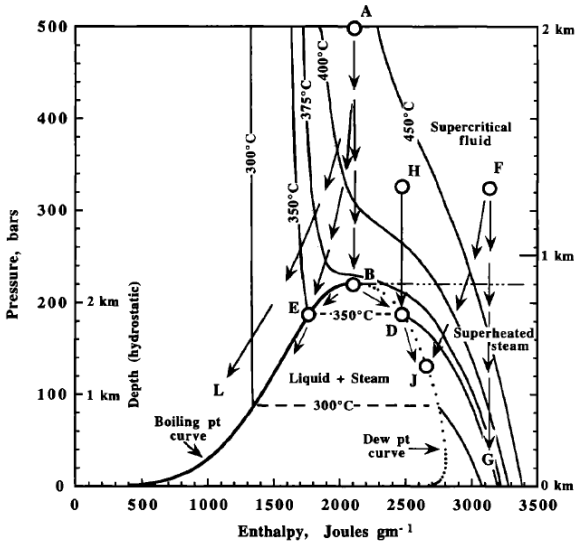

Figure 1-1: *Pressure-enthalpy diagram (Fournier, 1999) showing different possible fluid paths in hydrothermal systems. Paths originating from "F" are economically most interesting, due to highest enthalpy.*

Common features of hydrothermal systems include circulating fluids (E.g. liquid water, steam or brines to mention some end members.) responsible for convective heat transfer, mixing of different fluids, phase separation and conductive heat transfer from a magma chamber which represents the heat source. A sketch including some general features is shown in Figure 1-2. During the activity of a system the location of these features and processes may change due to cooling or heating during recharge of the magma chamber. Lifetime of hydrothermal systems is still an area of research but estimations range from 0.1 to 1 million years, while fluid circulation is in the range of hundreds to ten thousands of years (Arnórsson et al., 2007). Some Icelandic hydrothermal systems show water isotope signatures that correspond to fluids with a long residence time in wide aquifers (Arnórsson, 1995).

The surface near part of high enthalpy systems is understood pretty well due to its accessibility and economic use for energy generation. Fluid circulation is primarily driven by density difference at high temperatures. Fluids in Icelandic high temperature systems are mainly of meteoric origin but locally also seawater can be a major factor and degassing volatiles from an underlying magma reservoir may have an influence. Temperatures in hydrothermal systems range to about 350 to 370° C in drillholes under hydrostatic conditions in pore-space and may exceed 370° under pressures conditions above hydrostatic (Arnórsson et al., 2007; Fournier, 1991).

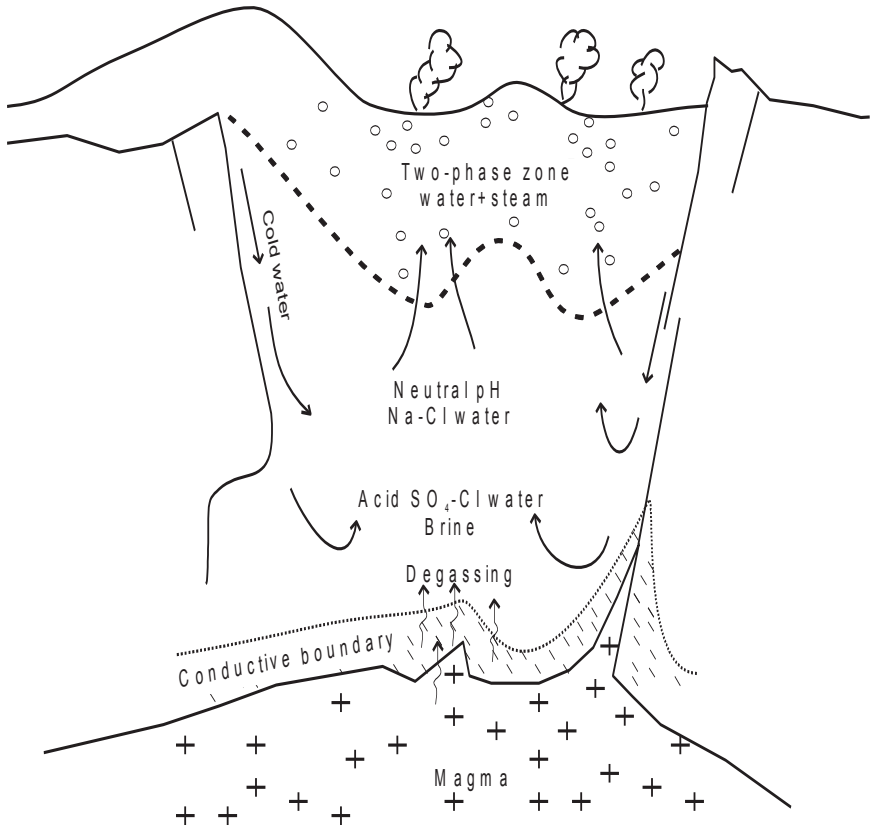

Figure 1-2: *Schematic sketch of a high enthalpy hydrothermal system (Arnórsson et al., 2007) main focus of research are the "roots" of hydrothermal systems as little is known about actual processes in the contact zone between heat source and circulating fluids*

Current research focuses on the "deep roots" of high enthalpy systems. These "roots" represent the contact zone between the magmatic heat source and the lowermost level of fluid circulation. It can be characterized by the transition from molten rocks in the magma chamber towards brittle host rock. This includes partly crystallized and brittle intrusive rocks as well as heated and therefore ductile host rocks. In these ductile rocks a narrow zone with self-sealing qualities develops (Fournier, 1999). Thickness of this zone can be derived from heat flux and size of the heat source. Geothermal gradients reach in active volcanic areas about 700 to 1000°C/km. Measured gradients from drilling into magma at surface pressure may be up to 1050°C/m in this extreme scenario. Estimated thickness hence is in the range of m to 10s of meters (Arnórsson et al., 2007).

Modelling, investigation of fossil systems and comparison to surface features as well as few drillholes are the methods used to increase our understanding. Research projects are often based on one geological background (E.g. geophysical or geochemical) (Driesner, 2012) to understand one part of the system (magmatic-volcanic or hydrothermal) (Elders and Friðleifsson, 2010). Processes in the roots of natural hydrothermal systems however strongly depend on changes due to interaction of both, magmatic and hydrothermal part of the system and are subject of projects like the Iceland Deep Drilling Project (IDDP) (Elders and Friðleifsson, 2010) or COTHERM (Driesner, 2012).

The efficiency of heat transfer from magma to fluids depends on physical properties of the rocks. Compared to conduction, convective fluids in cooled and brittle rocks are more efficient (Gillis and Roberts, 1999; Gillis, 2008). The temperature of this transition in felsic rocks is approximately 400° C. Fluid to rock ratio leading to intense alteration is based on fluid flux which is described by Darcy's Law. Interconnected porosity is based on the vesicularity of the host rock and increased by brittle fractures. Hydrothermal mineral growth form passing fluids may lead to self-sealing of pores (Hart et al., 1999). Depending on the efficiency of heat transfer, pressure and temperature various fluids from supercritical to vapor and water may be present in the system (Hayba and Ingebritsen, 1997). Eventually this also influences economic interest in geothermal systems. High enthalpy systems at shallow depths are therefore the most interesting energy producers. Within these systems supercritical fluids can directly transform to the superheated steam (Figure 1-1). In a pressure-enthalpy diagram this equals decompression with constant or near constant energy. To be able to maintain efficient energy generation over time, understanding for temporal as well as spatial evolution of the system must be increased.

Formation and composition of newly formed hydrothermal alteration minerals as well as breakdown of primary minerals strongly depends on pressure, temperature and chemical conditions in the system (German and Von Damm, 2006; Sveinbjörnsdóttir, 1991). Empirical temperatures for hydrothermal minerals growing in open spaces of alteration zones are derived from production wells, where measured temperatures were correlated with mineral occurrence. But drilling usually is restricted to the brittle zone. Approximate temperatures are summarized in Table 1-1. At various systems and drillholes slightly different temperatures and minerals may be described. E.g. temperatures below 200° C correspond to zeolite and smectite, followed by a clay and prehnite rich zone. Above 230° C epidote and

chlorite form and are eventually replaced by an actinolite zone. Locally contact metamorphism forms minerals like wollastonite, garnet and epidote (Kristmannsdóttir, 1975, 1979, 1981, 1982). Contact metamorphism also includes basaltic hornfels (Friðleifsson, 1983). Some minerals like epidote show a strong temperature dependence of the composition within alteration zones (Sveinbjörnsdóttir, 1991). Generally four alteration zones are described, based on the minerals actinolite, andradite, epidote and chlorite. These roughly correspond to temperature and depth in various hydrothermal systems. The problem remains that measured temperature does not necessary correspond to the deposition temperature of minerals as they may be stable over a certain temperature range.

Table 1-1: *Approximate temperatures assigned to mineral formation in four alteration zones and regional alteration (Bird et al., 1984; Friðleifsson, 1983)*

Mineral	Temperature [C]
Actinolite	>300°
Andradite	>300°
Epidote	230-300°
Chlorite	-
Zeolites	<120°

Hydrothermal alteration also leads to a change in the bulk chemistry of rocks. As elements show variable mobility within the system, their depletion or enrichment can be used as a proxy for intensity of alteration (Franzson et al., 2008; MacLean and Kranidiotis, 1987). K/Na and K/Ca ratios may help to determine degree of alteration based on the mobility of elements in hydrothermal systems (Berndt et al., 1988; Fournier and Truesdell, 1973; Giggenbach, 1988). Coexisting Fe-Ti oxides in silicate rocks, like titanomagnetite and ilmenite are regularly used to determine temperature, pressure and oxygen fugacity based on experimental results (Andersen et al., 1993; Sauerzapf et al., 2008). This is mostly applied to magmatic rocks and crystallization but these oxides also form under hydrothermal conditions (Matthews, 1976).

Therefore it is possible to gain information on the development (e.g. fluid to rock ratio (Franzson et al., 2008)) of active geothermal systems by looking at mineral assemblages and composition of these minerals and degree of alteration. Fluid inclusions can give additional information about the fluid temperatures, pH and composition during mineral growth (Arnórsson, 1995).

2 Geological setting

2.1 Geology of Iceland

Iceland is located at the intersection of a mantle plume with a mid ocean ridge. High production rate of magmas lifts this section of the north Atlantic ridge above sea level. Icelandic geology therefore is dominated by tholeiitic volcanism related to rifting of Tertiary and younger age (Figure 2-1). With a thickness of locally up to 45 kilometers, Icelandic crust is clearly thicker than average oceanic crust (Ágústsson, 2005; Allen et al., 2002; Foulger et al., 2003).

Due to the ocean ridge architecture Icelandic rocks become older with increasing distance from the active neovolcanic zone stretching southwest to northeast. The oldest tertiary rocks are located off axis in the northwest as well as along the southeast coast. Pliocene to Pleistocene rocks are found as stripes between the older rocks and the neovolcanic zone. Finally younger rocks which erupted during ice

cover and interglacial periods until historic times cover the center of Iceland. This neovolcanic zone branches in the southwest to two active zones. Within the thick crust, intrusive rocks and magma chambers below central volcanoes (Shield volcano along the neovolcanic zone) are abundant. However most of the surface is formed by extensive tholeiitic lava flows with thin interbasaltic layers of soil formation, tephra and mostly fluvial sediments. These lava layers generally dip 5-15° towards the neovolcanic zone.

Locally intrusive and extrusive evolved rocks can be found. Within tertiary rocks in Iceland basaltic lavas are deeply eroded by glaciers during Pleistocene. Exposed rocks represent up to about two kilometers of paleodepth in southeast Iceland (Guðmundsson and Kjartansson, 2007). Here all features of the systems along the active zone may be exposed and accessible for geologic interpretation. *Geitafell* is one of these locations, where a fossil hydrothermal system associated with an extinct central volcano is partly eroded down to its roots.

Geothermal heat flux is elevated everywhere in Iceland. Combined with the high amount of precipitation and groundwater recharge, this allows abundant hydrothermal systems to form (Friðleifsson, 1983). Low temperature systems are located all over Iceland in Tertiary and Pliocene to Pleistocene rocks, while high temperature areas are mostly associated with central volcanoes (Bödvarsson, 1961; Friðleifsson, 1979). Regional alteration with a depth and temperature related sequence of secondary zeolites and calcite forms from this hydrothermal activity (Walker, 1960). Therefore nearly all rocks buried deeper than 100-200 m below the surface show alteration (Guðmundsson and Kjartansson, 2007).

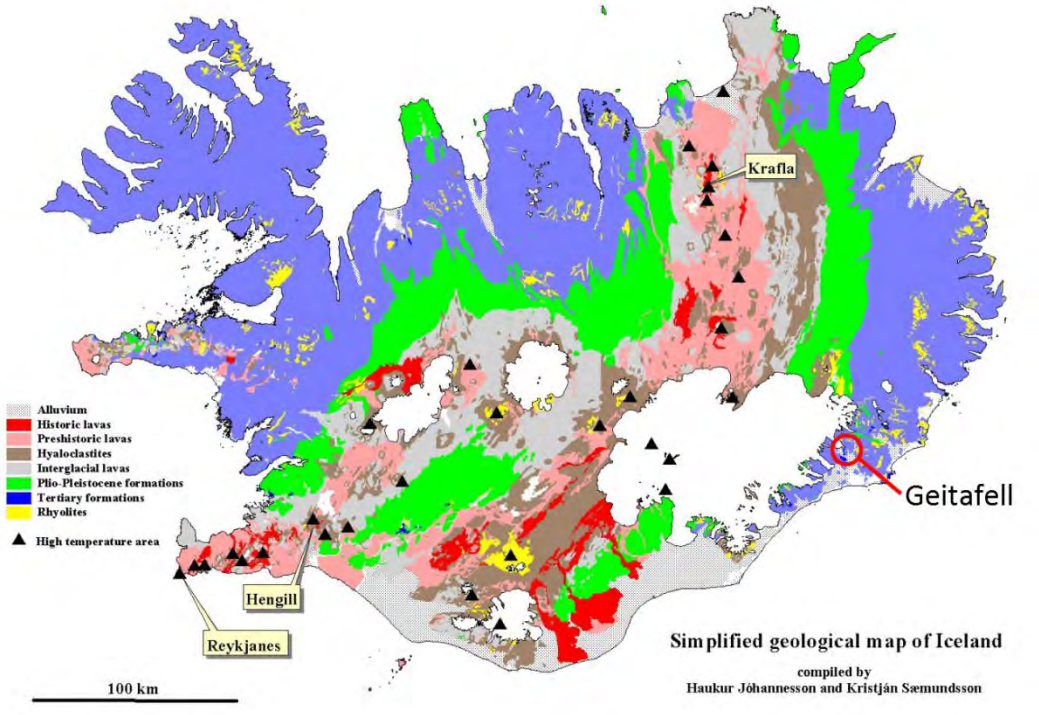

Figure 2-1: *Geologic map of Iceland including active high temperature areas with geothermal energy production (Sæmundsson K., 2009). Modification includes the locality of Geitafell field site.*

2.2 Geitafell Geology and Mineralogy

The *Geitafell* field area is located in southeast Iceland (Figure 2-1) and hosted in tertiary rocks. Geology at the extinct Geitafell central volcano is dominated by tholeiitic lava flows. The volcano was active about 6-5 Ma ago for approximately 1 Ma (Friðleifsson, 1983). Around *Geitafell*, lava flows have a dip of less than 10° towards the neovolcanic zone in the southeast and show a NE-SW trending flexure which increases the dip to more than 10° in northwest. This flexure extends across entire eastern Iceland and is related to the overload along the spreading axis. It is younger than the main volcanic activity and didn't influence the active phase of the hydrothermal system (Friðleifsson, 1983). Within the lava flows, remnants of a central volcano with several typical features are exposed to a paleodepth of about 1.6 kilometers due to erosion by the *Hoffell* glacier. Associated features include intrusive gabbro representing the ancient magma chamber, several phases of intrusive aphyric and porphyric dykes and cone sheets emerging from this chamber. Hyaloclasite, which is evidence for early glacial cover during active volcanism, formed at paleo surface level. Late rhyolitic intrusions and lavas represent evolved magmas. A total of twelve different intrusive phases were described (Friðleifsson, 1983). Other features associated with *Geitafell* include several alteration zones formed by a geothermal system which lies partly within the solidified gabbro. Similar alteration zonation is described from drill holes in active hydrothermal systems in Iceland as well as along mid ocean ridges (Bird et al., 1984; Humphris and Thompson, 1978; Marks et al., 2011; Sveinbjörnsdóttir, 1991). Time relations of the different events are resolved reasonably good trough intrusive contacts and vein relationships (Friðleifsson, 1983).

Gabbro and basaltic rocks at *Geitafell* is mainly composed of plagioclase (labradorite to bywtonite, few anorthite), clinopyroxene (augite) with minor olivine and ore minerals like magnetite and ilmenite. Secondary mineralization includes hematite and sulfides as mineral replacements. Vein and vesicle filling minerals include quartz, calcite, actinolite, zeolites, clay, garnet, and pyrite with decreasing abundance. Low grade alteration is represented by phyllosilicates like smectite and mixed clay layers including chlorite with higher Mg content towards higher temperatures in the actinolite alteration zone. Amphiboles are typically more Fe rich if found in veins or amygdales during replacement amphiboles show more typical, Mg rich actinolite composition. Epidote shows no correlation of composition to stratigraphic position but minor elements show higher variability within crystals than between different crystals (Exley, 1982; Friðleifsson, 1983). Zeolites occur in veins, amygdale and as pseudomorphs of feldspar. Several types can be found which usually are of consistent composition. Albite and adularia occurs as replacement of feldspar. Titanite occurs mainly with oxides and in actinolite veins and its composition is similar to host rock titanite. Rare sulfides are pyrite and chalcopyrite. Garnet of andradite to grossular composition is found as replacement mineral of hedenbergite indicating skarn formation (Friðleifsson, 1983).

3 Methods

3.1 Field work

Geological mapping and sampling was conducted at the field site at *Geitafell* between the glacial lagoon of *Hoffellsjökull* and *Geitafellsgil* gorge (Figure 4-1). Results of field mapping were digitized with ArcGIS software and merged with preexisting maps and findings of geophysical measurements. Any coordinates given are in the coordinate system "ETRS 1989 UTM Zone 28N".

Detailed mapping of magmatic and hydrothermal veining was done on outcrop "A" near *Hoffellsjökull* (see section 4.3.4). A grid laid on the outcrop was used for better correlation between individually mapped grid meshes. The grid was aligned along cardinal directions. As the mapped squares are on the outcrop surface with a dip westward towards the glacier the resulting map is adjusted to represent a horizontal plane. The map produced in ArcGIS is therefore squeezed in east-west extent by a factor of 0.963 calculated from $\cos \varphi_{dip}$ with $\varphi_{dip} = 25°$ to represent a horizontal layer.

In May 2014 a drill-hole campaign by Iceland GeoSurvey (ISOR) was conducted in the field area (Friðleifsson, 2014). Target was the Contact metamorphosed zone around Geitafell gabbro (Friðleifsson, 2014). One short granophyre core sample from drillhole 4 was used in this thesis.

3.2 Optical Microscopy

Petrography and alteration in the gabbroic magma chamber and the associated hydrothermal system was studied on 28 thin sections from 26 samples and direct observations on cut and polished hand samples. The samples are representative for the variability of gabbro and more evolved magmatic features as well as for hydrothermal alteration features, i.e. variable crystal-size and mineralogy, mineral replacement, vesicles and vein infill sequences. Six of the 28 thin sections were prepared as polished thin sections due to their high content of opaque minerals especially Fe-Ti-oxides.

For estimations of mineral volume percentages, point counting was used with grid spacing of 0.4 mm and 0.5 mm on thin sections of different samples. Number of points counted ranges from at least 200 up to about 2000 in samples where it was necessary to cover a wider area due to crystal-sizes. For coarse gabbro, point counting was applied on polished and scanned samples using a digital grid on the photograph.

3.3 Chemical Analysis

XRF

Whole rock composition of 14 samples was analyzed using X-ray fluorescence (XRF). Depending on crystal-size in each sample, 30-240g of each sample was crushed in a hydraulic press. 30g aliquots were ground to a fine powder in a tungsten-carbide mill. For one sample (P1), pieces including plagioclase phenocrysts were removed after crushing and sieving with a mesh size of 4 mm. This was done to measure whole rock composition of dyke filling melt without phenocrysts as these formed earlier than the dyke. Small phenocrysts might remain in the powder but these were diluted sufficient in the process of sorting. Therefore it is acceptable to assume nearly magmatic liquid composition in this whole rock analysis. All powder samples were dried at 378.15 K for more than 6 hours. After

weighting 1.5 gram into an aluminum-oxide crucible, the powder was dried for another two hours at 1323.15 K to determine the loss on ignition (LOI). The sample powder was then mixed with lithium tetraborate ($Li_2B_7O_7$) at a ratio of 1:5. One glass pill was cast from each powder and analyzed with a wave length dispersive X-ray fluorescence spectrometer (WD-XRF by Axios PANalytical). Measured major elements are shown in Table 4-1, Appendix B includes all results. Ga, Ce and Nd were not measured correctly during analysis and therefore results were not included in the results section.

XRD

Mineral identification based on crystal lattice parameters was accomplished by X-ray powder diffraction (XRD). Powder from six samples which were also analyzed with XRF was used as well as powder produced by grinding vein-filling material in an agate mortar. Due to the small amount of powder available from this sample it was measured on a glass waver while the other powders could be measured by adding powder directly into the sample holder.. High iron content is expected in most samples. With CuKα as source radiation, Fe can emit FeKα fluorescence radiation which will produce a high background in the measurement. To avoid this, an energy dispersive Sol-X detector is used for the measurement. Run *A* represents the first run with sample Q27 and run *B* the second run for all other samples. Peak match was done with "DIFFRAC.EVA" software from Bruker. Results are provided in Appendix D.

EPMA

Electron probe micro analysis was done on a JEOL (JXA-8200) device. Three polished section were chosen for analysis and coated with 20nm carbon. Wavelength-dispersive X-ray spectroscopy (WDS) mode was used to analyze ten major elements (Si, Na, Ca, K, Fe, Al, Mg, Cr, Ti, Mn) quantitatively by scanning areas at 100'000x and 300'000x magnification respectively for 20 seconds. Acceleration voltage was 15 kV and probe current was set to 2 nA. Compositional scanning mode was used to produce gray scale images of chosen mineral assemblages. Results are shown in Table 4-2.

3.4 Fluid inclusion measurements

Measurements of homogenization temperatures were done on a THMSG600 stage on Leitz Wetzlar and Nikon eclipse E600 pol microscopes. A H2O inclusion standard was used for calibration at 0° and 374.1°. Samples representing two locations within the roots of the hydrothermal system were chosen with the aim of observing spatial and temporal variation in fluid properties. Idiomorphic quartz in vesicles within *Aplite* matrix of an *Intrusive Breccia* was chosen for 150 µm thick sections. Pervasive alteration and weathering of the host basalt made it impossible to sample stable hand samples of open veins with intact epidote-garnet-quartz assemblages from *Kraksgil*. Therefore intact individual quartz crystals were collected. These 1.5- 4 mm wide and 5-20 mm long quartz crystals formed partly on and around garnet, epidote and chlorite crystals. About 30 of those crystals were examined under a binocular microscope for fluid inclusions. A selection of six was then prepared as 250 µm thick sections for thermometry studies. Focus in prepared samples was on growth zones within quartz and garnet crystals to attain conditions during mineral growth. Raw results are shown in Appendix C.

4 Results

4.1 Mapping

Mapping was done between *Hoffellsjökull* and along the southern end of *Geitafellsgil* with focus on magmatic and hydrothermal features. This restricted area includes the contact zone of a gabbroic intrusive body, swarms of sheets and dykes and basaltic host rock. Most of the mapping was done along the incision of *Geitafellsgil*. Outcrops are situated roughly along a cross section overlapping the contact zone as visible in Figure 4-1. The contact zone is strongly obliterated by intrusive dykes and sheets (Friðleifsson, 1983). A map with locations where rock types were identified is available in Appendix G. Further outcrops include strongly altered basalt host rock at *Kraksgil* and lava flows in *Hoffellsdalur* which were subject of the related geophysical study (Grab, 2014; Zürcher, 2014).

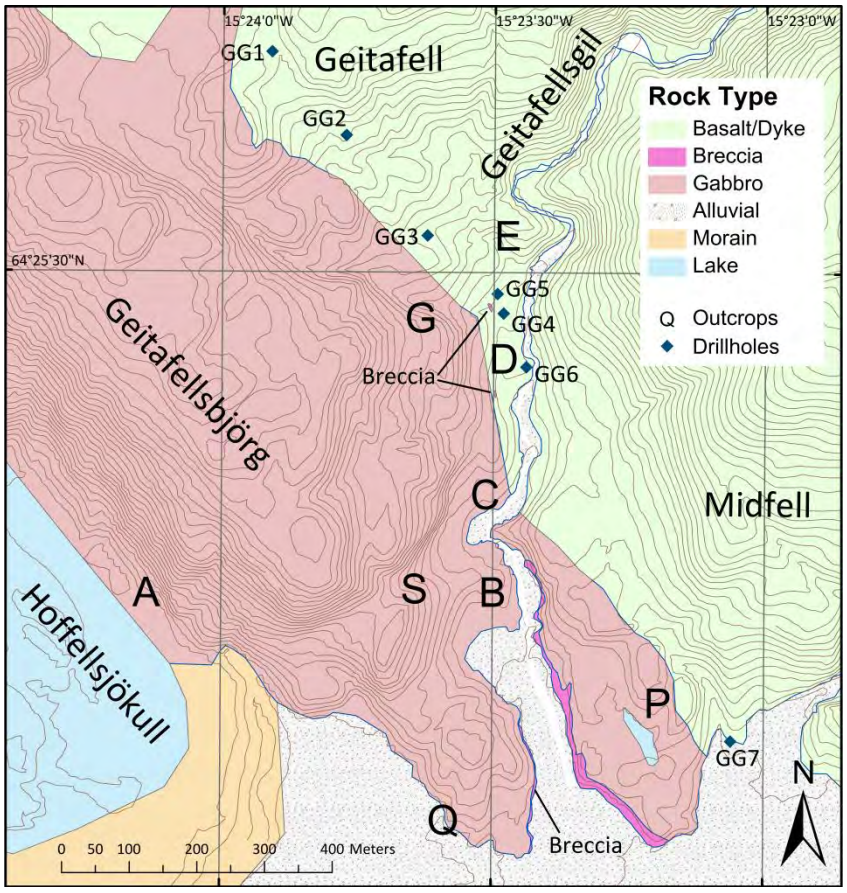

Figure 4-1: *Overview map of the field site. Drillholes from May 2014 (blue diamonds), approximate outcrops and sampling sites (capital letters) along a profile in Geitafellsgil and a geologic layer are included. The location Kraksgil is about 1.2 km southeast of location P. The contact zone is assumed to continue southward from P. Therefore Kraksgil is situated in a distance of several hundred meters from the contact.*

4.2 Intrusive magmatic features

Despite being part of the tholeiitic magmatic series in Iceland, intrusive features at *Geitafell* cover a wide range of variability in appearance as well as crystal-size and bulk composition. Total alkali versus silica (TAS) plots of analyzed rocks ranges from pircrobasalt to rhyolite equivalent (Figure 4-10). Detailed discussion of these results will follow later.

4.2.1 Petrography and mineralogy

Main intrusive lithologies

All rock types described herein are gabbro variations found at *Geitafell*. All variations correspond to "intrusive phase 2" of Friðleifsson 1983. Occurrences of the described gabbro types are shown on the map in appendix G.

"Gabbro A"

Main gabbro type observed along the glacial lagoon and towards the entrance of *Geitafellsgil*. Crystal-size is 2-8 mm. Mineralogy comprises ~40% subidiomorphic plagioclase, ~51% xenomorphic clinopyroxene, ~6% dendritic ilmenite and ~3% subidiomorphic spinel shaped magnetite (Figure 4-5 A). In some zones the abundance of plagioclase shows variations and weak modal layering may be observed (Figure 4-6 D). Locally also ophitic growth of few pyroxene crystals is observed at outcrop A. Structure of crystals does not show preferred orientation. Around outcrops A and Q this rock type includes *Pegmatoidal Gabbro* (described in detail below) and zones with bimodal crystal-size distribution, where coarse, pegmatoidal crystals (usually pyroxenes with minor plagioclase) are mixed with finer crystals (predominantely plagioclase). These zones have a roughly N-S strike if elongated. Dykes and sheets intruding this gabbro generally belong to late intrusive phases but are not as abundant as in other gabbro types. Intrusive contact towards other gabbro lithologies is not distinct. It is mainly observed as disappearance of *Pegmatoidal Gabbro* zones and increased abundance of thick dykes and sheets towards the rim of the magma chamber.

"Fine Gabbro"

This gabbro type occurs abundantly at the southern end of *Geitafellsbjörg* to the west of outcrop S. In other areas this gabbro was not observed frequently. Average crystal-size is <3 mm. The rock consists of ~50% subidiomorph plagioclase, ~43% xenomorphic clinopyroxene, ~7% oxides (Figure 4-5 B). Crystal size is very homogenous and crystals are evenly distributed. Ilmenite grows as elongated laths while magnetite is of nearly octahedral shape. Ilmenite laths may be oriented parallel or in 60°, 90° and 120° angles to each other on thin section scale. Growth of silicates may grow around and in between dendritic laths. Angles between silicate crystals are similar to the ones observed in oxides.

Transition towards *Gabbro B* is dominated by dm to m wide zones of *Fine Gabbro* enclosed in *Gabbro B*. At least one *Aphyric dolerite* sheet is found to penetrate this zone. Contact to *Gabbro A* is more abrupt but the restricted occurrence of *Fine Gabbro* does not allow extensive observations. Contact towards *Ophitic Gabbro* is not observed directly but is fairly abrupt following the width of a gully marking the contact. Crystal size of fine crystals in *Porphyritic Gabbro* and crystals in *Fine Gabbro* are very similar, a magmatic contact is therefore difficult to establish and might be transitional.

"Gabbro B"

At the southern end of *Geitafellsgil* (outcrops B) gabbro resembles *Gabbro A* in appearance and crystal-size. *Gabbro B* is, however, richer in subidiomorphic plagioclase (up to 72%). Further minerals are ~20% of xenomorphic clinopyroxene, ~8% oxides with isomorphic partly octahedral shape. Closer to the contact zone oxide content decreases slightly. Ilmenite is also found as lath-shaped crystal with a weakly oriented growth direction. Some up to 10 mm long and 0.5 mm wide crystals with a small spacing (<4mm) are sub-parallel oriented (Figure 4-2). Exsolution lamellae of magnetite are abundant in ilmenite. In magnetite rarer ilmenite lamellae are observed. Zones with interstitial crystallization are pervasively altered. Only plagioclase remains as recognizable mineral. Presence of this feature is found near contact to *Ophitic Gabbro*.

Within *Gabbro B* pegmatoidal pockets are not present. Local inhomogeneity however is found too. Zones of several centimeters to decimeter width and a few meter length include alternating "layers" of coarser and smaller crystals than the surrounding gabbro (Figure 4-3). Penetrating these zones are smaller, dyke-like intrusive bodies resembling the silica rich phases described below. Some layers are pronounced by slightly different weathering due to uneven extent of alteration, especially albitization. Strike is roughly N-S but zones are not straight. Dip is about 75-90° east.

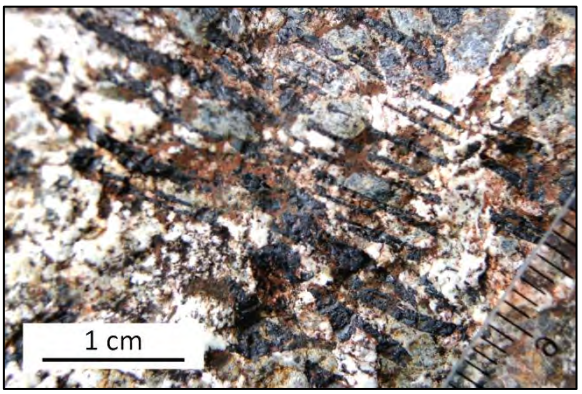

Figure 4-2: *Parallel oriented ilmenite laths in Gabbro B due to dendritic growth.*

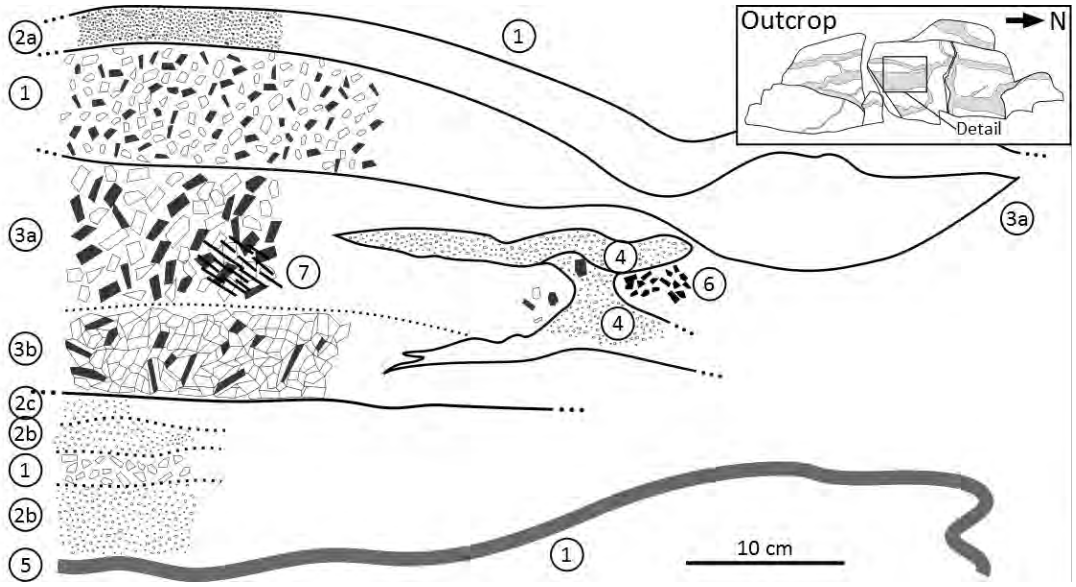

Figure 4-3: *Enigmatic zonation at outcrop B1 (Location in Appendix G): Gabbro B (1). Several "layers" of Fine Gabbro (2a, b, c) and coarse gabbro (3a, b) with slightly different crystal-size and mineral proportions. Gabbro is host for more silica rich rocks like White Acid (4) and Green Dykelet (5). Magnetite (6) and ilmenite laths (7) are locally enriched. Transition between gabbro types is not as distinct as in the sketch and crystal-size is slightly exaggerated for simplification.*

Contact towards *Ophitic Gabbro* is dominated by coarsening of *Gabbro B* and presence of interstitial crystallization. Intrusive contact to *Porphyritic Gabbro* is a not sharp as well but a several m wide zone. Average crystal size increases where bimodal crystal size distribution disappears. Contact to *Gabbro A* and *Fine Gabbro* is described in respective sections. *Gabbro B* is frequently penetrated by mafic sheets and dykes as well as evolved silica rich melts forming an *Intrusive Breccia* at *Geitafellsgil*.

"Xenolith Gabbro"

Similar gabbro type as *Gabbro B*. Alteration however is stronger and the rock has a bleached appearance. (Figure 4-5 C) This rock type was found as two xenoliths in a dolerite that cuts through *Gabbro B*. The host rock of the dyke is not of the same gabbro as the xenoliths as it is slightly ophitic while the xenoliths are equigranular and more plagioclase-rich.

"Ophitic Gabbro"

This gabbro type is made of coarse clinopyroxene crystals with ophitic growth around smaller plagioclase crystals. Outcrops are near the gabbro to host rock contact in *Geitafellsgil*. Crystal-size is <50 mm for clinopyroxene and <2.5 mm for plagioclase. Mineralogy comprises ~40% subidiomorphic to idiomorphic plagioclase, ~57% xenomorphic clinopyroxene, ~3% oxides. (Figure 4-5 D) Crystal-size of pyroxene increases northward along *Geitafellsgil* from an average diameter of about 1.5 cm to 4 cm. The texture of the finer *Ophitic Gabbro* tends to be subophitic with <3 mm long plagioclase laths. In plagioclase-rich zones, the texture becomes intergranular and resembles orthocumulate with elongated 10 µm long plagioclase crystals and replacement minerals (chlorite, epidote) due to intensive alteration.

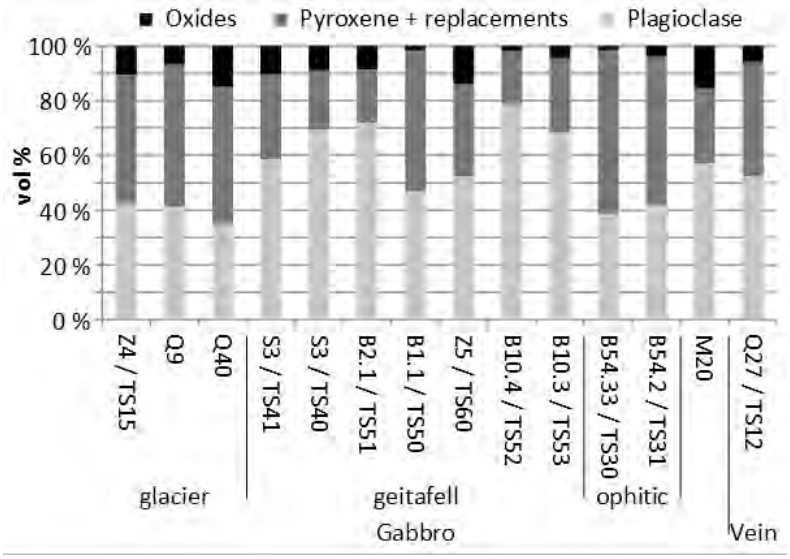

Figure 4-4: *Proportions of rock forming minerals determined by mineral counting. Replacements include secondary actinolite and chlorite. Sample Z4, Q9 and Q40 correspond to Gabbro A, S3 to Fine Gabbro, B2.1, Z5 and B10.4 to Gabbro B from Geitafellsgil without pegmatoidal pockets, B10.3 to Xenolith Gabbro, B1.1 to a sub Ophitic Gabbro from Geitafellsgil, B54.2 and B54.33 to Ophitic Gabbro, M20 to Porphyritic Gabbro. Proportions Q27 are a Green Dykelet.*

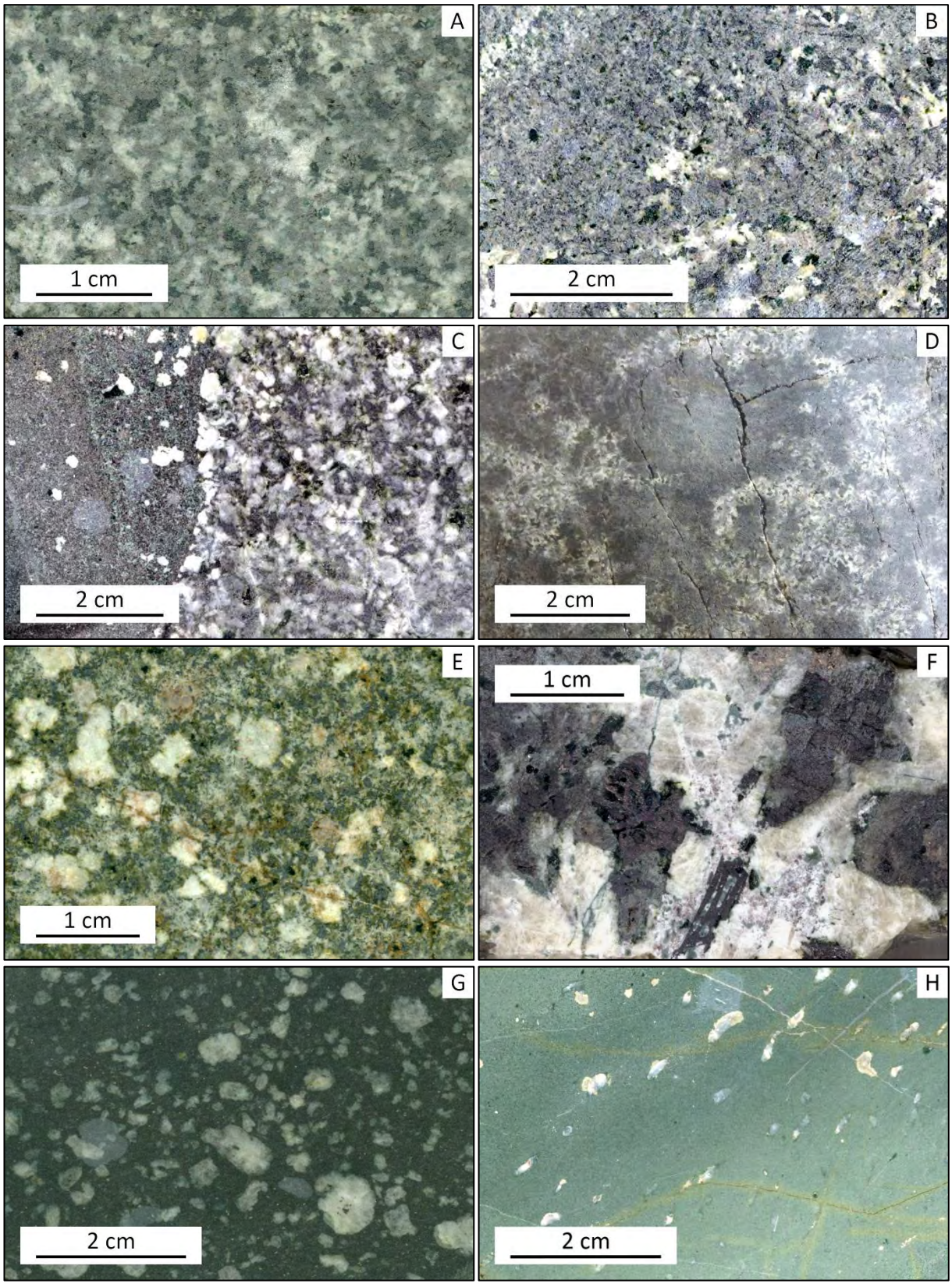

Figure 4-5: *Rock types at Geitafell central volcano. A) Gabbro A; B) Fine Gabbro with batches of Gabbro B; C) Rim of Xenolith Gabbro in dolerite host; D) Ophitic Gabbro; E) Porphyry Gabbro, strongly affected by alteration and weathering; F) Gabbro Pegmatite. A fine actinolite vein is visible; G) Porphyry dolerite; H) Aphyric Dolerite with squeezed and filled vesicles (cc-py) and veins (cc-py). Greenish color due to epidote-chlorite alteration;*

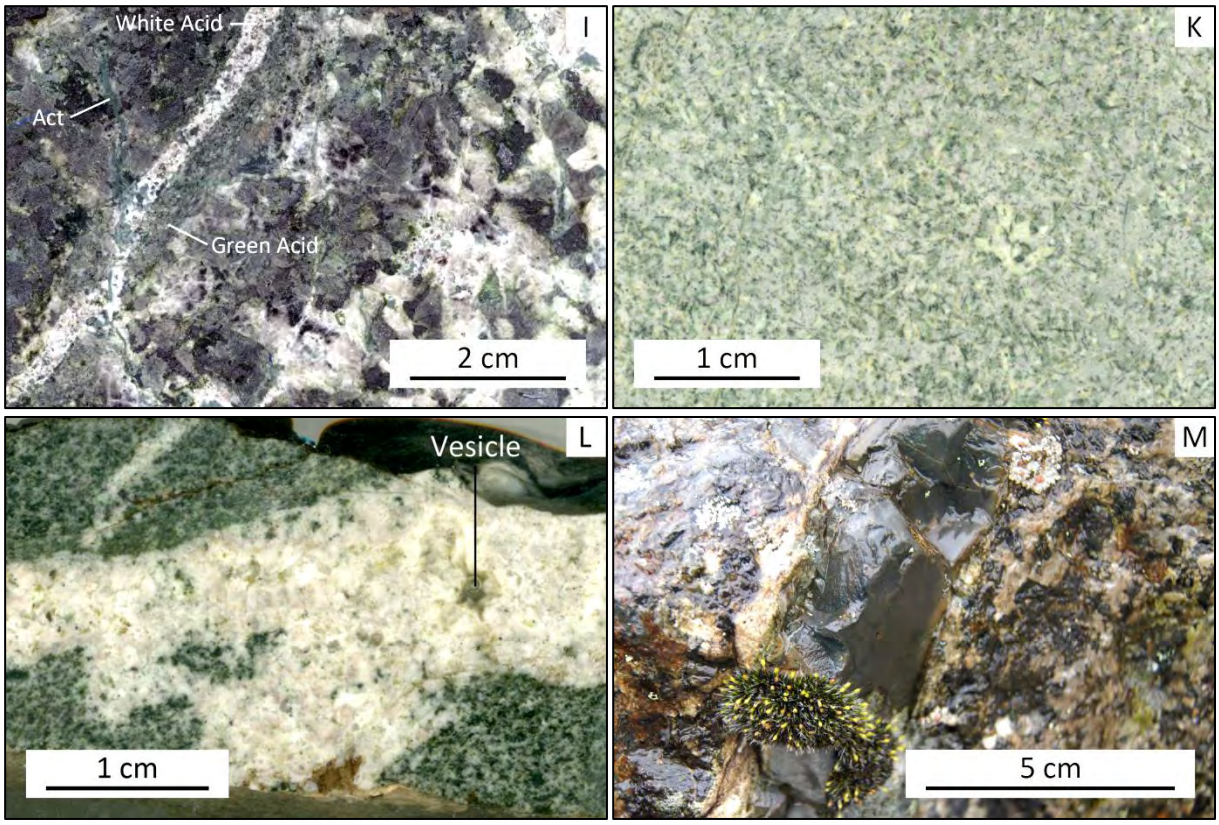

Figure 4-5 continued: *Rock types at Geitafell central volcano. I) Veins of Green Dykelet and White Acid within gabbro pegmatite; K) Granophyre (from core sample); L) Aplite vein in coarse dolerite breccia; M) Basalt dykelet following a White Acid vein (field photo); Samples are cut and wet to improve visibility of minerals. Image manipulation is restricted to improvement of white balance, brightness and contrast.*

"Porphyritic Gabbro"

Fine grained gabbro type with bimodal crystal-size distribution of plagioclase. Average crystal-size is <1.5 mm with additional 3-8 mm plagioclase crystals. Rock forming minerals include ~20% subidiomorphic coarse plagioclase, ~33% subidiomorphic fine plagioclase, ~40% clinopyroxene, ~7% oxides. (Figure 4-5 E) Abundant occurrences of this rock are found on the small hill south of *Geitafellsgil* and northwards along the gabbro to basalt contact. Contact to the host basalt is obliterated by abundant porphyric and aphyric dykes and sheets. Locally there are just meter-sized chunks squeezed in between seveal dykes indicating presence of *Porphyritic Gabbro*.

Subordinate intrusive lithologies

Subordinate intrusive bodies include pegmatoidal bodies within gabbro and different sets of silica rich dykelets. *Pegmatoidal Gabbro* is part of intrusive phase 2 while all silica rich rock types (A*cid Green*, A*cid White*, A*plite* and matrix of *Intrusive Breccia*) belong to intrusive phase 4 (Friðleifsson, 1983). Corresponding intrusive phases for dykes and sheets of near basaltic composition are mentioned in each section. For Structural relations see the map in Appendix E.

"Pegmatoidal Gabbro"

Coarse gabbro, occurring as irregular pods and dikelets around outcrop A and Q. Contact from *Pegmatoidal gabbro* to host gabbro is usually

sharp but as coarse crystals nucleate on host rock crystals may partly be obscured. Maximum crystal-size is up to 30 mm for plagioclase, 100 mm for clinopyroxene and 20 mm for oxides while typical sizes are around 15 mm for plagioclase laths, 20-30 mm for pyroxenes and 2-8 mm for oxides. Mineralogy consists of ~60% subidiomorphic plagioclase, ~30% subidiomorphic clinopyroxene, ~10% oxides (Figure 4-5 F). Ilmenite has strong dendritic shapes and magnetite is slightly dendritic. Exsolution lamellae along the crystal lattice plains are very abundant in ilmenite and slightly more rare in magnetite (Figure 4-9 C, D). Two types are described, straight long lamellae as well as short lamellae with rice grain shape. Lamellae may originate at the contact of ilmenite and magnetite crystals and percolate entire crystals. Biggest lamellae are up to 10 µm wide with a roughly regular spacing of 100 µm. Smaller lamellae in between the most obvious ones are common and Between laths of dendritic ilmenite plagioclase, pyroxene as well as *Granophyre* is found.

Shape and size of *Pegmatoidal Gabbro* occurences show strong variations (Figure 4-6 A, B, C). Occurrence and extent of each type of *Pegmatoidal Gabbro* is shown in Appendix E. There also spatial relations to more silicic rocks described below are shown.

Pegmatite dykelets are the most common feature. These are 3-10 cm wide, several meters long and have relatively sharp walls (Figure 4-6 B, C). Crystals in dykelets are often oriented perpendicular to the wall rock surface. Dykelets may overlap and branch. Strike is N-S and dip is sub-vertical. On vertical outcrops dykelets are sometimes forming a vertical "tail" emerging from more irregular pegmatite pods downward.

Irregular pegmatite pods are other common features. These are 5-30 cm wide and some are up to ~2 meter long with irregular shape. Pods are typically hosting an infill of more silicic rock types with occasionally loose crystals from the pegmatite floating in the silicic area (Detailed description below). Elongated structures have a N-S to NNE-SSW strike and are sub vertical. Alignment of several pods of this type forming 10-15 m long structure is observed. However smaller more roundish pod are also frequent. Vertical transition from pegmatoidal dykelets widening to pegmatite pods is occasionally observed.

Bigger pegmatite bodies with diameter up to 70 cm have irregular shape and extensions. As these are roughly isometric, no orientation is observed. Siliceous infill may show internal variation if present (Figure 4-6 B). Pods may have asymmetric rims, e.g. pegmatite is thinner or absent. The irregular rim is also present in roundish and oval pegmatite pods of about 10 to 20 cm diameter (Figure 4-6 A).

Enigmatic zones with pegmatoidal crystals floating in fine grained silica rich rock are observed but lack of distinct pegmatoidal rims. One of these zones is visible in the upper central part of Figure 4-6 A.

"Green Dykelet"

Fine grained rock type with plagioclase, clinopyroxene, oxides and vesicles. Crystal-size is <0.5 mm. Mineralogy consists of ~20% plagioclase, ~10% pyroxene, ~3% oxides and ~67% of very fine grained materials which are unidentifiable by optical methods but assumed to be mostly glass and secondary replacement minerals. (Figure 4-5 I) The green color is due to pervasive actinolite and chlorite replacement of pyroxenes.

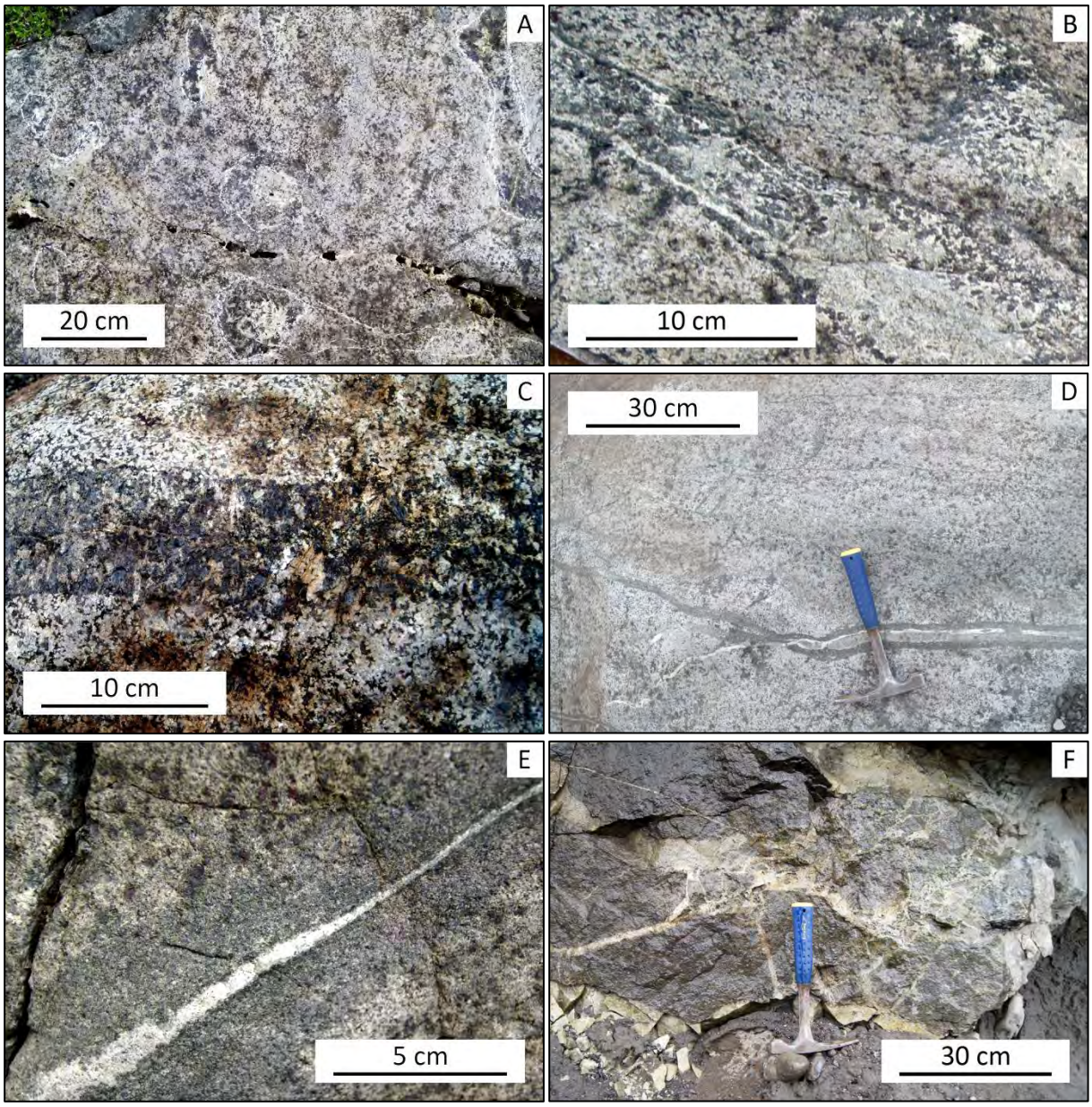

Figure 4-6: *Late magmatic features in Geitafell gabbro: A) Gabbro A outcrop including small pegmatoidal pockets and pegmatoidal zones with later White Acid rock; B) Pegmatoidal zone with later White Acid and Aplite infill. The transition of a pegmatite pocket to pegmatite veins with acid in its center is clearly visible; C) Wide pegmatoidal dykelet in Gabbro A. Pyroxene and plagioclase crystals are oriented preferably perpendicular to vein walls; D) Composite sheet with a sequence of dark dolerite, bright grayish acid and whitish Aplite within a weakly layered Gabbro A; E) Composite sheet including Aplite following after dolerite in Gabbro A. In the right part of the photo, the contact from dolerite to Aplite is brittle simultaneously the left part it is more ductile and diffuse; F) Small zone of brecciated gabbro with Aplite matrix near Hoffelsjökull. Not visible in the picture is a 20-30 cm wide Aplite sheet nearby to which the brecciated zone is associated;*

Green Dykelet rocks are restricted to thin dykelets within *Gabbro A, B* and *Pegmatoidal Gabbro*. Dykelets are <30 mm wide with irregular walls. Their orientation follows preferentially *Pegmatoidal Gabbro* dykelets with an average width of about 5mm. Depending on alteration appearance can be grayish.

"White Acid"

Fine grained rock with plagioclase, quartz, few clinopyroxene and abundant vesicles. Crystal-size mostly is <1 mm. Mineralogy comprises ~35% plagioclase, ~5% quartz, ~2% oxides, <1% pyroxene and ~57% of very fine grained materials, most of it glass or graphic intergrowth of plagioclase, orthoclase and quartz (Figure 4-5 I and Figure 4-9 B).

Occurrence of this rock is common near outcrops A and Q towards *Geitafellsgil*. Dyeklets with <3 cm width are found as well as "acid" infill within pods of *Pegmatoidal Gabbro* of up to 15 cm width. The shape of these pockets is often irregular and the fine grained material is intruding between coarse, pegmatitic crystals and truncating these (Figure 4-9 A). Dykelets often follow preexisting structures like pegmatite dykelets or *Green Dykelet*. Pieces of broken crystals from *Pegmatoidal Gabbro* are found on either side of dykelets. Xenocrystals entrapped from host gabbro are found in brittle dykelets.

"Granophyre"

Granophyre (Barker, 1970) is a plagioclase and orthoclase rich rock type mostly occurring within gabbro along *Geitafellsgil* (Figure 4-5 K). Crystal size is very fine with plagioclase as dominant rock forming mineral. Most of the coarser plagioclase (<2 mm) has a zoned rim while finer plagioclase is unzoned. Crystal-size is variable and local amphibole near small host basalt xenoliths along the gabbro contact may be up to 8 mm long but completely replaced by secondary minerals including oxides. Graphic intergrowth of quartz and orthoclase is observed mainly in the zones with small crystals and lack of amphibole.

Granophyre occurrence approximately following the *Intrusive Breccia* along lowermost *Geitafellsgil*. Surface outcrops are not very abundant but drillholes along *Geitafellsgil* regularly penetrated into *Granophyre*. Contacts towards basalt and hornfelsed basalt are sharp and small host fragments are observed as xenoliths.

"Aplite"

Fine grained rock with quartz and plagioclase. Dykelets with <35 mm width and occasionally thicker sheets or dykes of up to 250 mm width are observed. Vesicles of <2 mm width are abundant but more rare in wider dykelets or dykes. Outcrops of dykelets and dykes are found around A and Q as well as along *Geitafellsgil*. Most outcrops are dykelets or sheets with straight boundaries. At *Geitafellsgil* the matrix of an intrusive breccia is formed by *White Acid* to *Aplite* material. (Figure 4-5 L)

"Intrusive Breccia"

An *Intrusive Breccia* is found in outcrops along the southern end of *Geitafellsgil*. The northernmost outcrop is found near geophysical profile 7 on the road (See Appendix G). The breccia is matrix supported in the center and shows gradual transition to clast supported and relatively intact host gabbro with silicic dykelets. The latter become rarer with increasing distance from the breccia. Clasts are angular to sub-rounded and made of *Gabbro B* as well as fine grained, *Basaltic* to *Aphyric Dolerite,* P*orphyritic Dolerite* and host basalt upriver. Silica rich rocks like

Granophyre and *Aplite* form the matrix (Figure 4-7). Small (<2mm, rarely <5 mm) primary vesicles are common within the matrix and partly filled with idiomorphic quartz crystals.

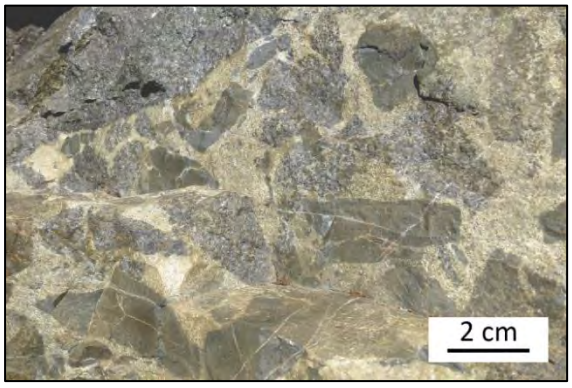

Figure 4-7: *Intrusive Breccia with gabbro and fine Aphyric Dolerite clasts.*

Several small outcrops and occurrences in drillholes along *Geitafellsgil* are assumed to form one zone of brecciation following the river and penetrating trough gabbro as well as the basalt lava flows.

"Rhyolite"

Dykes and sheets of rhyolitic composition are very rare but parts of a 100-200 mm wide sheet were found in *Geitafellsgil* near *Granophyre* from drillholes. There it shows chilled margins towards plagioclase-bearing basaltic dolerites. Crystal-size is <2 mm for longish plagioclase phenocrysts and <1.2 mm for possible amphibole phenocrysts. Mineralogy comprises ~60% subidiomorphic plagioclase with a grayish glassy matrix. Described *Rhyolite* is part of intrusive phase 4 from Friðleifsson (1983), where also phase 11 is referred as rhyolite it is not described in the mapped area.

"Aphyric Dolerite dykes"

Aphyric dykes and sheets are similar to *Porphyric Dolerite* but without phenocrysts of plagioclase. Chilled margins are an abundant feature. Several phases are visible in the field as indicated by Friðleifsson, 1983. Vesicles may be visible by naked eye (Figure 4-5 H). and few very tiny vesicles were present in all sample analyzed with petrophysical methods (Grab, 2014; Zürcher, 2014). *Aphyric Dolerite* is described as intrusive phase 5 (few augite crystals) and 12 (last phase, characterized by columnar jointing) (Friðleifsson, 1983). In this study it is used for phase 5 if not stated different.

"Porphyric Dolerite dykes"

Porphyric dykes and sheets, with a dense, homogenous and fine grained to glassy matrix. The matrix is made of plagioclase, pyroxene and oxides. Magnetite is present. Up to 10 ^{vol}% plagioclase phenocrysts are observed but the content is highly variable (Figure 4-5 G). Interior parts and rim of one dyke may have different appearance due to abundance of phenocrysts and presence of vesicles. Vesicles may not be visible by naked eye but are present in all samples analyzed with petrophysical methods. Chilled margins are a common feature. Several intrusive phases of *Porphyritic Dolerite* were described by Friðleifsson, 1983. Intrusive phase 3 dykes are rare and include bywtonite and augite phenocrystals. Clasts at the northernmost exposure of the *Intrusive Breccia* are from this phase. Phase 6 cone sheets are highly feldsparphyric with a fine matrix. Phase 7 dykes have chilled margins and are less feldsparphyric than phase 6. Both of those phases are common in the mapped area and the term *Porphyric Dolerite dyke* is used to describe them. Phase 10 dykes and sheets include big plagioclase crystals (>1cm) but were not described during mapping.

"Basalt Dykelets"

Dykelets and dykes of very fine grained intrusive rocks with basaltic composition occurring in the whole field area. Locally plagioclase phenocrysts and vesicles are

visible. Chilled margins are usual and even chilled margins between 100-200 mm wide members are common. Thickness may vary from 10mm to m (Figure 4-5 M). This rock type corresponds to intrusive phase 8 sheets and phase 9 dykes.

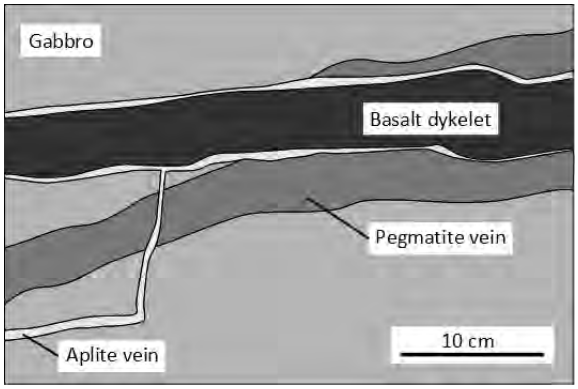

Figure 4-8: *Sequence of small magmatic dykelets following pre-existing structures in Gabbro A.*

4.2.2 Time Relations

Time relations of magmatic intrusive and extrusive rocks were described in detail in earlier work for mafic dykes and sheets, gabbro and roughly for more silica rich rocks (Friðleifsson, 1983). As finer distinctions of certain rock types were introduced, time relations are discussed here again.

Based on field relations, the sequence of above described rock types begins with smaller bodies of main intrusive lithologies (*Porphyritic gabbro*, *Ophitic Gabbro* and *Fine Gabbro* subsequently) followed by larger volumes of *Gabbro B* and eventually *Gabbro A*. Dykes and sheets form simultaneously to the intrusion of all of these lithologies along fractures in already cooled lithologies. Clear intrusive contacts between the main gabbro lithologies are absent and imply injection of magma into not yet completely solidified predecessors. Field relations indicate begin of crystallization in the main gabbro (*Gabbro A and B*) prior to pegmatoidal pockets and dykelets.

The sequence of subordinate lithologies begins with pegmatoidal pods and dykelets whose formation may overlap with the last stages of crystallization in gabbro (Fig 4-6 A, B, C). *Pegmatoidal Gabbro* is followed by fine dolerite sheets and *Green Dykelet*. Sheets and pockets of at more silicic magmas (*White Acid*) form subsequently (Fig 4-6 D, E) and intrude into crystallized *Pegmatoidal Gabbro* along fractures. Infill mainly occupies preexisting dyke–shaped structures (Fig 4-8), pods associated with pegmatite and occasionally space in between coarse pegmatite crystals. Pods including *White Acid* have a variable mixture of magma and floating crystals. Partly following these structures aplitic material forms brittle sheets and brecciates gabbro (Fig 4-6 F). As within the breccia also fine *Aphyric Dolerite* as well as *Porphyric Dolerite* (phase 3) are found as clasts, brecciation takes place later than these intrusive phases. Meanwhile aphyric dykes of phase 12 as well as phase 5 intrude the magmatic breccia as a composite dyke. Phase 8 *Basalt Dykelets* are not seen to intrude into breccia but are younger than *Aplite* dykelets (Fig 4-8) and always have chilled margins due to their later intrusion.

As the earliest clearly identified mafic intrusive phase intruding into *Gabbro A* is phase 8. All earlier phases may form contemporal with only small aphyric dykelets (e.g. *Green Dykelet*) reminding on their presence. Shortly after crystallization of gabbro.

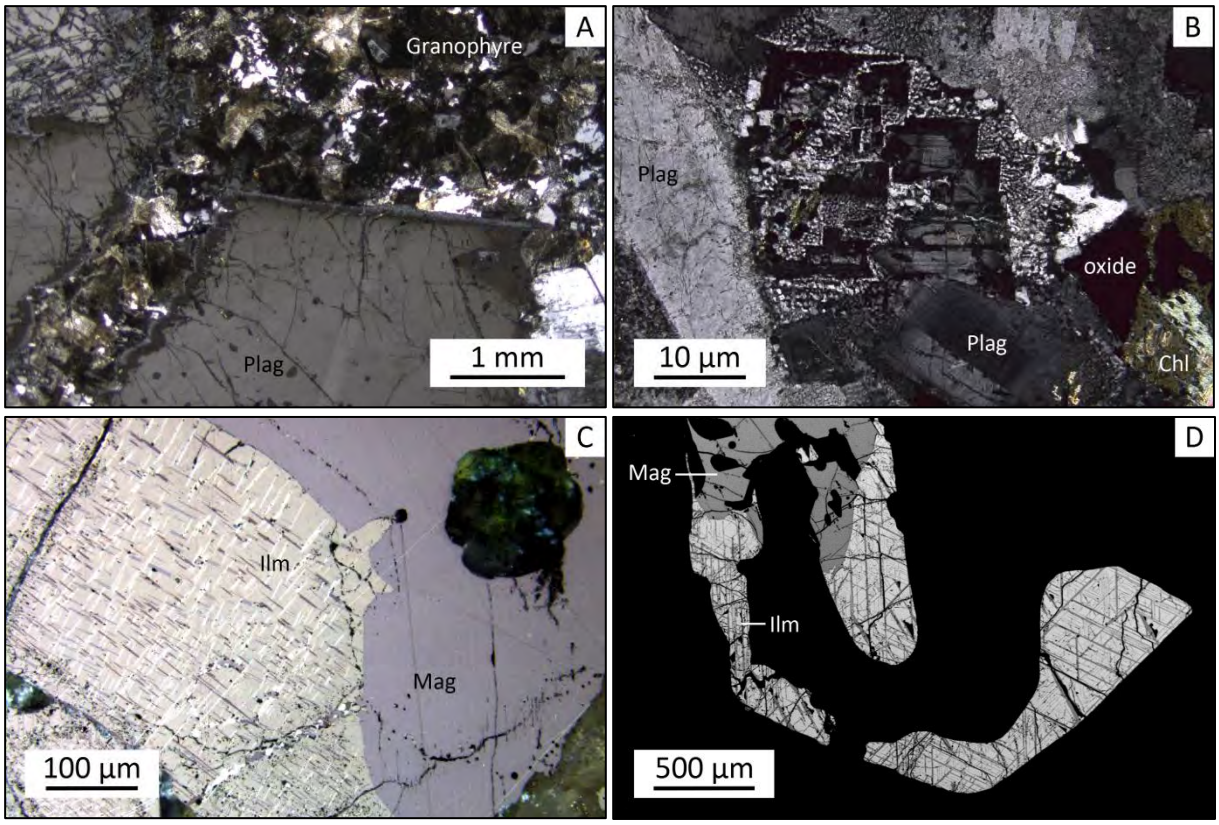

Figure 4-9: *Thin section photographs of textures formed by processes during and after crystallization. A) Intrusion of White Acid into gabbro pegmatite with continued plagioclase crystallization on a broken plagioclase crystal; B) Graphic intergrowth of orthoclase and quartz near albitized plagioclase; C) Exsolution lamellae of magnetite in ilmenite (wide lamellae) and ilmenite in magnetite (fine lamellae); D) EPMA photo of similar features as in C. Clear orientation parallel to crystal faces is visible.*

4.2.3 Rock chemistry

XRF analysis

XRF measurements on 14 samples resulted in bulk rock compositions for major elements and some minor elements. In the TAS diagram (Figure 4-10) the analyzed samples plot as two groups, one silica poor with picrobasalt to basalt composition and a silica rich with a composition equal to dacite or rhyolite. Exact numbers of major elements are given in Table 4-1. (For complete results including trace elements, see Appendix B)

The analyzed samples include two types of basalt from the host rock. One sample (L5.3) with no vesicles and just little alteration and another (K5) with abundant vesicles and pervasive alteration visible on hand specimen. Most major elements show just slight variations between these two samples. CaO and Al_2O_3 are slightly lower in the more pristine sample while Fe_2O_3, TiO_2 and K_2O are slightly higher. Only P_2O_5 is clearly depleted in sample K5. Representing the gabbroic magma chamber one *Ophitic Gabbro* (B55.3), one *Pegmatoidal Gabbro* (Q15) and one *Gabbro A* (Q9) were analyzed. Major elements are similar in all samples except for lower Fe_2O_3 and TiO_2 and higher SiO_2 in samples closer to the contact zone. Three samples from sheets and dykes representing intrusive phases 5, 6 and 7 were analyzed. Major elements in samples P1 and P2 (phase 6 and 7) are the

same yet B10.3 (Phase 5) includes more MgO but all other elements are slightly lower. Six samples from different acid rock phases cover the variability in these small volume intrusives. *Green Dykelet* (Q11), *White Acid* (Z4, Q27), *Aplite* (Br3) and *Granophyre* (GG-4, C1.4) were compared. SiO2 covers a trend from basaltic (Q11) to extremely silica rich rocks (Br3). Except for Q11 with values similar to a basaltic composition, all samples show a similar trend with Al_2O_3, Fe_2O_3, MgO, CaO and Na_2O decreasing with higher SiO_2 values. K_2O is higher in more silica rich rocks.

For minor elements samples show a similar bimodal distribution following the trend in TAS diagram and major elements.

Transitional metals (Zn, Cu, Ni, Co, Cr and V) show depletion with increasing silica content. For Cu and Ni silica rich samples with elevated values exist. For Zn and Cu average content decrease slightly from 80-135 ppm to 20-125 ppm in silica rich samples. Co and Cr drop from45-135 ppm to 4-25 ppm. Ni decreases slightly from 40-110 ppm to 7-80 ppm. V decreases from 310-590 ppm ito 10-90 ppm.

Incompatible LILE (Rb, Ba, Sr) are more enriched in silica rich rocks by several orders of magnitude. An exception is Sr without a clear trend but much higher variability in content from 140 to 415 ppm in acid samples. Basic samples have 280-380 ppm Sr. Rb increases from 5-22 ppm up to 50-130 ppm in silica rich samples. Ba rises from below 120 ppm to 260-400 ppm.

Incompatible HFSE (Nb, Zr, Hf, Y, Th, and REE: Sc, La) generally increase in abundance with higher silica contents. In average Nb and Y are about 1.5 times as abundant in samples with <63% of SiO_2. Hf is enriched by a factor of two, Zr by three, Th is enriched ten times and La about 25 times. Sc is the only element with a decrease to 0.2 times the abundance in silicate poor rocks.

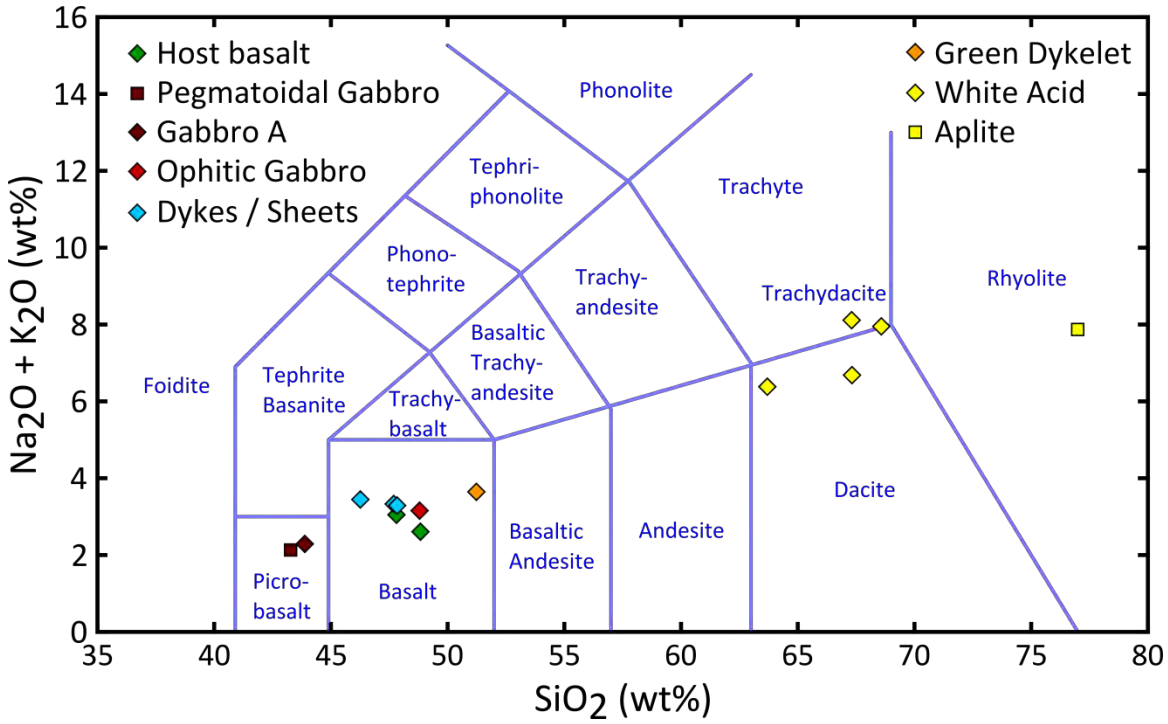

Figure 4-10: *Total alkali versus silica diagram (Le Maitre et al., 1989) (IUGS classification) of analyzed samples.*

Table 4-1: *Results of XRF analysis.*

Rock type	Pegmatite	Gabbro A	Ophitic Gabbro	Aphyric Phase 5	Phyric Phase6	Aphyric Phase 7	Green Acid
Sample	Q15	Q9	B55-3	B 10-3	P 1	P 3	Q 11
SiO_2 [wt%]	43.3	43.9	48.8	46.3	47.8	47.7	51.2
TiO_2	5.4	4.0	2.2	2.7	2.8	2.8	2.1
Al_2O_3	12.6	16.3	14.4	14.4	14.6	14.6	15.4
FeO_{tot}	17.0	14.6	10.8	13.1	13.3	13.4	9.2
MnO	0.21	0.15	0.15	0.18	0.19	0.19	0.14
MgO	7.1	5.6	6.6	7.3	5.5	5.5	5.7
CaO	12.5	13.0	13.3	10.4	11.0	11.0	11.3
Na_2O	1.9	2.1	2.3	2.9	2.8	2.8	3.3
K_2O	0.2	0.2	0.9	0.5	0.5	0.5	0.4
P_2O_5	0.05	0.06	0.20	0.26	0.29	0.29	0.46
Cr_2O_3	0.01	0.02	0.06	0.02	0.02	0.02	0.01
NiO	0.01	0.01	0.01	0.01	0.01	0.01	0.01
LOI	0.20	0.20	0.35	2.25	1.19	1.21	1.13
Total	100.44	100.08	100.05	100.33	100.15	100.01	100.24

Table 4-1 continued: *Results of bulk rock XRF analysis.*

Rock Type	White Acid	White Acid	White Acid	Grano-phyre	Aplite	Vesicular Basalt	Basalt
Sample	Z4	C1-4	Q 27	GG-4	Br3	K5	L5-3
SiO_2 [wt%]	63.7	68.6	67.3	67.3	77.0	48.8	47.8
TiO_2	1.1	0.7	0.8	0.9	0.2	3.0	3.9
Al_2O_3	15.3	14.2	14.4	13.8	10.9	14.0	13.2
FeO_{tot}	5.9	4.4	4.2	4.7	1.4	14.2	15.6
MnO	0.05	0.07	0.03	0.07	0.02	0.22	0.23
MgO	1.8	0.8	1.3	1.0	0.1	5.1	5.1
CaO	4.3	2.4	2.0	3.4	1.4	10.7	9.8
Na_2O	4.5	3.9	5.1	3.2	2.2	2.6	2.5
K_2O	1.9	4.1	3.0	3.5	5.7	0.0	0.6
P_2O_5	0.23	0.14	0.28	0.19	0.03	0.35	0.56
Cr_2O_3	0.00	0.00	0.00	0.00	0.00	0.01	0.01
NiO	0.00	0.00	0.01	0.00	0.00	0.01	0.01
LOI	1.36	0.71	1.31	1.99	1.06	0.94	0.85
Total	100.13	99.98	99.79	100.01	100.04	99.98	100.08

Uranium is with <3 ppm very rare and only enriched in very silica rich samples. Lead has a low abundance with the same range of 7-22 ppm in all samples.

XRD analysis

XRD measurements of 6 bulk rock powder samples (Q9, Q15, Q27, GG4, K2, and L5.3) resulted in 2θ angle plots with matched peaks shown in Appendix D. Each of these samples was also analyzed by XRF.

Primary minerals in all samples are consistent with optical microscopy. Plagioclase (albite, labradorite, anorthite), pyroxenes (augite diopside), ilmenite and magnetite are identified in gabbro and host basalt samples. Additional orthoclase and quartz are found in silica rich samples. Secondary minerals include chlorite in all samples. Actinolite occurrence is restricted to silica poor samples like gabbro and basalt. Andradite garnet is only found in host basalt. Epidote, titanite and pyrite are occasionally found in gabbro, pegmatite and basalt samples. Quartz is restricted to host basalt and a silica rich sample. Except for apparently common titanite no additional mineral missed by optical microscopy is found. Within glassy and fine grained basalt samples andradite and actinolite as high temperature hydrothermal minerals were identified in addition to the minerals from optical microscopy.

EPMA analysis

49 analyses on 23 crystals in three thin sections were performed. Due to analytical problems all measurements on one thin section resulted in total element mass of <25% for 10 major elements. One another analysis also resulted in <10% total element mass. These measurements are therefore neglected in further discussion. 31 analysis representing 14 minerals or zones in minerals remain. For each mineral an average of two to three conducted analysis is used and given as oxide mass percent normalized to 100% (Table 4-2).

Measurements of magnetite and ilmenite confirmed expected compositions indicating magnetite to contain up to 5.9 oxide mass% of Ti. Analyzed augite has xMg of ~75%.

Analysis of vein forming minerals reveals composition matching a Fe-Mg chlorite and titanite in one vein. Titanite is also found as exsolution lamellae in augite within pegmatite.

Within *White Acid* intruding into *Pegmatoidal Gabbro* plagioclase was analyzed. Comparison included the center and a 5 µm wide zoned rim of plagioclase in *Pegmatoidal Gabbro* and a small plagioclase crystal in *White Acid*. Anorthite content within of the three analyzed samples decreases from 85.8% for the core to 73.3% for the rim and to 54.3% in the younger rock (Fig 4-9 A). K_2O shows increase for the three analyzed zones with time of formation. Evolution of White Acid and plagioclase growth continued during flow along fractures in *Gabbro A* and *Pegmatoidal Gabbro*. Graphic exsolution and myrmekite textures in *White Acid* are alkali feldspars with 67.9%-76.9% orthoclase intergrown with quartz.

Table 4-2: *Results of EPMA analysis on 14 minerals or mineral zones. The measurement for mineral 14.03 lead to two different compositons, labelled as "a" and "b". All measured points were above 85% for 8 major elements (El.% EPMA) except 14.02 which was about 49 oxide % before*

Point	12.01	12.02	12.03	12.04	14.01	14.02	14.03a	14.03b	14.40	14.05	14.06	14.07	14.08	14.09	14.10
Mineral	Mag lam.	Ilm host	Chl	Tt	Ilm	Mag	Aug	Tt	Aug	Plag rim	Plag center	Plag small	Myrm	Myrm	Myrm
Proportion	xTi = 5.9	xTi = 46.0	xMg = 57.7	xTii= 91.4	xTi = 45.1	xTi = 1.2	xMg = 74.5	Ti = 94.9	xMg = 74.4	An% = 85.8	An% = 73.3	An% = 54.3	Orth% = 74.9	Orth% = 67.9	Orth% = 76.9
SiO_2	4.3	6.4	32.6	32.7	0.01	0.00	46.3	32.5	46.6	59.7	65.1	69.3	75.6	83.0	80.0
Na_2O	0.01	0.06	0.01	0.04	0.02	0.01	0.34	0.02	0.27	5.3	7.7	9.9	3.0	2.8	2.3
CaO	4.5	5.6	0.32	33.6	0.01	0.01	22.0	34.3	22.1	16.0	10.5	5.91	0.24	0.14	0.12
K_2O	0.02	0.02	0.02	0.02	0.01	0.01	0.01	0.02	0.01	0.18	0.40	0.30	9.0	6.0	7.7
FeO_{tot}	84.5	46.4	23.7	2.4	53.9	98.1	7.4	1.6	7.4	0.70	0.40	0.28	0.15	0.14	0.16
Al_2O_3	1.2	0.49	10.6	3.8	0.09	0.37	1.0	1.2	1.1	17.9	15.8	14.3	11.9	7.8	9.6
MgO	0.13	0.21	32.3	1.9	0.34	0.14	21.7	0.26	21.5	0.14	0.07	0.03	0.00	0.00	0.03
Cr_2O_3	0.04	0.03	0.01	0.01	0.02	0.09	0.00	0.01	0.01	0.00	0.00	0.00	0.01	0.01	0.00
TiO_2	5.3	39.6	0.26	25.6	44.3	1.2	0.91	30.0	0.73	0.10	0.02	0.03	0.02	0.07	0.05
Mn	0.09	1.2	0.11	0.03	1.3	0.10	0.27	0.01	0.22	0.00	0.01	0.01	0.00	0.01	0.01
Total:	100.0	100.0	100.0	100.0	100.0	100.0	100.0	100.0	100.0	100.0	100.0	100.0	100.0	100.0	100.0
El % EPMA	90.85	97.47	86.08	92.13	99.45	48.92	95.79	95.63	96.47	89.50	89.12	90.47	88.35	88.68	89.25

4.3 Hydrothermal features

Hydrothermal features include pervasive alteration and veining in all rock types. However it is possible to indicate a difference of alteration depending on rock type and location. Alteration is always more pervasive in mafic rock types and along zones of structural weakness or enhanced porosity.

4.3.1 Mineralogy and alteration

Secondary minerals

Actinolite

Vein forming and vesicle filling mineral. Abundant within gabbro but more rare in host basalt samples. Length of crystals is usually <50 µm. As alteration mineral it is found as extensive replacement of pyroxenes (Figure 4-11 C) and rare magmatic amphibole. Around magmatic oxides rims of actinolite fibers are found but extensive replacement is not observed (Figure 4-11 E, F).

Quartz

Idiomorphic and xenomorphic hydrothermal quartz is abundant in veins and vesicles across all observed gabbro outcrops as well as the surrounding host basalt. It is found as intergrowth together with garnet, epidote, chlorite, calcite and zeolite. Crystals grow up to 20 mm long and 5 mm wide. Fluid inclusions in hydrothermal quartz are described below.

Garnet

Hydrothermal garnet is only found in veins as well as vesicles within the host basalt. Occurrence together with quartz, epidote and chlorite is common while calcite and zeolite are rare. Biggest crystals have a diameter of about 1 mm. Fluid inclusions within hydrothermal garnet are described below.

Epidote

Epidote occurs in veins, vesicles as well as due to hydrothermal alteration replacing plagioclase, amphibole and basaltic glass. Occurrence in the same vesicles and veins as quartz, chlorite and calcite is a common feature but with actinolite, garnet and zeolite it is found more rarely.

Chlorite

Chlorite is found in veins, vesicles as well as due to hydrothermal alteration replacing pyroxene, amphibole, basaltic glass and secondary actinolite in veins. Occurrence together with all other secondary minerals is observed as it is common in all analyzed samples and occurs in at least three variations. In vesicles from *Kraksgil* two types can be distinguished with optical microscopy due to color variation from brown to green in polarized light, corresponding to bigger crystal-size for green chlorite (Figure 4-11 M). Interference colors of these chlorites also change from brownish to anomalous blue. In sections of *medium gabbro* and *gabbro pegmatite*, <20 µm clusters of radially grown chlorite are found where under cross polarized light the inner zone tends to have an anomalous blue-purplish color, while rim zone is of anomalous blue interference color (Figure 4-11 A). Pervasive replacement chlorite is found in intergranular space of orthocumulate, where fine grained zone in rocks (pyroxene, glass) are replaced (Figure 4-11 B, D). XRD measurements indicated chlorite to be clinochlore.

Titanite

Titanite is found rarely as primary magmatic mineral in evolved rocks. It is very abundant in

one chlorite vein analyzed by XRD, as exsolution lamellae in augite analyzed by EPMA and within a small vein associated with chlorite and pyrite in the reaction rim around ilmenite-magnetite crystals. Crystal-size in these veins is <5 µm. In optical microscopy very small crystals with a typical titanite crystal shape are found while it was not possible to confirm titanite finding by EPMA measurements.

Calcite

Calcite is a common vesicle and vein filling mineral forming in mm-cm wide veins and vesicles within host basalt as well as in vesicles within dykes and sheets. Veins with predominant calcite infill often occur as multiple fine (<mm) veins which branch from bigger (<cm) veins and are oriented roughly parallel. Calcite forming after other hydrothermal minerals like quartz, zeolite, chlorite and pyrite is common however with garnet, epidote and actinolite it is rare. In open spaces calcite crystals often show signs of corrosion or re-solution which is most likely due to weathering as in thin section it looks more pristine. Calcite as secondary replacement mineral is observed plagioclase associated with albitization and in completely replaced pyroxene (Figure 4-11 C).

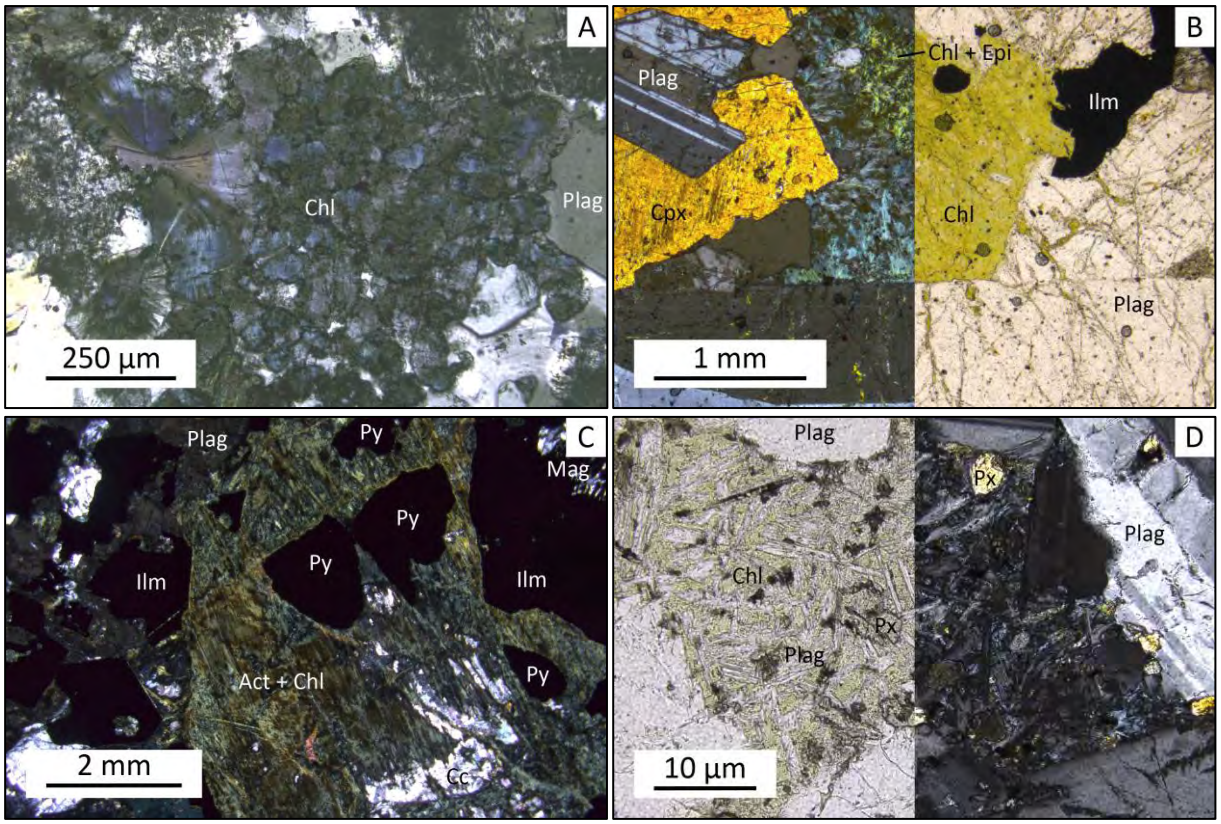

Figure 4-11: *Secondary mineralogy in veins, vesicles and as replacement of primary magmatic minerals. (Figures B, D, I and M are partly with crossed polarizers .) A) Chlorite replacing glass or small crystals of White Acid; B) Chlorite filling intergranular space and microcracks in plagioclase within gabbro; C) Pyroxene in pegmatite near a Tt-Chl vein. Completely replaced by actinolite, calcite and pyrite. D) Fine plagioclase laths in intergranular space surrounded by chlorite replacing glass in orthocumulate gabbro; E) White acid with granophyre texture in Pegmatoidal Gabbro. Intact dendritic ilmenite and minor magnetite, partly replaced by actinolite; Further description see next page.*

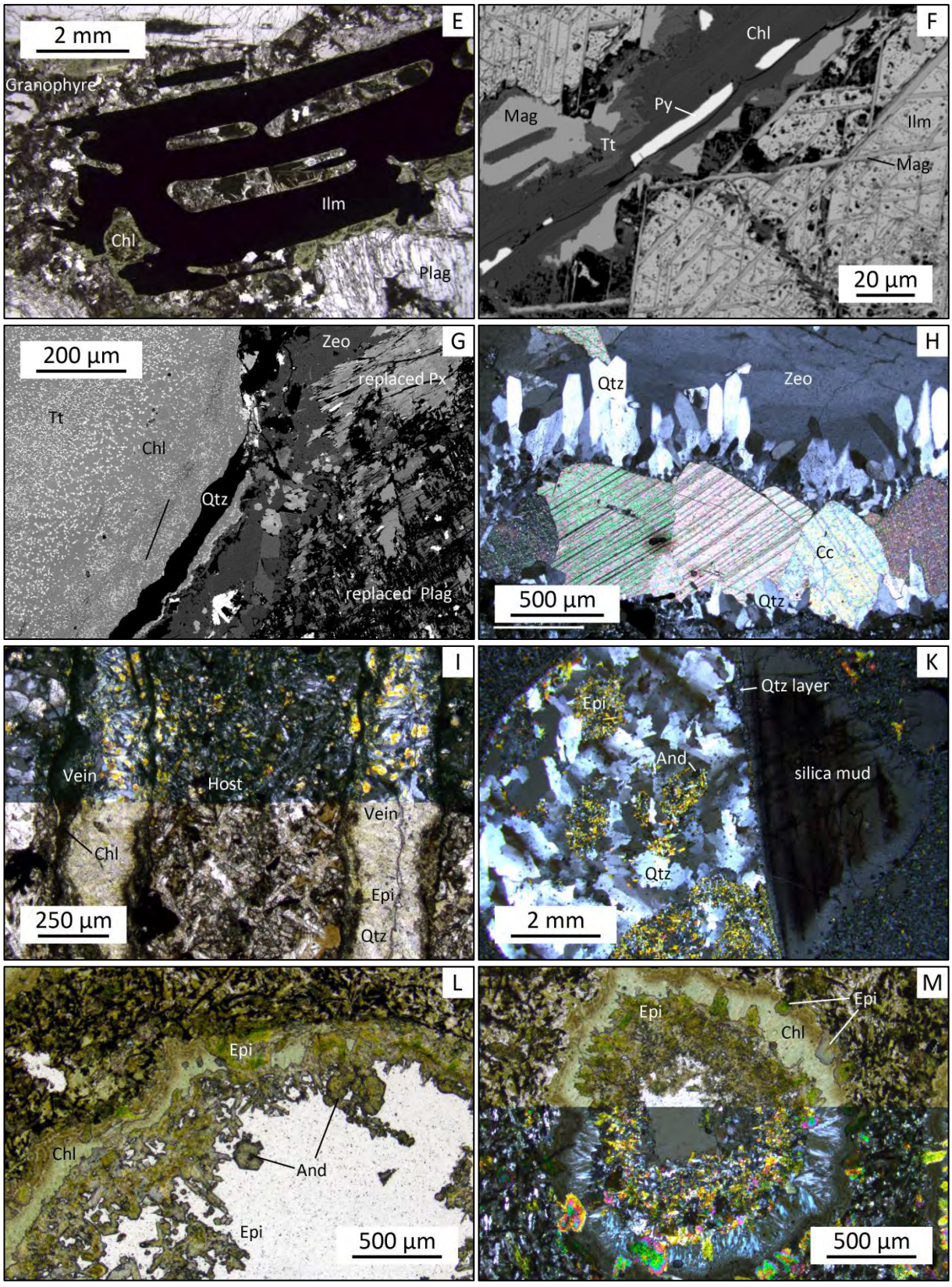

Figure 4-11 continued: *F) Backscatter EPMA compositional image, Ilm Mag partly resolved along a Tt Chl py vein; G) Backscatter EPMA compositional image, Tt-Chl vein rim; H) Vein with Qtz-CC-Qtz-Zeo infill sequence; I) Two Chl-Epi veins with halo; K) Vesicle with clay-silica-Chl-Epi-Zeo infill sequence; L) Vesicle rim with Epi-Chl-Chl-Epi-Gt infill; M) Vesicle infill sequence.*

Pyrite

Hydrothermal pyrite occurs in host rocks as well as aphyric dikes (phase 5 and later) together with calcite. It is relatively rare and occurs in vesicles and veinlets (Figure 4-11 F). Rarely also epidote and zeolite occur in the same zone but other secondary minerals are not found. In dykes and host basalt pyrite is found sparsely spread in the matrix. As replacement mineral pyrite is found in completely replaced pyroxene (Figure 4-11 C) and rare amphibole and occasionally after Fe-oxides in *Gabbro A* and *Gabbro B* (Figure 4-12).

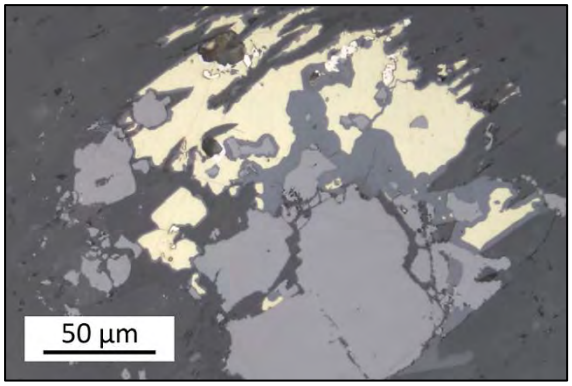

Figure 4-12: *Sulfides and Fe-hydroxides replacing ilmenite.*

Chalcopyrite

Observed as secondary mineral in clusters together with pyrite replacing oxides. It is usually coated with Fe-hydroxides (Figure 4-12).

Zeolite

Zeolites are common minerals forming in at least two types of veins. Within gabbro at outcrop "A", thin ≤mm veins with white, fine grained zeolites are abundant. These veins have mostly parallel vein walls and show intense branching (Figure 4-13 E). Another type of zeolite veins is abundant in the basaltic host rocks and dykes within but close to the contact. Here zeolite occurs in multiple fine veins (<2 mm) which branch from wider veins (<2 cm) and follow these vein. (Figure 4-11 G and Figure 4-13 E) Within dykes, veins preferentially follow dyke margins and also form networks of fractures across the dyke. These veins are not completely filled and zeolite may grow idiomorphic into the free space. Zeolite associated with other hydrothermal minerals however usually occurs as vein filling material and rarely shows idiomorphic growth. One exception is outcrop K at *Kraksgil*, where few big (<5mm) zeolite crystals grow within open vesicles and veins.

4.3.2 Veins and Vesicles

Mineral assemblages in veins match vesicle filling sequence. Well-preserved veins are abundant in gabbro, sheets and dykes, while in basalts minerals in vesicles are more common. Vein density based on analysis with ArcGIS measuring total length of veins per square meter but neglecting vein width. It is $> 6.3 \frac{m}{m^2}$ for hydrothermal veins at outcrop A (Location shown in Appendix G). This is a minimum value as certainly veins were missed during mapping and closely spaced multiple veins of the same type were drawn as one vein. The vein map of outcrop A in *Gabbro A* is shown in Appendix F.

Actinolite

Actinolite veins are up to 5 mm wide but mostly <1 mm with straight vein-walls (Figure 4-13 A). Length of veins is usually few dm but several veinlets may be aligned forming several m long structures. Veins are straight and no branching is observed. Haloes are represented by extensive replacement of pyroxene crystals next to veins. Vein abundance in gabbro is relatively high, veins in dykes and sheets are more rare and smaller. In basalt actinolite veins are very rare. Orientation of veins on outcrop A is N-S with slight

variations (~350°-015° strike). Vein density on outcrop A is $> 0.67 \frac{m}{m^2}$ but clearly too low due to the small size. Veins in mafic sheets and dykes are oriented parallel to the host and follow the intrusive contact along silicate intrusives (Figure 4-14).

Quartz

Rare vein type at outcrop A. Width is <8 mm with straight and parallel vein walls. Fine idiomorphic quartz (<mm) grows from vein walls (Figure 4-13 B, C). Orientation is N-S for veinlets crosscutting only actinolite veinlets. Fine quartz veinlets crosscutting epidote veins are NW-SE oriented. Chlorite veining will later reuse quartz veinlets.

Clinochlore-Titanite-(Pyrite)

Clinochlore veins with contemporal titanite and possibly later pyrite are <15 mm wide and have irregular vein-walls. Small fragments of wall rock can be enclosed within the vein. Haloes are <5 mm wide and show characteristic disintegration of ilmenite while magnetite is more stable (Figure 4-11 F, G). Pyrite occurrence is restricted to presence of Fe-oxides along the vein walls. Vein occurrence is restricted to gabbro outcrops southwest of *Geitafellsbjörg* Clinochlore may replace earlier actinolite. Chlorite vein density on outcrop A is $> 0.15 \frac{m}{m^2}$. Orientation is following existing structures when replacing actinolite veins.

Epidote-(Quartz)-(Calcite)

Epidote veins are <8 mm wide and often occur as multiple sub-parallel and branching veins. Vein walls are irregular and <80 mm wide haloes with elevated epidote abundance and albitization of plagioclase are prevalent (Figure 4-13 D). Quartz is occasionally and calcite regularly found in the center of these veins. Veins are abundant in gabbros and mostly oriented E-W (usually 085°-095° strike and few members with ~045° and ~130°). Vein density on outcrop A is $> 2.3 \frac{m}{m^2}$. Similar veins are found in host basalt and *Porphyric Dolerite* dykes in a distance of several hundred meters from the contact. Veins are accompanied by pervasive alteration haloes. Orientation is generally E-W but with abundant conjugate fractures.

(Clay)-Chlorite-Epidote-(Andradite)-(Quartz)-(Calcite)-(Zeolite)

Irregular, often strongly interconnected vein type similar to "Epidote-(Quartz)-(Calcite)" veins. Apparently this vein type covers a much wider range of hydrothermal activity compared to other veins which only contain parts of the hydrothermal mineral sequence. This vein type is found at only one outcrop in highly vesicular basalt or heavily fractured dolerites assumed to be more than 500 m away from the contact at *Kraksgil* (Figure 4-13 F and Fig 4-11 I, K, L, M). A nearly complete sequence of hydrothermal minerals formed as this vein remained open for fluid circulation during elevated hydrothermal activity.

Vein width is usually <30 mm but where bigger squeezed vesicles are part of the vein it may be wider. Haloes are present as extensive replacement of basalt by chlorite and epidote as well as a bleaching of the wall rock due to albitization . Clay is found rarely in subvertical veins which possibly represent older fractures formed during cooling of the basalt flow. Chlorite may cover walls of veins and vesicles in two different compositions. Epidote is partly growing together with chlorite but as slightly smaller crystals also after chlorite. Andradite, idiomorphic quartz, calcite and zeolites form in this order and are mostly restricted to open zones, where veins still include open space.

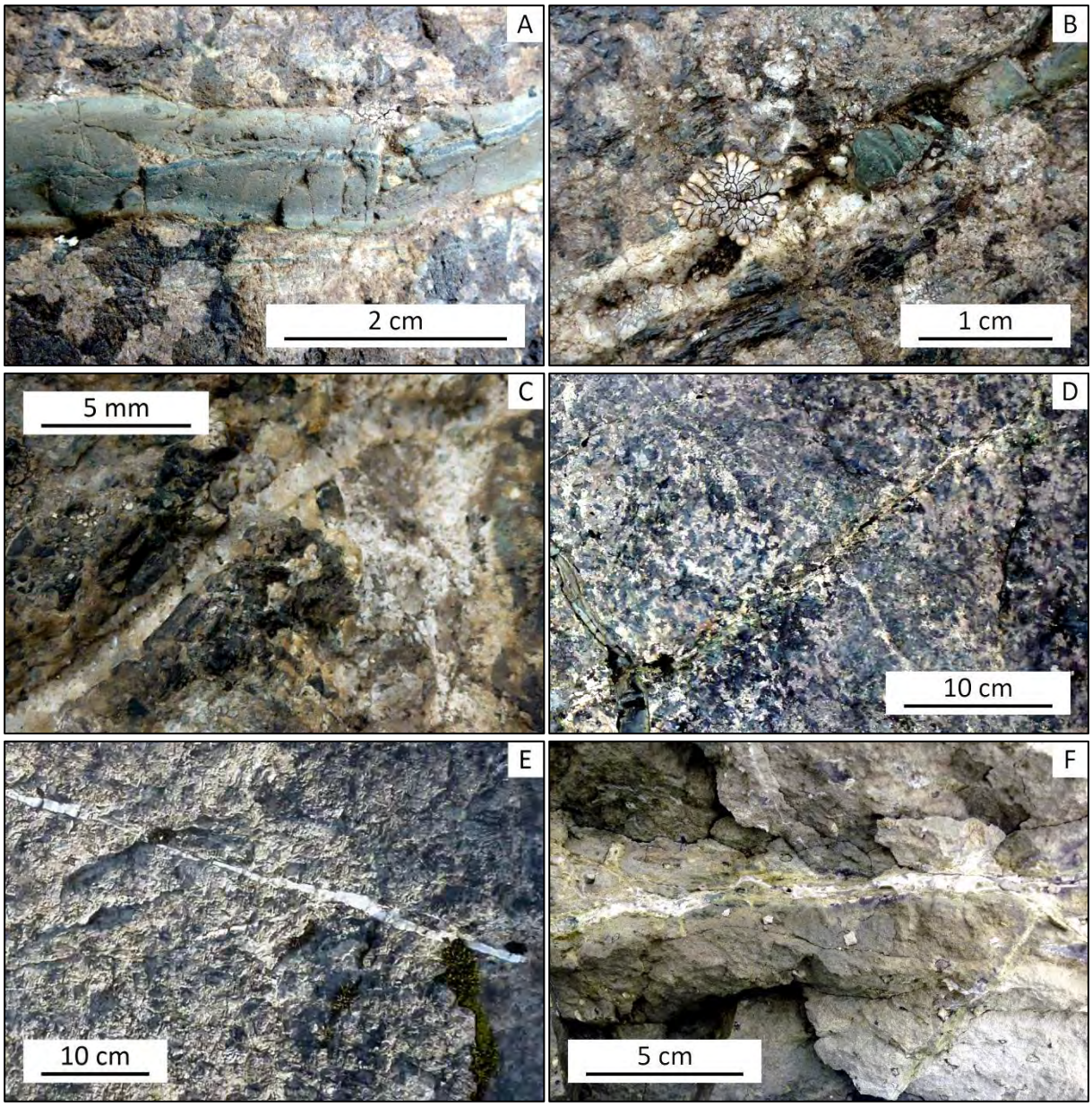

Figure 4-13: *Hydrothermal veins at Geitafell. A) Actinolite vein following a basalt vein whose chilled margins were chloritized; B) End of a basalt vein and continuation as a quartz vein with later chlorit formation in its center; C) Quartz vein and halo of an epidote veinlet; D) Epidote-(calcite vein) with halo crossing a pegmatite vein; E) Thin zeolite vein; F) Chlorite-epidote-(garnet)-quartz vein at Kraksgil;*

Vesicles with the same infill sequence are observed nearby. Small vesicles tend to be completely filled by chlorite, hence completeness of the infill sequence depends on size of vesicles. Chlorite garnet assemblage is also found in vesicles in *Hoffellsdalur*, where measurements of physical rock properties were conducted within garnet alteration zone (Zürcher, 2014).

Fine Quartz

Very thin quartz veins <0.5 mm connecting vesicles in *Aplite*. Vein walls are parallel, partly cutting plagioclase crystals. Haloes are not cleary visible but epidote and albitization is

observed. Small vesicles (<1.5 mm) in *Aplite* have the same type of fine quartz crystal infill. Crosscutting with other veins is only observed by younger zeolite vein.

Quartz-Calcite-Quartz-(Zeolite)

Well preserved <4 mm wide veins with straight and parallel vein walls. Haloes are weak and < 1 cm wide and are characterized by calcite within the host rock. Infill sequence is clearly related to width. Wider veins include a more complete sequence with more than one fluid pulse leading to quartz precipitation (Figure 4-11 H). Best preserved veins are found in dykes and sheets but similar veins are also found in gabbro (Figure 4-13 C) and basalt.

(Pyrite)-Calcite (H)

Calcite veins are <3 mm wide and are usually thinner if pyrite is present. Vein walls are straight and sub-parallel. Haloes are not observed and the occurrence is restricted to dolerite and basalt. Vesicles with pyrite-calcite infill are usually found in the vicinity of these veins.

Calcite-Zeolite (I)

Huge vesicles (>5cm) in basalt are filled with calcite and zeolite and represent relicts of regional calcite-zeolite alteration. Veins formed after magmatic activity dominantly follow dolerite sheets and dykes. Veins are < 15 mm wide but with many sub-parallel and branching thinner veins. Vein walls are irregular and small fragments of host rock may be included in the vein. Abundance is high in all rock types including intrusive phases until phase 12.

Zeolite (K)

<3 mm wide zeolite veins appear very irregular, have no haloes but are very abundant all over the field area. Vein density is $> 1.6 \frac{m}{m^2}$ at outcrop A. majority of veins has an E-W orientation but often a bunch of fine veinlets frazzles radially from one point (~090°-130° strike and fewm members with completely different strike). Many veins do not show any systematics in orientation and are controlled by local stress along and within existing structures like dolerite sheets and dykes during regional alteration.

4.3.3 Alteration

Alteration not apparently related to veins affects mainly mafic minerals, zones of structural weakness, high porosity and rocks with small crystal-size or glass. This includes *Pegmatoidal Gabbro* dykelets hosting later silica rich dykelets and contacts between brecciated gabbro and matrix (Figure 4-14). Preexisting fractures controlled by dykes and vesicle bearing silica rich intrusive and vesicular basaltic host rocks as associated with fine quartz veins. Combination of these effects facilitates pervasive alteration. Clinopyroxene crystals in gabbro and *Pegmatoidal Gabbro* closely associated with actinolite veins or vesicular dykelets of silica rich rocks represent the most completely replaced zones.

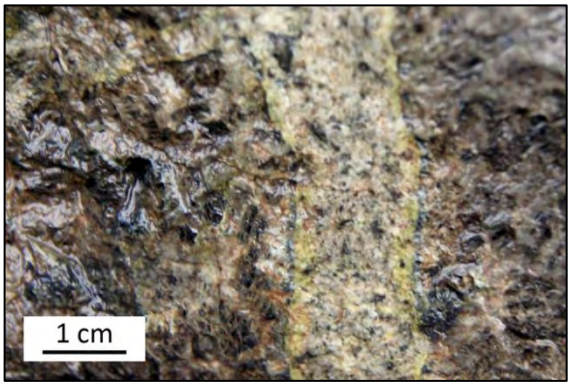

Figure 4-14: *Actionlite veins with epidote halo along a contact of White Acid in brecciated Gabbro A.*

Coarse, rock forming minerals (>5mm) tend to be affected by alteration only along rims or

cracks. Plagioclase may be extensively affected by albitization along microscopic cracks. Replacement by chlorite-epidote-calcite is restricted to plagioclase rims, except for crystals in xenoliths and porphyric crystals in vesicular host rock. Nearly complete clinopyroxene pseudomorphs are found near actinolite veins and are represented by actinolite-chlorite-(pyrite-calcite-Fe-hydroxides) mineralization (Figure 4-11 C). Extensive replacement is also found in coarse (>15 mm) pyroxene crystals entrapped by silicic magma. Pyroxene crystals tend to be replaced along crystal margins and fine cracks. Cracks may form due to exsolution of titanite in clinopyroxene lamellae. Magnetite and ilmenite in gabbro are affected by the alteration only at crystal rims. Both are surrounded by chlorite. Ilmenite is clearly less stable (Figure 4-11 F). Alteration affecting oxides clearly starts after formation of exsolution lamellae of magnetite within ilmenite.

Comparison of XRF results from host basalt samples with different grade of alteration but similar primary mineralogy reveals nearly constant values for most major elements. Only TiO_2 is about 25% lower in a strongly altered basalt sample. This relevant difference is only explained by much lower primary oxide content in the sample. CaO is enriched by about 10% and K_2O is depleted to less than 1% but is a minor element (<1 wt%). Trace elements show similar patterns. Transitional metals are roughly constant (within 10% of a sample with low alteration) except Cr (30% increase) and Zn (20% decrease). HFSE (high field strength elements) and REE (rare earth elements) show a decrease of 10-25% LILE (large ion lithophile elements) decrease Rb by 70%, Sr by 20% and Ba is not present in the hydrothermally altered sample.

4.3.4 Time Relations

Veins include variable mineralogy representing a sequence of minerals precipitating. Within basaltic host rock the earliest secondary minerals in vesicles are clay and amorphous silica as pre-hydrothermal infill (Friðleifsson, 1983) (Figure 4-13 K). These are followed by epidote and chlorite coating vesicle walls. A compositional change of chlorite is observed as interference color change and is accompagned by epidote disappearance in *Kraksgil*. Epidote reappears after chlorite (Figure 4-11 L, M) and its growth overlaps whith andradite garnet and quartz. Andradite often grows on fine epidote or chlorite crystals. All these minerals are included within quartz crystals (Figure 4-15 A, B). Most quartz crystals however form after garnet and epidote. Remaining open space is subsequently filled by calcite and at least two types of zeolite (Laumontite, Stilbite). If free space remains it is often due to absence of calcite and zeolites.

Vesicles within *Porphyry Dolerite* dykes cross-cutting host rock contain the same infill sequence as vesicles in basalt starting after brown chlorite. Garnet is absent and quartz less idiomorphic due to restricted space.

Sequence of hydrothermal veins forming at outcrop A within the gabbros begins with actinolite alteration representing the highest alteration temperature based on estimated temperature from Table 1-1. It forms after intrusion of *Aplite* sheets and fluid partly flows along these intrusive contacts (Figure 4-14). It is followed by quartz veinlets with changing strike towards E-W representing cooler conditions during mineralization. A change in stress is also accompanied by basalt dykelets intruding into gabbro at temperatures below basalt solidus as these develop chilled margins.

In and along those veins, local reheating allows further actinolite veinlets to form. However, most pervasive hydrothermal alteration is restricted to epidote veins crosscutting earlier structures and only locally following pre-existing structures. Lower temperature alteration represented by chlorite replacing higher temperature actinolite forming microscopic veinlets and in existing open space is observed mainly on thin section scale and by greenish appearance of altered rocks. Finally regional calcite to zeolite alteration forms fresh veins rarely following preexisting structures.

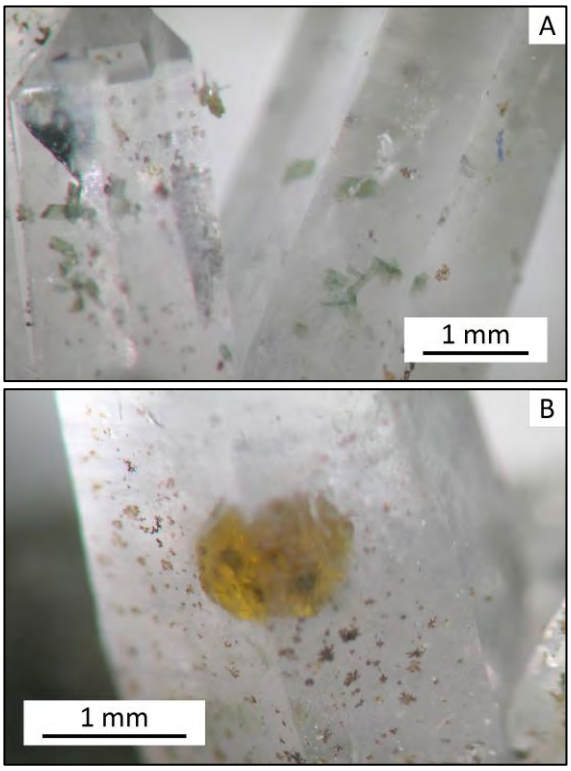

Figure 4-15: *Hydrothermal mineral intergrowth of quartz enclosing epidote (A) and garnet (B).*

4.4 Fluid Inclusions

Fluid inclusion thermometry was done on 79 fluid inclusions belonging to 26 assemblages within different crystals. The inclusion bearing crystals were sampled at two locations within the fossil hydrothermal system. Assemblages in seven quartz crystals of about 2 mm width from vesicles within the matrix of the *Intrusive Breccia* from outcrop B55 (Location shown in Appendix G) were analyzed as well as six quartz crystals of 4-8 mm length from veins and vesicles at *Kraksgil*. Garnet crystals all are from *Kraksgil* and did show intergrowth with quartz from the same location (Section 4.3.2 and Figure 4-15).

4.4.1 Petrography

Fluid inclusions in quartz form clear assemblages with negative crystal shape as well as inclusions with irregular shapes and necking down features. Vapor to liquid proportions (V:L ratio) range from nearly pure vapor to dense liquid inclusions. Size of inclusions is about 2-270 µm yet most inclusions are 10-20 µm wide. Abundance of inclusions is highly variable from rare assemblages and inclusions in idiomorphic quartz and garnet at *Kraksgil* to abundant growth zones and secondary inclusions at *Geitafellsgil*. Only one very small example of a brine inclusion with a halite crystal was discovered, which showed evidence of possible necking down were apparent.

There are several types of fluid inclusions found at *Geitafell* with a number of subtypes. The classification of assemblages is based on estimated density (volumetric vapor to liquid ratio in inclusions), shape (negative crystal shape, irregular shape), occurrence in growth zones and host mineral. Nomenclature of fluid inclusion types starts with G for garnet hosted and Q for quartz hosted inclusions. It is followed by V for vapor and the estimated volumetric percentage of vapor). A second G is included after V for inclusions from *Geitafellsgil*. For distinction of inclusions with similar vapor volume the letter i was added for inclusions with an irregular shape.

Fluid inclusions in garnet

Vapor rich inclusions are spatially associated with mineral inclusions. Two elongated inclusions (GV90) at the tip of fibrous mineral inclusions in sample FL01_C1 are 15-20 µm long and have a vapor to liquid ratio (V:L) of 2:1 and 9:1. Rectangular vapor rich inclusions (GV66) squeezed in between mineral inclusions 10-20 µm long and have a V:L ratio of about 2:1. Similar inclusions are found in several garnet crystals.

Rare, nearly rectangular inclusions (GV20) with negative crystal shape of garnet are 5-8 µm long and have an estimated V:L ratio of about 1:5.

Aqueous inclusions in garnet include irregularly shaped inclusions (GV11) which are about 10 µm wide and have a V:L ratio of 1:8. These inclusions are rare in sample FL01_C1. Two rectangular inclusions (GV08) next to mineral inclusions in FL01_C2 are 10 µm long oriented along the crystal lattice and have a V:L ratio of about 1:11.

Fluid inclusions in quartz (*Kraksgil*)

Elongated, rectangular, aqueous inclusions (QV10) are 5-50 µm long with a V:L ratio of about 1:9. The orientation of these primary inclusions is perpendicular to the orientation of growth zones.

Rectangular to nearly cubic inclusions (QV25) with negative crystal shape are < 20 µm wide and have a V:L ratio of about 1:3. The orientation of elongated members of this inclusion type is elongated parallel to the assemblage. Inclusions with similar shape and V:L ratio are described as QV25l and QV25h based on two different ranges of homogenization temperatures (T_{hom}, see section 4.4.3)

Irregular inclusions with negative crystal shape (QV16) are <25 µm long and have a V:L ratio of 1:4 to 1:6 and are pseudo secondary. Elongated inclusions are elongated parallel to the assemblage.

Irregular inclusions (QV20) within a growth zone including epidote crystals are 5-80 µm wide and have a V:L ratio of 1:4. Similar inclusions with necking down are found outside of the growth zone with similar V:L ratio of 1:2 to1:6. These 5-100 µm wide inclusions are of secondary origin as some assemblages crosscut primary assemblages and not considered for further measurements.

Irregular inclusions (QV12) with low relief and partly negative crystal shape have a V:L ratio of 1:5 to 1:10. These inclusions are oriented perpendicular to the assumed crystal surface during growth. Inclusions with the same V:L ratio and appearance are found in apparently younger zones of the crystal indicating a pseudo secondary or secondary origin.

Irregularly shaped vapor rich inclusions (QV90) are <25 µm wide and contain little amounts of fluid in pointy edges. Vapor inclusions are found as secondary and possibly pseudo secondary inclusion assemblages. A subtype of these vapor inclusions with occasional negative crystal shape consists of nearly pure vapor and also forms secondary inclusions.

Vapor inclusions (QV95) are <20 µm wide and often have negative crystal shape. Vapor inclusions are found as secondary and possibly pseudo secondary inclusion assemblages.

Fluid inclusions in quartz (*Geitafellsgil*)

Rectangular and irregular inclusions (QVG25) with negative crystal shape are 5-20 µm long and have a V:L ratio of about 1:3. The

orientation of these primary inclusions within growth zones is perpendicular to growth zones with the irregular inclusions preferably in areas with a kink in the growth zone.

Rectangular inclusions (QVG20) with negative crystal shape are 5-50 µm wide and have a V:L ratio of 1:4. These primary inclusions form in extensive multiple growth zones parallel to crystal surfaces. Irregular inclusions (QVG20i) with occasional necking down have the same V:L ratio of 1:4. They are <10 µm wide and are of secondary or pseudo secondary origin.

Irregular inclusions (QVG15) with mostly negative crystal shape are <20 µm wide and have a V:L ratio of about 1:6. Pseudo-secondary inclusion assemblages are restricted to the inner zone of quartz crystals.

Vapor rich inclusions (QVG90) are <10 µm wide and of secondary or pseudo secondary origin.

4.4.2 Time Relations

As indicated in 4.4.1 there are primary, pseudo secondary and secondary fluid inclusions. Appearance, restricted occurrence and growth zones provide clear evidence for relative age of some assemblages. However crosscutting relationships of pseudo-secondary and secondary with earlier inclusions are not always clear. Spatial and temporal relations of fluid inclusions in quartz are shown in Figure 16.

Within garnet, vapor-rich inclusions may formed earlier than aqueous inclusions as they are associated with mineral inclusions in the center of garnet crystals. GV20 inclusions are the earliest aqueous inclusions observed, but clear relative ages could not be determined as the few inclusions are too widespread over several garnet crystals.

For fluid inclusions in a single quartz crystal from *Kraksgil*, the oldest possibly primary inclusions in a growth zone are QV20 coexisting with epidote mineral inclusions. Subsequently type QV25h homogenizes as first trustworthy inclusion assemblage in a sequence of assemblages with decreasing homogenization temperatures. These are followed by primary aqueous inclusions QV12. Subsequently pseudo secondary type QV16 and primary QV25l (Figure 4-17 I) form after another with a small spatial gap. During the latest stage of quartz crystal growth primary QV10 inclusions form, which are restricted to few zones near the surface of the crystal. They are followed by secondary aqueous inclusions QV30, and vapor inclusions QV90 are found in all quartz crystals. Exact timing of QV30 and QV 90 is not clear due to the presence of both as loosely confined secondary inclusion trails. However both of them occur in zones assumed to have formed later than QV10 due to their spatial relation. As vapor rich inclusions show no clear secondary trails but often pseudo secondary trails they are considered as older.

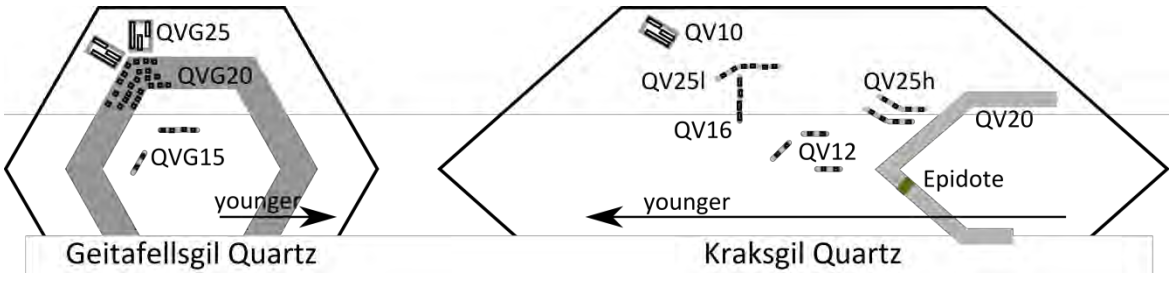

Figure 4-16: *Temporal and spatial sequence of fluid inclusion assemblages for quartz.*

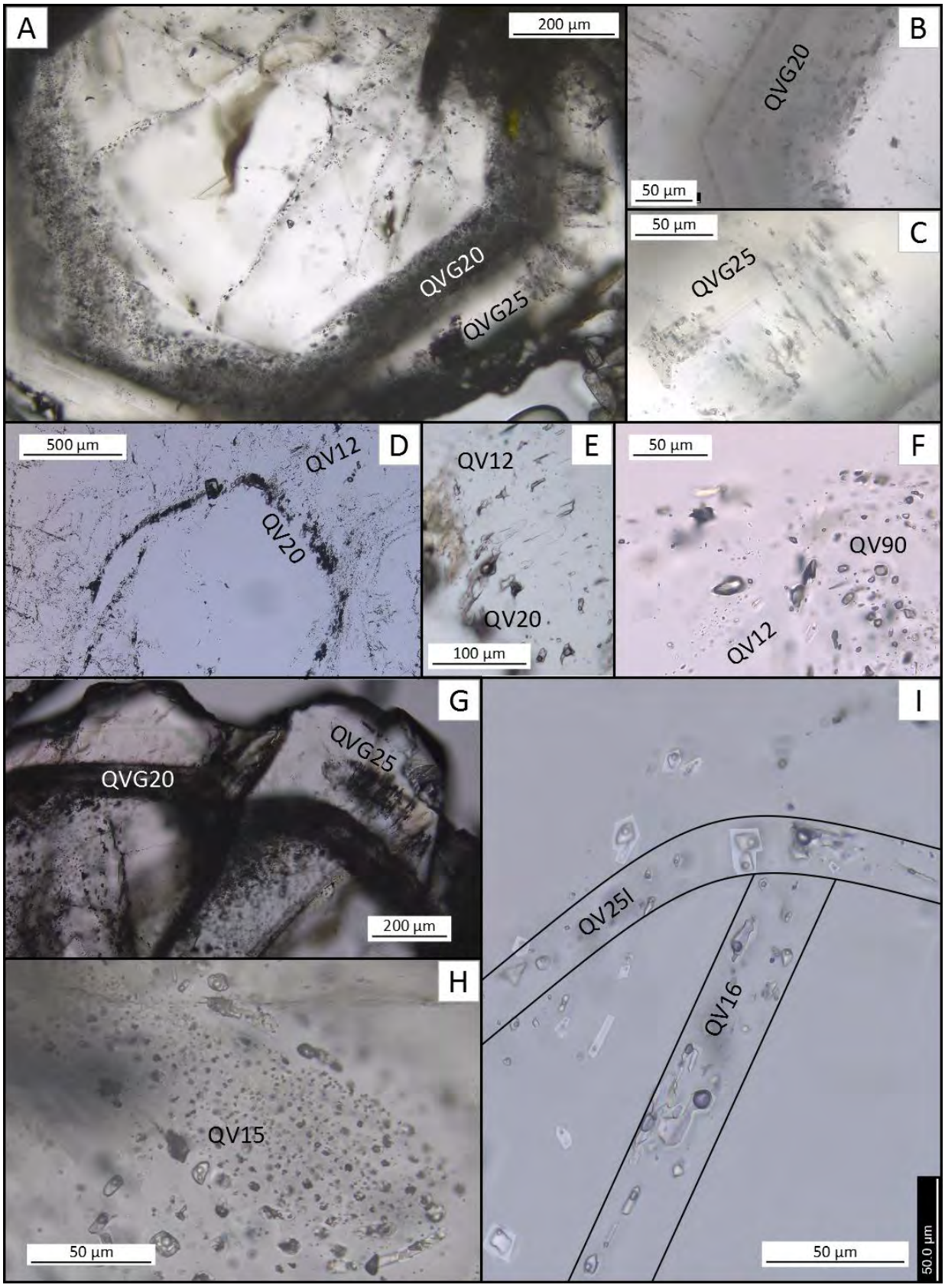

Figure 4-17: *Fluid inclusions at Geitafell. Explanation see next page.*

.

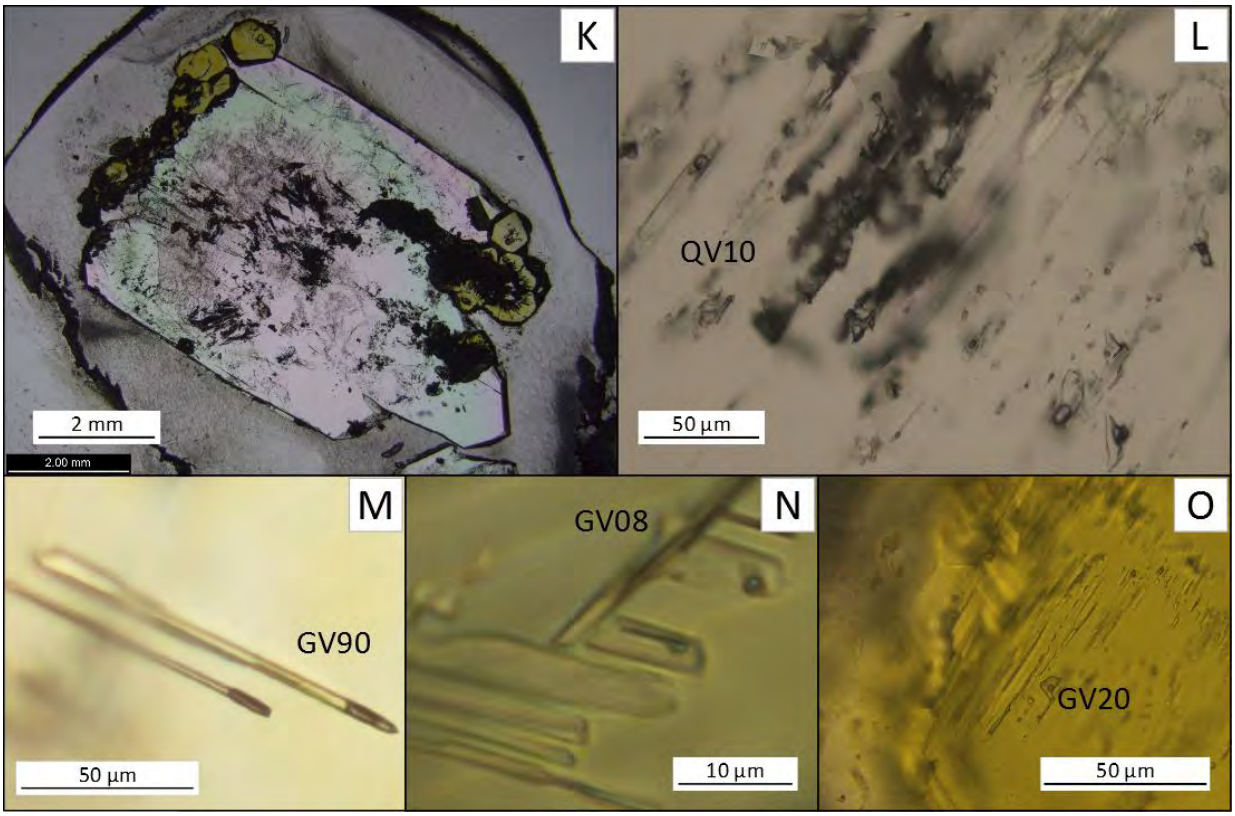

Figure 4-17 continued: *Fluid inclusions at Geitafell. A) Quartz crystal from Geitafellsgil with fluid inclusions in growth zones and secondary fluid inclusion traces; B & C) Two types of growth zones (QVG20 and QVG25) within the crystal shown in A; D) Growth zone in a quartz crystal from Kraksgil, including tiny epidote crystals within the growth zone. Further primary, secondary and pseudo secondary assemblages are recognizable; E) Detailed view with irregular fluid inclusions (QV20) as well as low relief fluid inclusions (QV12) within the crystal shown in D; F) Pseudo secondary vapor inclusions (QV90/95) with some low relief inclusions (QV12); G) Another crystal from Geitafellsgil with two types of growth zones (same as in A); H) Primary aqueous fluid inclusions from Geitafell (QVG15); I) Primary and pseudo secondary aqueous fluid inclusions from Kraksgil; K) Overview sample Fl01.1, garnet quartz assemblage ; L) Aqueous fluid inclusion assemblage (QV10) from Fl01.1; M) elongated vapor rich fluid inclusions in garnet (GV90) from sample Fl01.1; N) Possible aqueous fluid inclusions (GV08) in garnet from sample Fl01.2; O) Aqueous fluid inclusion assemblage (GV20) oriented along the crystal lattice in garnet from sample Fl01.1; [Variability in brightness of pictures is an artifact of image processing to merge pictures from different focal plains into one picture]*

In quartz form *Geitafellsgil* the temporal correlation is easier due to the presence of extensive growth zones (Figure 4-16 and Figure 4-17 A). Aqueous inclusions QVG15 of primary and or pseudo secondary origin are the earliest discriminable inclusions occurring only within the distinct growth zones of primary QVG20. However, most of the quartz lies inside these growth zones (Figure 4-17 A). Primary QVG25 formed thereafter in another, spatially more restricted growth zones. The last inclusions forming are secondary QVG20i and eventually QVG90 clearly distinguishable by crosscutting relations. QVG20i may be younger than QVG90 as assemblages clearly

crosscut the entire crystal while QVG20i assemblages are more enigmatic.

As garnet is overgrown by quartz (Figure 4-15 B) it clearly formed before or while the earliest stages of quartz precipitation. Therefore all fluid inclusions within garnet are classified as older than those in quartz. Correlation between *Kraksgil* and *Geitafellsgil* quartz inclusions is clearly possible for secondary vapor inclusions while for aqueous inclusions it is more demanding. Based on results of petrography and thermometry sections, growth of quartz including primary and secondary inclusions most likely did not take place simultaneously at both sites from the same fluid.

4.4.3 Thermometry

Cooling of fluid inclusions revealed constant ice melting temperatures of -0.1° to 0° C in all measured quartz inclusions. This represents salinities of 0 to 0.2 wt% NaCl and correlates to meteoric water. In garnet -0.2° to 0° is observed. This represents meteoric water with salinities of up to 0.35 wt%. Homogenization temperatures are highly variable and cover temperatures from 200° up to 370° (Figure 4-18).

Vesicles within Aplite breccia matrix in the outermost zone of the magma chamber at *Geitafellsgil* formed at magmatic temperatures of 700°. The hydrothermal quartz however forms at much lower temperatures. Homogenization temperatures combined with time relations between different fluid inclusion types in quartz indicate a prograde temperature evolution during quartz precipitation. The increase of temperature was about 100° C with variations in the range of about 20° C. Type QVG15 inclusions with T_{hom} around 250° are only found in the innermost zone of quartz crystals surrounded by extensive growth zones of QVG20 type inclusions. Within these growth zones T_{hom} are around 300° C, with the lowermost measurements (~295°) at the inner rim and slightly higher T_{hom} with increasing distance from the center. Less extensive QVG25 assemblages in growth zones homogenize from 320-350°. Subsequently secondary inclusions (QVG20i) formed below peak temperatures. Measurements on a secondary vapor inclusion trail (GVG90) reveal a minimum temperature of 420° which is not trusted due to difficulties in observing homogenization.

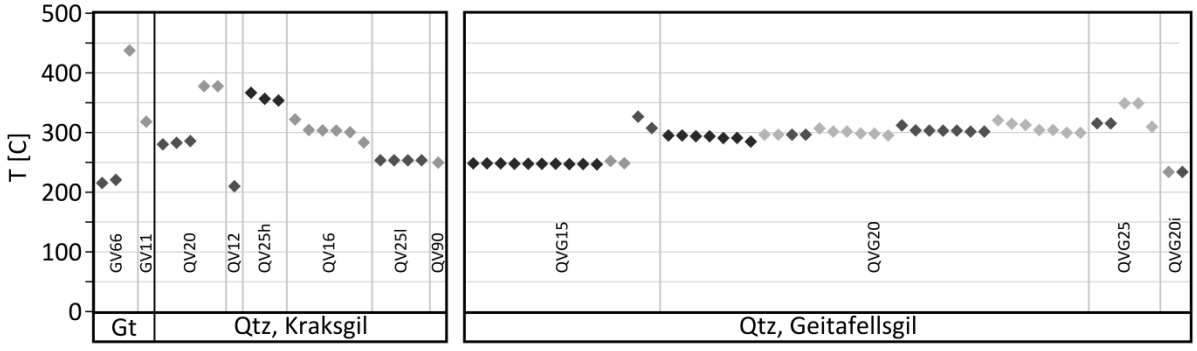

Figure 4-18: *Homogenization temperatures of fluid inclusions. Inclusion types are arranged from left to right according to time relations discussed in section 4.4.2 for Kraksgil and Geitafellsgil separately. Garnet inclusions from Kraksgil are plotted separately even though garnet formation overlaps with early quartz. Grayscale of diamonds next to each other indicates inclusions of the same assemblages. A table with measured temperatures is given in Appendix C.*

At *Kraksgil* temperature evolution is not as well constrained. The few inclusions in garnet have a high variability of T_{hom}. Best measurements of a small assemblage (GV66) homogenize at around 220°. Further measurements of T_{hom} for potentially younger fluid inclusions are at ~320°. T_{hom} in quartz is higher than in garnet for earlier inclusions and eventually decreases. QV20 inclusions are located in a very distinct but irregular growth zone. For sub euhedral inclusions T_{hom} is near supercritical at ~380° (Figure 4-17 D) but for more irregular inclusions in the same zone it is ~285°. Primary or possibly pseudo secondary QV12 inclusions outside of this assemblage homogenize at 220°. Further measurements of this inclusion type elsewhere were inhibited due to overheating and destruction during measurements in garnet. T_{hom} in the next generation of fluid inclusions (QV25h) is up at ~350°. Temperature decreases again to T_{hom} of ~300° for QV16 and ~250° for QV25l (Figure 4-17 I). Observation of vapor inclusions also suggests homogenization around 250°.

Trustworthy homogenization temperatures above the critical temperature for pure water are not observed. However few results above 400° were measured in small assemblages, single inclusions with irregular shape and necking down or in vapor inclusions where homogenization was hard to establish optically. Without necking down these T_{hom} may represent fluids without meteoric water composition. Mineral inclusions in garnet mistaken for fluid inclusions due to the limits of optical microscopy lead to destruction of quartz inclusion. Results above 420° in Appendix C therefore are equivalent to abortion of heating. Those temperatures are not presented in Figure 4-18, and are not included in further discussion.

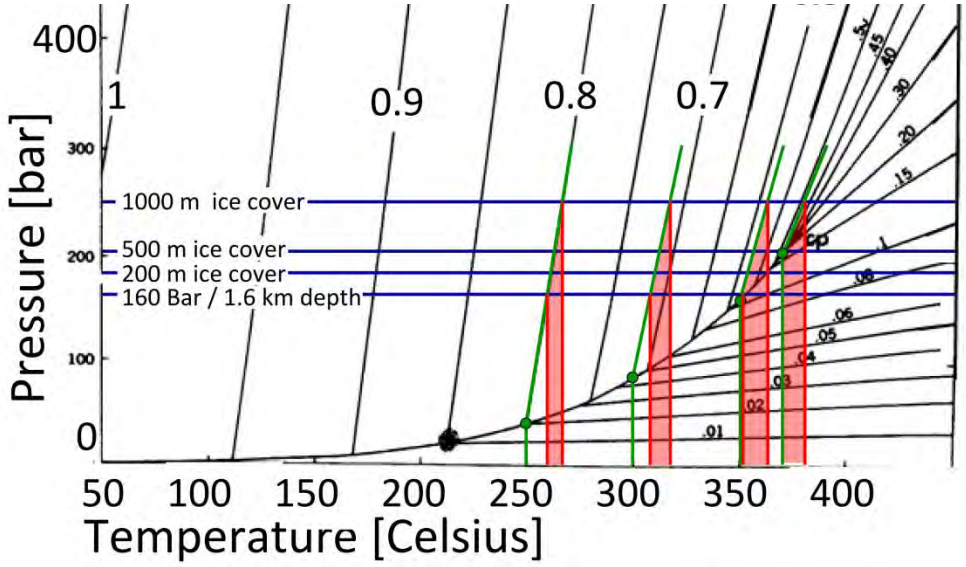

Figure 4-19: *Maximum temperatures derived from fluid inclusion density and homogenization temperatures. Blue lines represent estimated pressure for hydrostatic conditions assuming variable ice cover. Green lines are measured homogenization temperatures and possible paths of entrapment at higher pressures. Red lines represent Maximum and minimum temperature derived by intersection of blue and green. Red areas cover the Temperature variability for ice cover between 0 and 1000 m. Temperature may be about 10-20° higher due to high pressure entrapment.*

Estimates for higher pressure of fluid inclusions while formation is shown in Figure 4-19. Paleo depth is 1600 m (Friðleifsson, 1983) and variable ice cover is assumed. Densities of 1 g/cm^3 for water and 0.9 g/cm^3 for ice are used in pressure estimates. Homogenization temperatures at 250°, 300°, 350° and 370° are plotted. With 1 km of ice cover, temperatures are elevated by up to about 20° compared to T_{hom} at atmospheric pressure. Without ice cover temperatures are only up to 10° higher. Thus the impact of fluid inclusion entrapment at higher pressures is relatively small. For the measured inclusions, supercritical entrapment temperatures in a hydrostatic system at this depth are only possible if ice cover is more than 500 m.

5 Discussion

5.1 Magmatic Evolution

During the activity of Geitafell central volcano the magmatic heat source evolved. This is represented in the variability of mineral proportions within gabbro (mainly plagioclase and pyroxene) as well as the occurrence of subordinate intrusive lithologies including evolved silicic rocks. Trends in major elements (AFM diagram and xMg) follow evolution of tholeiitic rocks

Occurrence of rock types with variable mineral proportions and rock chemistry lead to the idea of multiple pulses of magma, recharging a partly solidified magma chamber eventually forming *Geitafell* gabbro. Various gabbro units were already described in previous work for the outcrops east of *Geitafell* at *Viðborðsfjall* (Annels, 1967; Friðleifsson, 1983; Newman, 1967*)*. Variability in gabbro at the southern end of *Geitafellsbjörg* roughlycorresponding to outcrops of *Gabbro A* and *B* were described in earlier studies but were restricted to magnetic rock properties (Schoenharting, 1979). Magma pulses crystallized around *Geitafellsbjörg* must follow temporally relative close after each other as no sharp intrusive contacts are found between different gabbro types. However, mineral volume percentage as well as bulk rock chemistry suggest that there were at least two types of magma from which gabbro crystallized. Further differences in mineralogy may originate in changes of cooling rate and crystal nucleation.

A first, partly feldsparphyric magma pulse crystallized as *Porphyry Gabbro* along the contact zone. It most likely intruded as relatively small body in a considerably cooler host rock with a fine matrix representing fast cooling. Patches of fine *Fine Gabbro* are found further towards southeast up to a distance of 250 meter from the contact. All of these subtypes of gabbro are interpreted as recharges in a partly solidified small sill-shaped magma chamber (Gudmundsson, 1986). Due to high cooling rates, small crystals formed and ilmenite grew dendritic in *Fine Gabbro*.

As recharge continued and cooling rate decreased due to heating up of host rocks, crystal-size in intrusive rock increases. About 70 meter from the contact in inward cooling rock, sub ophitic to ophitic texture developed by growth of pyroxene around plagioclase. This texture is typical for thick sills (Kretz, 2003) supporting the theory of multiple sills preceding the main magma chamber. Away from the contact, the imbalance between growth of plagioclase and pyroxene decreases which is represented by decreasing pyroxene size and content. Orthocumulate texture with fine interstitial plagioclase crystals in coarse *Gabbro B* corresponds to higher plagioclase

content. Dykes and sheets crosscutting these gabbros and the surrounding host rock have lower bulk silica content and therefore represent a less evolved magma. This is taken as evidence for multiple magma recharge of variable composition.

Further towards the center of the magma chamber in *Gabbro A*, silica content is lower (Figure 5-2). This may represent another, more primitive batch of magma. As silica will increase during crystallization of pyroxenes and plagioclase (Bowen, 1928) this part of the magma chamber does not represent a residual magmatic liquid derived by fractional crystallization. It can though represent a corresponding crystal mush. Evidence for this is found in a weak layering. Good knowledge about spatial extent of magma types along the contact is lacking but outcrops clearly indicate a bigger body for the more mafic gabbro than the gabbro bodies crystallized from first a batch of magma. During crystallization of this gabbro several types of small magmatic bodies formed. Within Figure 5-1 the evolution described in the following sections is shown graphically.

Pegmatoidal gabbro pods may originate from water saturated melt in crystal mush. Apatite and dendritic ilmenite forms due to enrichment and saturation of Fe, Ti and P in unmixing interstitial liquids. Simultaneously diffusivity is enhanced by H_2O saturation (Holness et al., 2011; Namur et al., 2012). Density contrast can drive these melts upward following structural weaknesses in the crystal mush and form the characteristic elongated shape of pegmatite pods (Larsen and Brooks, 1994). High diffusivity due to H_2O saturation enables pyroxene megacrysts to crystallize and dendritic ilmenite growth. Thus dendritic growth can also be achieved without fast cooling in sills (McBirney, 2007).

Dykelet shaped *Pegmatoidal Gabbro* forms a network of interconnected structures possibly overprinting itself and is loosely connected to pegmatitic pods. N-S orientation of dykelets and elongated pods is approximately parallel to the gabbro contact could be related to cooling processes or follow a stress field in cooling and shrinking magma. Tearing in crystal mush with a vertical cooling front as it is assumed at *Geitafell Gabbro* may originate in settling of nearly solid blocks of crystal mush (Humphreys and Holness, 2010). Within *Pegmatoidal Gabbro* exsolution lamellae in dendritic oxides form during cooling when solid solutions become unstable. Ilmenite lamellae in ulvöspinel–rich magnetite form at temperatures of 600-800° depending on f_{O2} (Haggerty, 1976). Temperature during formation of *Pegmatoidal Gabbro* is magmatic, enabling solid solutions to be stable. Exsolution took place before silicic intrusives formed as solidus temperatures for typical magmas with rhyolite composition are about 600-700° (Larsen, 1929).

Lack of chilled margins in *Green Dykelet* and *White Acid* dykelets and sheets, pods and other silicic intrusives support a formation relatively shortly after solidification of gabbro. Gabbro temperature may well be above the solidus of rhyolitic magma facilitating movement of the magma within solid gabbro. Walls of dykelets however are mostly brittle in gabbro and pegmatite (Figure 5-1; Detail α). Fracturing in crystal mush may be equivalent to crystal lock up with 10% intergranular hydrous melt (Hibbard and Watters, 1985). Coarse crystals without trunctations, floating in silicic rock indicate about 30% intergranular melt present and negligible crystal interlocking.

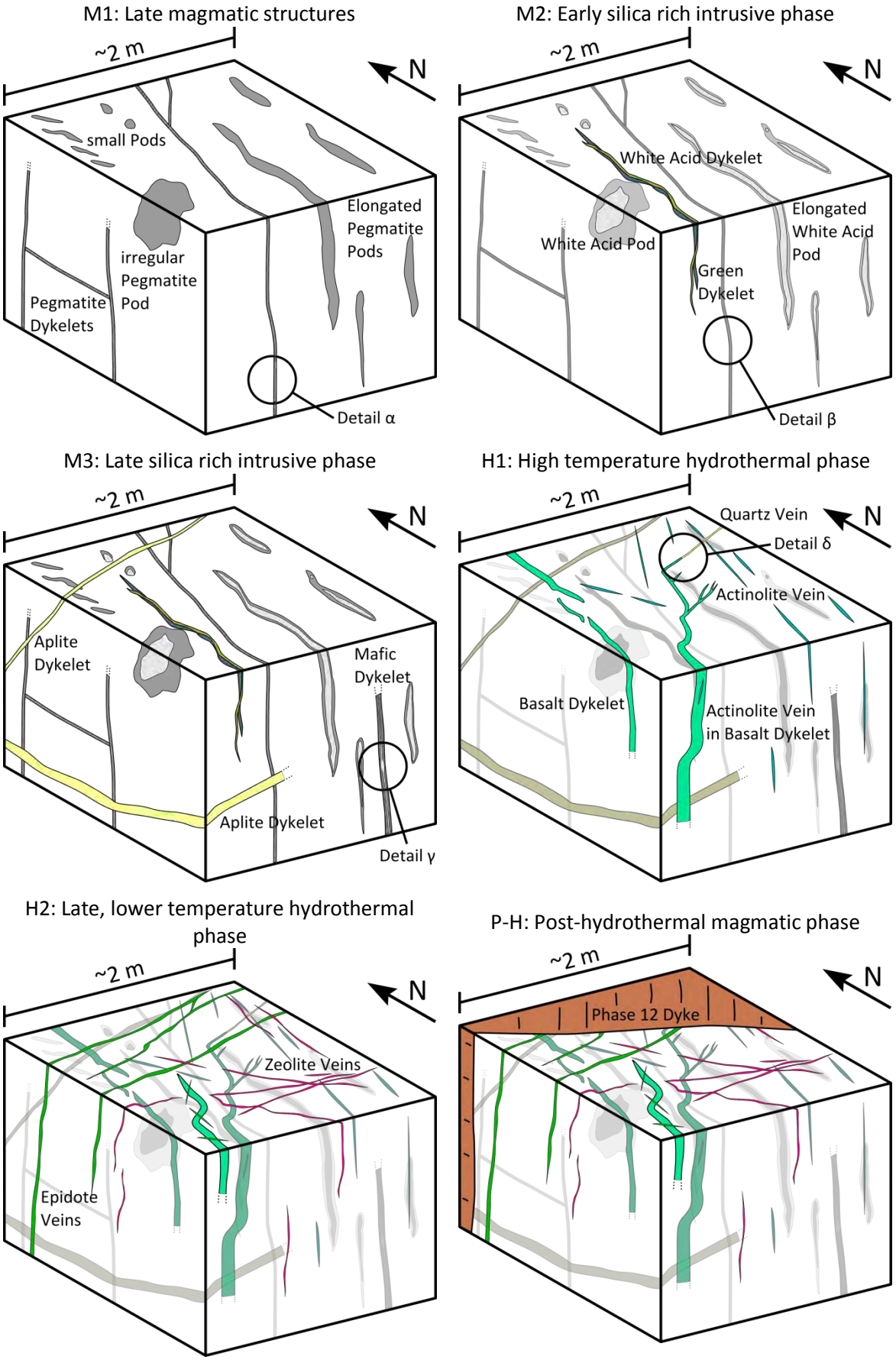

Figure 5-1: *Late magmatic and hydrothermal evolution (discussion see text).*

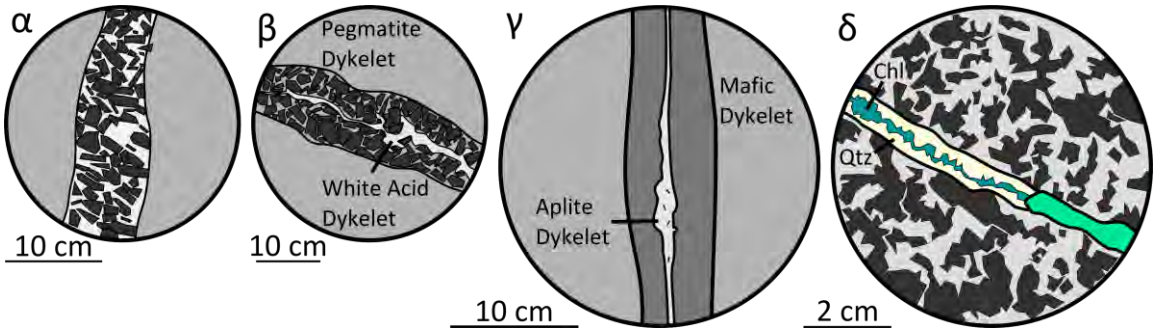

Figure 5-1 continued: *Details of sketches on previous page. Phase M1 represents cooling of the gabbro and forming of gabbro pegmatite. Phase M2 and M3 are represented by intrusion of small silicic bodies with a temporal evolution in composition and the ductile to brittle transition as separator. H1 is the peak temperature hydrothermal phase with actinolite veining. The latest occurrence of actinolite is within dykes of intrusive phase 8 (Friðleifsson, 1983). H2 with epidote and zeolite veining and detail δ with chlorite represent the decreasing temperature in the system. Detailed discussion of the figures is done in section 5 of the text.*

If shear stress was present during crystallization of gabbro, silicic dykelets could operate as a lubricant in between more stiff blocks of crystal mush. Zones with enigmatic mixing of fine silicic rocks with relatively coarse gabbro may represent incomplete aggregation of interstitial melt in dykelets. Composition of entrapped silicic melt should represent magmatic evolution with decreasing melt remaining in the crystal mush (Figure 5-2). As buoyancy may drove the extracted melt upward, it is not necessary representing interstitial melt expelled from nearby host rock at the site of crystallization.

During injection of silicic rocks, growth of fractured host plagioclase continued with substantially decreased anorthite compared to the crystal core content (85.8% to 73.3%). Composition of intruding silicic magma evolved during crystallization and anorthite content in plagioclase crystals within the silicic intrusive is even lower (54.3%) (Fig 4-8 A). Finally graphic intergrowth of orthoclase and quartz represents cotectic crystallization. Rare wider dyklets and sheets not following gabbro pegmatite intruded brittle after cooling of the gabbro. This includes evolved *Granophyre* and *Aplite* dykelets which crosscut several more mafic aphyric dykelets. They represent a second phase of silicic intrusives and orientation is controlled by a changing stress field. If frequency of these dykelets increases, *Intrusive Breccia* is formed. Breccia includes clasts of intrusive phase 3 and is intruded by phase 5 dykes (Friðleifsson, 1983). It therefore represents the last stages of phase 4 intrusives. As breccia matrix is fine but unchilled, it intruded into relatively hot rock. Rare hornblende crystals in *Granophyre* and abundant primary vesicles in *Aplite* indicate volatile saturation in these magmas. Fluid inclusions in hydrothermal quartz within *Aplite* vesicles however have salinities comparable to meteoric water and formed later.Volatiles in evolved magmas approach saturation during ascent which is represented in occurrence of primary vesicles within dykelets (Sparks, 1978). This enhanced porosity will facilitate later hydrothermal circulation. A partly syngenetic formation of acid intrusives and gabbro at *Geitafell* is already described in earlier work (Schoenharting, 1979).

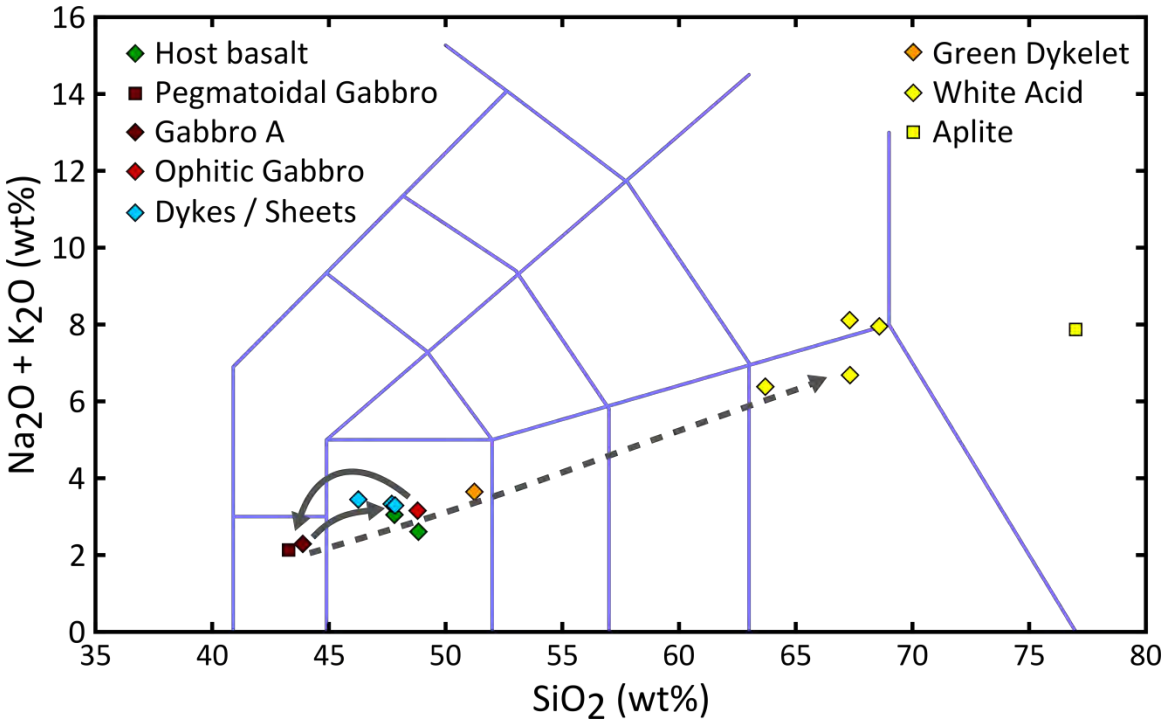

Figure 5-2: *Possible temporal evolution of magmas as Geitafell central volcano. Gray arrows represent subsequent formation of intrusive rocks. Dotted arrow represent melt extracted from crystal mush.*

Mafic intrusive phases 5 to 7 (Friðleifsson, 1983) are found frequently in gabbro along *Geitafellsgil* while *Gabbro A* along *Hoffellsjökull* only phase 8 and younger are observed. As these smaller intrusions have silica content between *Gabbro A* and *Ophitic Gabbro* they could represent evolved melt from *Gabbro A*. Small dolerite dykelets in *Gabbro A* preceding more silicic dykelets are thus interpreted as zones of magma ascent or the "roots" of dykes. A temporal overlap of the inward cooling and crystallization of the gabbro with mafic dyking is assumed and also applies to silica rich intrusives equivalent to phase 4 in earlier work (Friðleifsson, 1983).

5.2 Hydrothermal Evolution

Hydrothermal veins and alteration haloes are found in all rock types. Extensive alteration is restricted to the victinity of fractures and along contacts form silicic intrusives to *Pegmatoidal Gabbro*. Low volatile content of about 0.25 % in tholeiite melt (Moore, 1970) provided only small amounts of magmatic fluids compared to the big supply of meteoric water in Iceland. In brittle rocks magmatic fluids mixed fast with percolating meteoric hydrothermal fluids and therefore leave hardly any traces of their presence. The only brine inclusion observed is interpreted as product of necking down. Evidence for magmatic CO_2 in fluid inclusions was not found at all.

Two paths of hydrothermal evolution are found. One within the basaltic hostrock and outermost parts of the former magma chamber with a pro- and retrograde evolution preserved and a second path in gabbro where the decreasing temperatures are recorded beginning with hydrothermal actionlite

formation. Overprint of lower temperature alteration is present in all rock types. Andradite alteration (Friðleifsson, 1983) was not observed in gabbro. As it is best seen in open veins within host rock the lack of high porosity in these rocks may prevented conditions for andradite formation. Hydrothermal reaction with primary minerals by replacement is predominantly affecting pyroxene and earlier secondary minerals. Oxides are corroded only if directly affected by microscopic chlorite veining.

In host rocks pro- and retrograde alteration temperature evolution is preserved in hydrothermal minerals. Mainly chlorite and epidote are preserved during higher temperature alteration. Both of them are reported as stable even at high temperatures (Bird et al., 1984). Peak temperatures of about 370° are observed for fluids in host rock within a zone of pervasive alteration and continuing fluid flow during all stages of hydrothermal activity until late stage regional alteration characterized by zeolite precipitation. Boiling trails and meaningful homogenization temperatures above 380° as found in earlier work could not be observed (Troyer, 2007). However possibly primary vapor rich inclusions in garnet could indicate boiling while formation. Clearly secondary vapor inclusions in quartz are evidence for boiling after precipitation of hydrothermal quartz in the cooling system.

Mineralization sequence in vesicles and veins is in agreement of findings by Friðleifsson (1983). Fluctuations in fluid properties or pressure temperature conditions are observed as subsequent quartz-calcite-quartz overgrowth in veins as well as epidote appearance and disappearance in vesicles. Epidote can be stable over a wide temperature range (Bird and Spieler, 2004) and therefore may not be indicative for the high temperature evolution in the system.

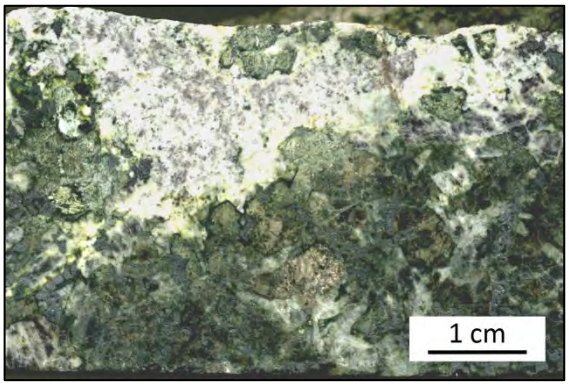

Figure 5-3: *Typical Granophyre-Pegmatite sample with most intense epidote and actinolite alteration along the contact and replacing pyroxene crystals.*

Highest temperature of alteration in gabbro is represented by actinolite. Within gabbro it is mostly restricted to fine veinlets (Figure 5-1) with N-S strike roughly parallel to the assumed gabbro contact. It is also abundant along the contact of early silicic intrusions towards mafic minerals (Figure 5-3). These zones provided higher porosity and are structural weaknesses allowing higher flux rates of fluids. Formation of veinlets is supported by cooling and shrinking of the intrusive body. Actinolite veins outside of the magma chamber are restricted to dykes and sheets providing elevated temperatures for a short time (Friðleifsson, 1983) the same is observed for late intrusive sheets. Lower temperatures are represented by quartz veinlets. Re-heating may occurred along those basaltic dykelets partly follow these structures. Cooling continued to temperatures of epidote-chlorite alteration. Overprint is pervasive and accompagned by more abundant epidote veins and chlorite veins following earlier veins. Chlorite replaces pyroxenes as well as actinolite while plagioclase is partly albitized and replaced by

epidote and calcite. Increasing vein abundance with lower alteration is interpreted as corresponding to higher permeability due to the propagating cracking front.

Titanite and pyrite formation in a chlorite vein crosscutting ilmenite and magnetite implies small scale redistribution of Ti and Fe. As pyrite occurrence usually corresponds to lower temperatures and calcite veins in basaltic host rock, it might be the availability of Fe leading to precipitation.

In *Granophyre* and *Aplite* the highest alteration temperature visible as mineral is represented by albitization and epidote replacement of plagioclase. Within *Granophyre* and *Aplite* matrix of *Intrusive Breccia*, fine quartz veinlets connect small vesicles. Hydrothermal quartz within these vesicles in *Aplite* breccia matrix bear near supercritical fluid inclusions and shows rising homogenization temperatures. A temperature rise of about 100° in distinct growth zones of quartz crystals must be related to a considerable increase of heat flow from the source. This temperature rise took place after cooling of the *Aplite* from magmatic temperatures (~700° for rhyolitic melt) below 250° for the lowest homogenization temperatures in primary fluid inclusions. The recharge with continuously hotter fluids must cool down within the already cool parts of the magma chamber allowing SiO_2 to saturate. The temperature rise also indicates an increase of energy in the heat source. Secondary vapor rich inclusions at the assumed paleodepth in *Geitafell* may indicates boiling in a later phase of the hydrothermal system.

The stress field in gabbro during formation of late magmatic dykelets and high temperature actinolite veinlets lead to a N-S orientation of these features. Veins with lower temperature mineralization such as epidote, chlorite, calcite and zeolite have an overal E-W orientation. This is looked at as a clear indication of change in the stress field around the cooling magma chamber during hydrothermal alteration. Highly evolved silicic intrusions with brittle vein walls have no obvious main orientation, but too few were observed to see a trend.

Approximate vein density supports the overall idea of epidote alteration as the most pervasive alteration. As it forms at temperatures below the brittle to ductile transition in host rocks, there is a chance to produce fractures which remain open and allow sufficient amount of fluid interacting with rock to imprint a signature. However all estimates for vein abundances might be substantially higher than values given due to missed veinlets. Especially actinolite forming alteration along contacts and microscopic chlorite veins are missed. Comparison of bulk rock measurements between basalt of diffeernt degree of alteration suggests a small impact of hydrothermal fluids on rock chemistry. Late regional zeolite alteration is abundant across all outcrops.

6 Conclusion and Outlook

The central theme of this master thesis is the occurrence of many processes as repetitive events. Magmatic as well as hydrothermal processes may repeat several times.

- Gabbro at *Geitafellsbjörg* represents three (or more) phases of compositionally slightly different magma recharge. However subsequent batches not necessarily intrude into completely crystallized predecessors.
- Formation of silica rich intrusives including pods, veins and magmatic

breccias, accompany the solidification of gabbro and its transition from a ductile mush to brittle solid rock. They show a big variability in shape and structure as well as bulk composition indicating a magmatic evolution during formation. Weather the smaller intrusive are remnants from bigger volumes of rising magma or small batches of remaining interstitial liquid rising within a crystal mush is unclear.

- Highest temperatures within the hydrothermal system were reached after emplacement of the gabbroic magma chamber when cracking front propagated into intrusive rocks. During further cooling, abundance of cracks and therefore permeability increases.
- Orientation of veins with lower temperature minerals compared to silicic magmatic features and high temperature hydrothermal veins suggest a change in the stress field during active hydrothermal circulation.
- Fluid inclusions in hydrothermal quartz suggest re-heating of fluid by at least 100° towards near critical temperatures in cooled gabbro. As mineral precipitation is triggered by sharp changes in the system (P, T, …), minerals form at a cooling front where subsequently hotter fluids cool.
- In more distal parts of the system preserved mineral assemblages in veins and vesicles preserved nearly complete sequence formed during heating and cooling.
- Near supercritical inclusions may indicate a minimal ice cover of about 500 m if formed under hydrostatic conditions.
- Hydrothermal fluids derive from meteoric waters as neither halite nor CO_2 bearing fluid inclusion assemblages are observed.

Some of these ideas were already introduced by earlier authors (Friðleifsson, 1983; Schoenharting, 1979).

Development of alteration is generally strongly controlled by the type of rock affected. Mafic, pyroxene bearing rocks are more sensitive to mineral replacement by actinolite and chlorite than silica rich rock. Therefore the effect of these types of alteration might be partly overlooked within *Granophyre* and *Aplite* rocks.

A better distinction of variable gabbro intrusive phases and further investigation of silicic rocks and their compositional evolution in comparison of shape of small intrusives, may provide further insight into the evolution of the magma chamber during crystallization. This could provide better constraints on the thermal energy available in the source of the natural geothermal system. Investigation of fluid paths on a bigger scale could then provide better understanding of the development of the system.

The conducted work started with its focus on hydrothermal features but drifted towards magmatic petrology over time as I assumed it to control the temporal and spatial occurrence of earliest hydrothermal activity. Magmatic structures, developing during crystallization and solidification of the magma chamber, might be crucial as early fluid paths for the hydrothermal fluid circulation.

7 Acknowledgements

My gratitude belongs to everybody who made this project possible. This includes Thomas Driesner as my supervisor, Guðmundur Ómar Friðleifsson and Knútur Árnason from Iceland GeoSurvey (ISOR) for the introduction to the

field site, Melchior Grab for shipping rock samples, Benjamin Zürcher for help and ideas during the fieldwork. Remy Lüchinger for preparation of fluid inclusion chips from tiny quartz crystals. Lydia Zehnder for XRF measurements. A big "Thank You" also goes to Ingibjörg and Dutti for being very kind hosts at *Hoffell* during fieldwork in Iceland and providing delicious *Kryddbrauð*.

8 References

Ágústsson, K., and Ó. G. Flóvenz, The thickness of the seismogenic crust in Iceland and its implications for geothermal systems, in Proceedings Proceedings of the World Geothermal Congress 2005, Antalya, Turkey, 24–29 April 2005, Volume Paper 0743, International Geothermal Association.

Allen, R. M., Nolet, G., Morgan, W. J., Vogfjörd, K., Bergsson, B. H., Erlendsson, P., Foulger, G. R., Jakobsdóttir, S., Julian, B. R., Pritchard, M., Ragnarsson, S., and Stefánsson, R., 2002, Imaging the mantle beneath Iceland using integrated seismological techniques: Journal of Geophysical Research: Solid Earth, v. 107, no. B12, p. 2325.

Andersen, D. J., Lindsley, D. H., and Davidson, P. M., 1993, QUILF: A pascal program to assess equilibria among Fe・Mg・Mn・Ti oxides, pyroxenes, olivine, and quartz: Computers & Geosciences, v. 19, no. 9, p. 1333-1350.

Annels, A. E., 1967, The Geology of the Hornafjordur Region, S.E. Iceland [PhD: University of London, 279 p.

Arnórsson, S., 1995, Geothermal systems in Iceland: Structure and conceptual models—I. High-temperature areas: Geothermics, v. 24, no. 5–6, p. 561-602.

Arnórsson, S., Stefánsson, A., and Bjarnason, J. Ö., 2007, Fluid-Fluid Interactions in Geothermal Systems: Reviews in Mineralogy and Geochemistry, v. 65, no. 1, p. 259-312.

Barker, D. S., 1970, Compositions of Granophyre, Myrmekite, and Graphic Granite: Geological Society of America Bulletin, v. 81, no. 11, p. 3339-3350.

Berndt, M. E., Seyfried, W. E., and Beck, J. W., 1988, Hydrothermal alteration processes at midocean ridges: Experimental and theoretical constraints from Ca and Sr exchange reactions and Sr isotopic ratios: Journal of Geophysical Research: Solid Earth, v. 93, no. B5, p. 4573-4583.

Bertani, R., 2012, Geothermal power generation in the world 2005–2010 update report: Geothermics, v. 41, no. 0, p. 1-29.

Bird, D. K., Schiffman, P., Elders, W. A., Williams, A. E., and McDowell, S. D., 1984, Calc-silicate mineralization in active geothermal systems: Economic Geology, v. 79, no. 4, p. 671-695.

Bird, D. K., and Spieler, A. R., 2004, Epidote in geothermal systems: Reviews in Mineralogy and Geochemistry, v. 56, no. 1, p. 235-300.

Björnsson, H., Björnsson, S., and Sigurgeirsson, T., 1982, Penetration of water into hot rock boundaries of magma at Grimsvotn: Nature, v. 295, no. 5850, p. 580-581.

Bödvarsson, G., 1961, Physical characteristics of natural heat resources in Iceland: Jökull, v. 11, p. 29-38.

Bowen, N. L., 1928, Evolution of the Igneous Rocks, Princeton, Princeton University Press.

Driesner, T., 2012, COTHEMRM - COmbined hydrological, geochemical and geophysical modeling of geoTHERMal systems: Zurich.

Elders, W. A., and Friðleifsson, G. Ó., 2010, Implications of the Iceland Deep Drilling Project for Improving Understanding Of Hydrothermal Processes at Slow Spreading Mid-Ocean Ridges, Diversity Of Hydrothermal Systems On Slow Spreading Ocean Ridges, American Geophysical Union, p. 91-112.

Exley, R. A., 1982, Electron microprobe studies of Iceland Research Drilling Project high-

temperature hydrothermal mineral geochemistry: Journal of Geophysical Research: Solid Earth, v. 87, no. B8, p. 6547-6557.

Foulger, G. R., Du, Z., and Julian, B. R., 2003, Icelandic-type crust: Geophysical Journal International, v. 155, no. 2, p. 567-590.

Fournier, R. O., 1991, The transition from hydrostatic to greater than hydrostatic fluid pressure in presently active continental hydrothermal systems in crystalline rock: Geophysical Research Letters, v. 18, no. 5, p. 955-958.

-, 1999, Hydrothermal processes related to movement of fluid from plastic into brittle rock in the magmatic-epithermal environment: Economic Geology, v. 94, no. 8, p. 1193-1211.

Fournier, R. O., and Truesdell, A. H., 1973, An empirical Na・K・Ca geothermometer for natural waters: Geochimica et Cosmochimica Acta, v. 37, no. 5, p. 1255-1275.

Franzson, H., Zierenberg, R., and Schiffman, P., 2008, Chemical transport in geothermal systems in Iceland: evidence from hydrothermal alteration: Journal of volcanology and geothermal research, v. 173, no. 3, p. 217-229.

Friðleifsson, G. Ó., 1983, The geology and alteration history of the geitafell central volcano, southeast iceland [PhD: Faculty of Science, University of Edinburgh, 371 p.

Friðleifsson, G. Ó., 2014, pers. communication.

Friðleifsson, I. B., 1979, Geothermal activity in Iceland.: Jökull, v. 29, p. 47-56.

German, C., and Von Damm, K., 2006, Hydrothermal processes: The oceans & marine geochemistry (Treatise on geochemistry series, Vol. 6), Elsevier, p. 181-222.

Giggenbach, W. F., 1988, Geothermal solute equilibria. derivation of Na-K-Mg-Ca geoindicators: Geochimica et Cosmochimica Acta, v. 52, no. 12, p. 2749-2765.

Gillis, K., and Roberts, M., 1999, Cracking at the magma–hydrothermal transition: evidence from the Troodos Ophiolite, Cyprus: Earth and Planetary Science Letters, v. 169, no. 3, p. 227-244.

Gillis, K. M., 2008, The roof of an axial magma chamber: A hornfelsic heat exchanger: Geology, v. 36, no. 4, p. 299-302.

Grab, M., 2014, pers. communication.

Gudmundsson, Å., 1986, Formation of crystal magma chambers in Iceland: Geology, v. 14, no. 2, p. 164-166.

Guðmundsson, A. T., and Kjartansson, H., 2007, Living earth: outline of the geology of Iceland, Reykjavík, Iceland, Mál og menning.

Haggerty, S., 1976, Oxidation of opaque mineral oxides in basalts: Oxide minerals, p. Hg1-Hg100.

Hart, S. R., Blusztajn, J., Dick, H. J. B., Meyer, P. S., and Muehlenbachs, K., 1999, The fingerprint of seawater circulation in a 500-meter section of ocean crust gabbros: Geochimica et Cosmochimica Acta, v. 63, no. 23–24, p. 4059-4080.

Hayba, D. O., and Ingebritsen, S. E., 1997, Multiphase groundwater flow near cooling plutons: Journal of Geophysical Research: Solid Earth (1978–2012), v. 102, no. B6, p. 12235-12252.

Hibbard, M. J., and Watters, R. J., 1985, Fracturing and diking in incompletely crystallized granitic plutons: Lithos, v. 18, no. 0, p. 1-12.

Holness, M. B., Stripp, G., Humphreys, M., Veksler, I. V., Nielsen, T. F., and Tegner, C., 2011, Silicate liquid immiscibility within the crystal mush: late-stage magmatic microstructures in the Skaergaard intrusion, East Greenland: Journal of Petrology, v. 52, no. 1, p. 175-222.

Humphreys, M. C. S., and Holness, M. B., 2010, Melt-rich segregations in the Skaergaard Marginal Border Series: Tearing of a vertical silicate mush: Lithos, v. 119, no. 3–4, p. 181-192.

Humphris, S. E., and Thompson, G., 1978, Hydrothermal alteration of oceanic basalts by seawater: Geochimica et Cosmochimica Acta, v. 42, no. 1, p. 107-125.

Kretz, R., 2003, Dendritic Magnetite and Ilmenite in 590 Ma Grenville Dikes near Otter Lake, Quebec, Canada: The Canadian Mineralogist, v. 41, no. 4, p. 1049-1059.

Kristmannsdóttir, H., 1975, Clay minerals formed by hydrothermal alteration of basaltic rocks in Icelandic geothermal fields: Geologiska Föreningen i Stockholm Förhandlingar, v. 97, no. 3, p. 289-292.

-, 1979, Alteration of Basaltic Rocks by Hydrothermal-Activity at 100-300° C, Developments in sedimentology, Volume 27, p. 359-367.

-, 1981, Wollastonite from hydrothermally altered basaltic rocks in Iceland: Mineral. Mag, v. 44, p. 95-99.

-, 1982, Alteration in the IRDP drill hole compared with other drill holes in Iceland: Journal of Geophysical Research: Solid Earth, v. 87, no. B8, p. 6525-6531.

Larsen, E. S., 1929, The temperatures of magmas: American Mineralogist, v. 14, p. 81-94.

Larsen, R. B., and Brooks, C. K., 1994, Origin and Evolution of Gabbroic Pegmatites in the Skaergaard Intrusion, East Greenland: Journal of Petrology, v. 35, no. 6, p. 1651-1679.

Le Maitre, R. W., Bateman, P., Dudek, A., Keller, J., Lameyre, J., Le Bas, M., Sabine, P., Schmid, R., Sorensen, H., and Streckeisen, A., 1989, A classification of igneous rocks and glossary of terms: Recommendations of the International Union of Geological Sciences Subcommission on the Systematics of Igneous Rocks, Blackwell Oxford.

Lund, J. W., Freeston, D. H., and Boyd, T. L., 2011, Direct utilization of geothermal energy 2010 worldwide review: Geothermics, v. 40, no. 3, p. 159-180.

MacLean, W. H., and Kranidiotis, P., 1987, Immobile elements as monitors of mass transfer in hydrothermal alteration; Phelps Dodge massive sulfide deposit, Matagami, Quebec: Economic Geology, v. 82, no. 4, p. 951-962.

Marks, N., Schiffman, P., and Zierenberg, R. A., 2011, High-grade contact metamorphism in the Reykjanes geothermal system: Implications for fluid-rock interactions at mid-oceanic ridge spreading centers: Geochemistry, Geophysics, Geosystems, v. 12, no. 8, p. Q08007.

Matthews, A., 1976, Magnetite forrnation by the reduction of hematite with iron under hydrothermal conditions: American Mineralogist, v. 6, p. 927-932.

McBirney, A. R., 2007, Igneous petrology, Jones & Bartlett Learning.

Moore, J., 1970, Water Content of Basalt Erupted on the ocean floor: Contributions to Mineralogy and Petrology, v. 28, no. 4, p. 272-279.

Namur, O., Charlier, B., and Holness, M. B., 2012, Dual origin of Fe–Ti–P gabbros by immiscibility and fractional crystallization of evolved tholeiitic basalts in the Sept Iles layered intrusion: Lithos, v. 154, no. 0, p. 100-114.

Newman, T. C., 1967, The geology of some igneous intrusions in the Hornafjordur Region of S.E. Iceland [PhD: University of Manchester.

Sæmundsson K., A. G., Steingrímsson B., 2009, Geothermal systems in a global perspective, Short Course on Surface Exploration for Geothermal Resources: Ahuachapan and Santa Tecla, El Salvador, ISOR - Iceland GeoSurvey, p. 14.

Sauerzapf, U., Lattard, D., Burchard, M., and Engelmann, R., 2008, The titanomagnetite–ilmenite equilibrium: new experimental data and thermo-oxybarometric application to the crystallization of basic to intermediate rocks: Journal of Petrology, v. 49, no. 6, p. 1161-1185.

Schoenharting, G., 1979, Magnetic properties of rocks from the Geitafell gabbro complex, SE Iceland: Bull. Geol. Soc. Den, v. 28, p. 21-29.

Sparks, R., 1978, The dynamics of bubble formation and growth in magmas: a review and analysis: Journal of volcanology and geothermal research, v. 3, no. 1, p. 1-37.

Sveinbjörnsdóttir, Á., 1991, Composition of geothermal minerals from saline and dilute fluids — Krafla and Reykjanes, Iceland: Lithos, v. 27, no. 4, p. 301-315.

Troyer, R. R., M. H.; Elders, W. A.; Fridleifsson, G. O., 2007, Iceland Deep Drilling Project (IDDP): (IV) Fluid Inclusion Microthermometry of the Geitafell Hydrothermal System - a Possible Analog of the Active Krafla System, American Geophysical Union, Fall Meeting 2007, abstract #V41A-0392: San Francisco.

Walker, G. P. L., 1960, Zeolite Zones and Dike Distribution in Relation to the Structure of the Basalts of Eastern Iceland: The Journal of Geology, v. 68, no. 5, p. 515–528.

Zürcher, B., 2014, Petrophysical and geophysical field study of a fossilised hydrogeothermal system in Geitafell, Iceland [MSc: ETH Zürich.

9 Appendix

A. Existing geological map of Geitafell

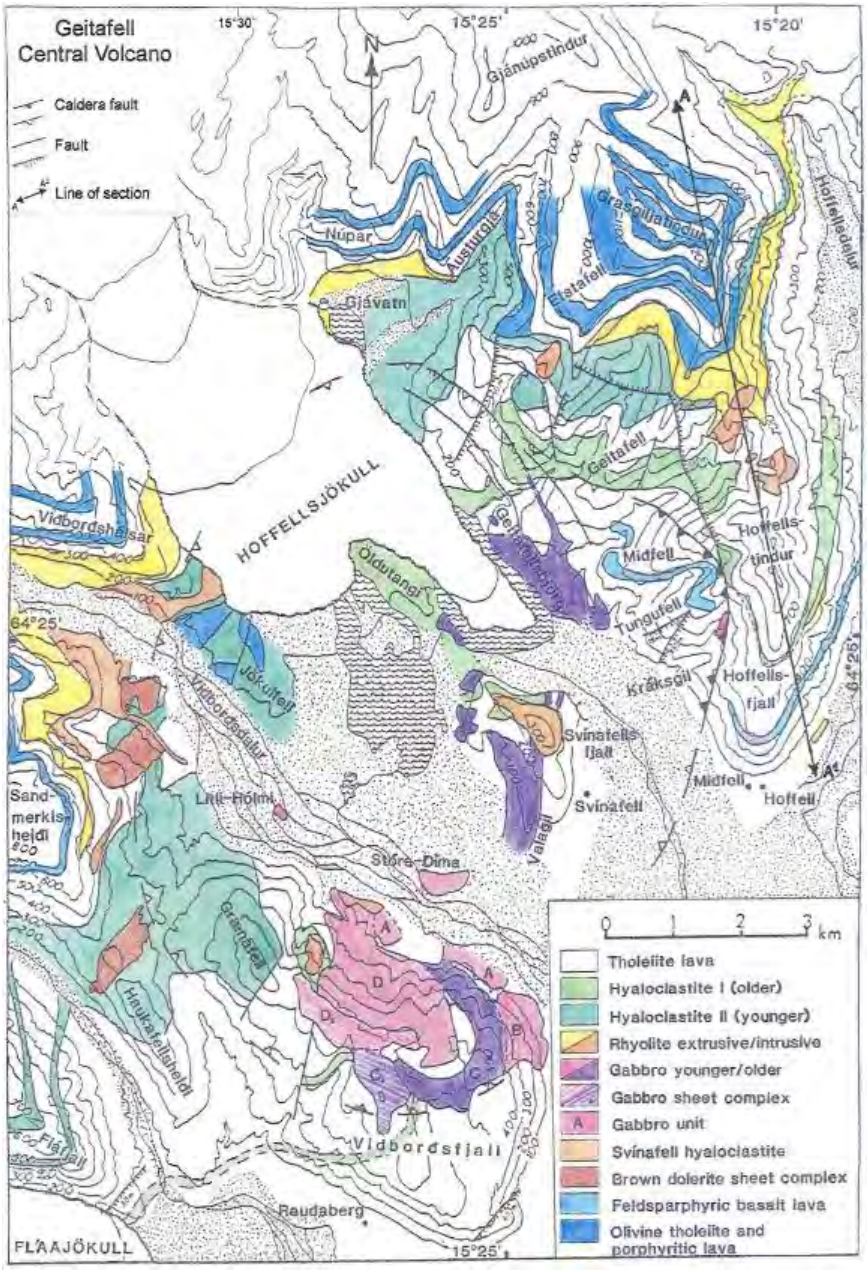

Geological map of Geitafell central volcano by Friðleifsson (1983).

B. XRF Results

Tables with results of XRF analysis. Results below limit of detection (LOD) are given as <LOD.

Rock type	Pegmatite	Gabbro	Ophitic. gabbro	Aphyric phase 5	Phyric phase 6	Aphyric phase 7	Grren acid
Sample	Q15	Q9	B55-3	B 10-3	P 1	P 3	Q 11
SiO_2 [wt%]	43.279	43.890	48.807	46.261	47.837	47.693	51.227
TiO_2	5.411	3.975	2.243	2.683	2.810	2.824	2.063
Al_2O_3	12.579	16.307	14.364	14.387	14.633	14.564	15.356
FeO_{tot}	17.019	14.591	10.767	13.098	13.328	13.365	9.185
MnO	0.214	0.151	0.150	0.182	0.189	0.190	0.136
MgO	7.074	5.603	6.601	7.292	5.539	5.529	5.741
CaO	12.471	13.002	13.348	10.443	11.001	10.988	11.273
Na_2O	1.936	2.068	2.288	2.923	2.810	2.845	3.272
K_2O	0.198	0.222	0.866	0.526	0.484	0.483	0.378
P_2O_5	0.049	0.056	0.198	0.263	0.293	0.292	0.457
Cr_2O_3	0.009	0.015	0.062	0.018	0.019	0.016	0.011
NiO	0.006	0.005	0.008	0.009	0.014	0.007	0.006
LOI	0.200	0.199	0.348	2.246	1.193	1.213	1.133
Total	100.444	100.084	100.051	100.330	100.152	100.010	100.238
Rb [ppm]	7.8	7.0	22.4	12.6	9.8	9.4	6.8
Ba	<20.1	<19.8	120.8	40.2	55.6	68.7	109.7
Sr	303.3	367.3	322.7	361.4	373.6	372.0	387.0
Nb	9.2	5.9	6.8	11.7	13.0	12.8	8.1
Zr	78.8	61.1	92.9	163.9	183.2	184.4	194.9
Hf	6.3	4.8	6.9	6.9	8.1	8.0	7.9
Y	17.6	15.4	24.4	33.2	37.1	36.5	45.7
Zn	99.9	85.2	81.0	105.8	107.2	108.5	45.3
Cu	109.1	126.8	84.4	125.7	134.5	128.9	56.8
Ni	47.0	41.9	62.1	75.0	108.7	53.8	43.9
Co	60.6	63.8	42.5	53.2	47.4	47.0	44.8
Cr	63.4	99.9	423.5	123.2	135.0	110.2	72.9
V	584.7	559.4	313.7	340.7	358.3	356.1	256.6
Sc	49.6	36.5	48.4	39.7	34.3	39.1	35.1
La	<18.2	<18.1	<18.1	<18.1	<18.1	<18.1	<18.0
Pb	21.1	21.7	19.6	8.3	6.8	8.8	8.3
Th	<2.7	<2.7	<2.6	<2.6	<2.6	<2.6	<2.6
U	<1.9	<1.7	<1.7	<1.7	<1.7	<1.7	<1.7

Rock type	White Acid	White Acid	White Acid	Granophyre	Aplite	Vesicular basalt	Basalt
Sample	Z4	C1-4	Q 27	GG-4	Br3	K5	L5-3
SiO_2 [wt%]	63.699	68.583	67.313	67.319	76.995	48.841	47.813
TiO_2	1.085	0.740	0.842	0.912	0.214	2.982	3.906
Al_2O_3	15.349	14.186	14.406	13.787	10.947	14.038	13.208
FeO_{tot}	5.921	4.402	4.169	4.664	1.395	14.159	15.576
MnO	0.050	0.070	0.031	0.073	0.020	0.219	0.229
MgO	1.789	0.781	1.293	1.005	0.133	5.099	5.119
CaO	4.260	2.411	2.016	3.386	1.378	10.734	9.759
Na_2O	4.453	3.893	5.085	3.234	2.203	2.570	2.485
K_2O	1.927	4.055	3.029	3.453	5.666	0.038	0.559
P_2O_5	0.229	0.144	0.284	0.188	0.028	0.345	0.561
Cr_2O_3	0.002	0.001	0.004	0.001	0.001	0.009	0.007
NiO	0.004	0.002	0.010	0.001	0.001	0.006	0.006
LOI	1.364	0.710	1.306	1.986	1.057	0.944	0.849
Total	100.133	99.976	99.787	100.009	100.038	99.983	100.076
Rb [ppm]	48.5	111.1	67.2	92.8	129.0	4.7	16.4
Ba	268.7	395.6	259.8	374.5	281.1	<19.3	64.2
Sr	414.6	199.7	419.0	202.7	141.7	279.8	357.8
Nb	13.8	22.6	9.5	21.0	15.0	15.3	20.1
Zr	646.4	613.2	390.3	405.1	375.7	234.8	306.0
Hf	19.9	19.5	12.1	12.1	14.1	8.6	11.4
Y	50.7	64.0	44.0	55.7	51.6	44.0	50.4
Zn	25.7	54.6	24.3	55.8	21.6	112.3	136.3
Cu	127.8	53.6	82.4	32.5	25.4	107.3	101.1
Ni	29.1	12.5	79.6	7.7	7.4	48.3	44.9
Co	24.7	18.8	16.8	10.2	6.0	45.2	46.7
Cr	15.4	6.6	27.4	5.9	4.2	62.3	47.3
V	87.5	39.9	72.3	61.3	11.2	389.2	400.1
Sc	14.1	7.5	7.7	9.0	<3.2	31.6	35.1
La	27.2	38.4	34.1	33.4	43.0	<18.1	<18.1
Pb	17.9	22.2	6.8	8.4	17.6	21.8	22.0
Th	6.9	9.0	8.8	9.6	14.0	2.7	<2.7
U	<1.6	<1.6	<1.6	2.8	2.1	<1.7	<1.7

C. Results, fluid inclusion thermometry

Sample	Mineral	Assemblage	P, PS, S	Content	Shape	$T_{m\,ice}$ [°]	T_{hom} [°]	Type	Comment
Fl01C1	gt	2	p	v, l	euhedral	0	404	GV90	
Fl01C1	gt	1	P	v, l	euhedral	0	438	GV66	T when FI broke?
Fl01C2	gt	1	P	v, l	euhedral	-0.1	216	GV66	
Fl01C2	gt	1	P	v, l	euhedral	-0.2	221	GV66	between needle inclusions
Fl01C1	gt	6	p	v, l	sub-euhedral	0	318.7	GV11	
Fl01C2	gt	2	p	v, l	sub-euhedral	0	440	GV08	min T
Fl01C2	gt	1	P	v, l	euhedral	-0.2	450	GV08	min T; bubble might be an artifact
Fl02C1	qtz	1	P?	v, l	sub-euhedral	0.1	280.5	QV20	in growth zone with epi
Fl02C1	qtz	1	P?	v, l	sub-euhedral	0.1	283	QV20	in growth zone with epi
Fl02C1	qtz	1	P?	v, l	irregular	0.1	286.1	QV20	in growth zone with epi
Fl02C1	qtz	2	P?	v, l	sub-euhedral	0.1	378	QV20	in growth zone with epi
Fl02C1	qtz	2	P?	v, l	sub-euhedral	0.1	378	QV20	in growth zone with epi
Fl02C1	qtz	2	P?	v, l	irregular	0.1	476	QV20	in growth zone with epi
Fl02C1	qtz	3	P?	v, l	euhedral	0	210.2	QV12	outside of growthzone
Fl02C1	qtz	7	?	v, l	sub-euhedral	0	354.2	QV25h	
Fl02C1	qtz	7	?	v, l	euhedral	0	357	QV25h	
Fl02C1	qtz	7	?	v, l	irregular	0	366.8	QV25h	
Fl02C1	qtz	5	PS?	v, l	sub-euhedral	0.1	284	QV16	sligthtly further away form rest of assemblage (inhomogenous trapping?)
Fl02C1	qtz	5	PS?	v, l	irregular	0.1	300.9	QV16	
Fl02C1	qtz	5	PS?	v, l	sub-euhedral	0.1	303.5	QV16	
Fl02C1	qtz	5	PS?	v, l	irregular	0.1	304.2	QV16	
Fl02C1	qtz	5	PS?	v, l	sub-euhedral	0.1	304.3	QV16	
Fl02C1	qtz	5	PS?	v, l	sub-euhedral	0.1	322.2	QV16	
Fl02C1	qtz	4	P	v, l	euhedral	0.1	254	QV25l	primary trail with 120° bend (qtz)
Fl02C1	qtz	4	P	v, l	sub-euhedral	0.1	254	QV25l	primary trail with 120° bend (qtz)

Sample	Mineral	Assemblage	P, PS, S	Content	Shape	$T_{m\ ice}$ [°]	T_{hom} [°]	Type	Comment
Fl02C1	qtz	4	P	v, l	euhedral	0.1	254	QV25l	primary trail with 120° bend (qtz)
Fl02C1	qtz	4	P	v, l	euhedral	0.1	254	QV25l	primary trail with 120° bend (qtz)
Fl02C1	qtz	6	?	v	irregular	0	250	QV90	approx T; not very clear homogenization, part of trail
FI11C4	qtz	3a	S	v, l	irregular	0	249	QVG15	towards innermost end
FI11C4	qtz	3a	S	v, l	irregular	0	252.5	QVG15	innermost end
FI11C4	qtz	3	S	v, l	irregular	0	308	QVG15	
FI11C4	qtz	3	S	v, l	irregular	0	327	QVG15	necking down
Fl11C3	qtz	1	S	v, l	variable	-0.1	247	QVG15	
Fl11C3	qtz	1	S	v, l	variable	-0.1	247.5	QVG15	
Fl11C3	qtz	1	S	v, l	variable	-0.1	247.5	QVG15	
Fl11C3	qtz	1	S	v, l	variable	-0.1	247.8	QVG15	
Fl11C3	qtz	1	S	v, l	variable	-0.1	248	QVG15	
Fl11C3	qtz	1	S	v, l	variable	-0.1	248	QVG15	
Fl11C3	qtz	1	S	v, l	variable	-0.1	248.1	QVG15	
Fl11C3	qtz	1	S	v, l	variable	-0.1	248.3	QVG15	
Fl11C3	qtz	1	S	v, l	variable	-0.1	248.6	QVG15	
Fl11C3	qtz	1	S	v, l	variable	-0.1	249	QVG15	
Fl10C2A2	qtz	1	P	v, l	euhedral	0	302	QVG20	innermost growth zone
Fl10C2A2	qtz	1	P	v, l	sub-euhedral	0	302	QVG20	innermost growth zone
Fl10C2A2	qtz	1	P	v, l	sub-euhedral	0	304	QVG20	innermost growth zone
Fl10C2A2	qtz	1	P	v, l	euhedral	0	312.5	QVG20	innermost growth zone
Fl11C7	qtz	7b	P	v, l	irregular	0	285.1	QVG20	
Fl11C7	qtz	7b	P	v, l	sub-euhedral	0	291.3	QVG20	
Fl11C7	qtz	7b	P	v, l	euhedral	0	291.3	QVG20	
Fl11C7	qtz	7b	P	v, l	euhedral	0	294	QVG20	
Fl11C7	qtz	7b	P	v, l	euhedral	0	294	QVG20	
Fl11C7	qtz	7b	P	v, l	euhedral	0	295.4	QVG20	
Fl11C7	qtz	7b	P	v, l	sub-euhedral	0	295.4	QVG20	
Fl11C7	qtz	8	P	v, l	sub-euhedral	0	295.5	QVG20	in growth zone

Sample	Mineral	Assemblage	P, PS, S	Content	Shape	$T_{m\ ice}$ [°]	T_{hom} [°]	Type	Comment
Fl11C7	qtz	2a	P	v, l	euhedral	0	296.8	QVG20	innermost zone
Fl11C7	qtz	2a	P	v, l	euhedral	0	296.8	QVG20	innermost zone
Fl11C7	qtz	2b	P	v, l	sub-euhedral	0	296.8	QVG20	innermost zone, towards outside
Fl11C7	qtz	2b	P	v, l	sub-euhedral	0	296.8	QVG20	innermost zone, towards outside
Fl11C7	qtz	8	P	v, l	sub-euhedral	0	298.5	QVG20	in growth zone
Fl11C7	qtz	8	P	v, l	sub-euhedral	0	299	QVG20	in growth zone
Fl11C7	qtz	7a	P	v, l	irregular	0	300	QVG20	approx. T
Fl11C7	qtz	7a	P	v, l	sub-euhedral	0	300	QVG20	approx. T
Fl11C7	qtz	8	P	v, l	sub-euhedral	0	302	QVG20	in growth zone
Fl11C7	qtz	8	P	v, l	sub-euhedral	0	302	QVG20	in growth zone
Fl11C7	qtz	1	P	v, l	irregular	0	303.5	QVG20	between two inner zones
Fl11C7	qtz	1	P	v, l	euhedral	0	303.5	QVG20	between two inner zones
Fl11C7	qtz	1	P	v, l	euhedral	0	303.6	QVG20	between two inner zones
Fl11C7	qtz	7a	P	v, l	euhedral	0	304.5	QVG20	
Fl11C7	qtz	7a	P	v, l	euhedral	0	304.5	QVG20	
Fl11C7	qtz	8	P	v, l	sub-euhedral	0	307	QVG20	in growth zone
Fl11C7	qtz	7a	P	v, l	sub-euhedral	0	312.9	QVG20	
Fl11C7	qtz	7a	P	v, l	euhedral	0	315.3	QVG20	
Fl11C7	qtz	7a	P	v, l	sub-euhedral	0	320.6	QVG20	
Fl10C2	qtz	2	P	v, l	sub-euhedral	0	310	QVG25	outer growthtzone
Fl10C2	qtz	2	P	v, l	sub-euhedral	0	349.5	QVG25	outer growthtzone
Fl10C2	qtz	2	P	v, l	sub-euhedral	0	349.5	QVG25	outer growthtzone
Fl11C7	qtz	3	P	v, l	sub-euhedral	0	315.5	QVG25	outside of fine growth zones
Fl11C7	qtz	3	P	v, l	sub-euhedral	0	315.9	QVG25	outside of fine growth zones
FI11C4	qtz	2	S	v, l	irregular	0	234.4	QVG20i	
FI11C4	qtz	2	S	v, l	irregular	0	234.4	QVG20i	
Fl11C7	qtz	4	?	v	euhedral	0	420	QV90	vapor trail min temp

D. XRD spectra of measured samples

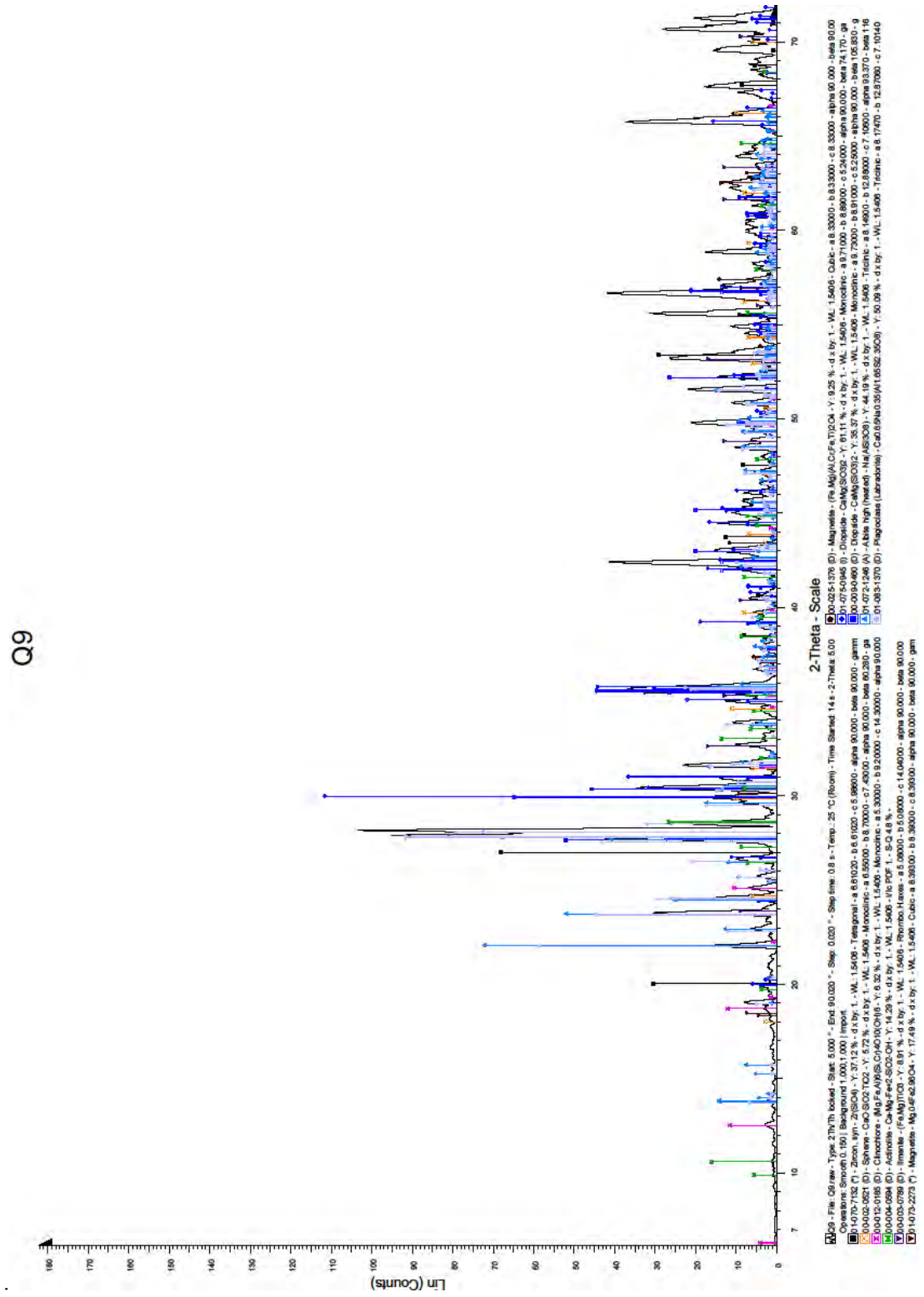

Plot of 2θ angle for sample Q9, *Gabbro A*.

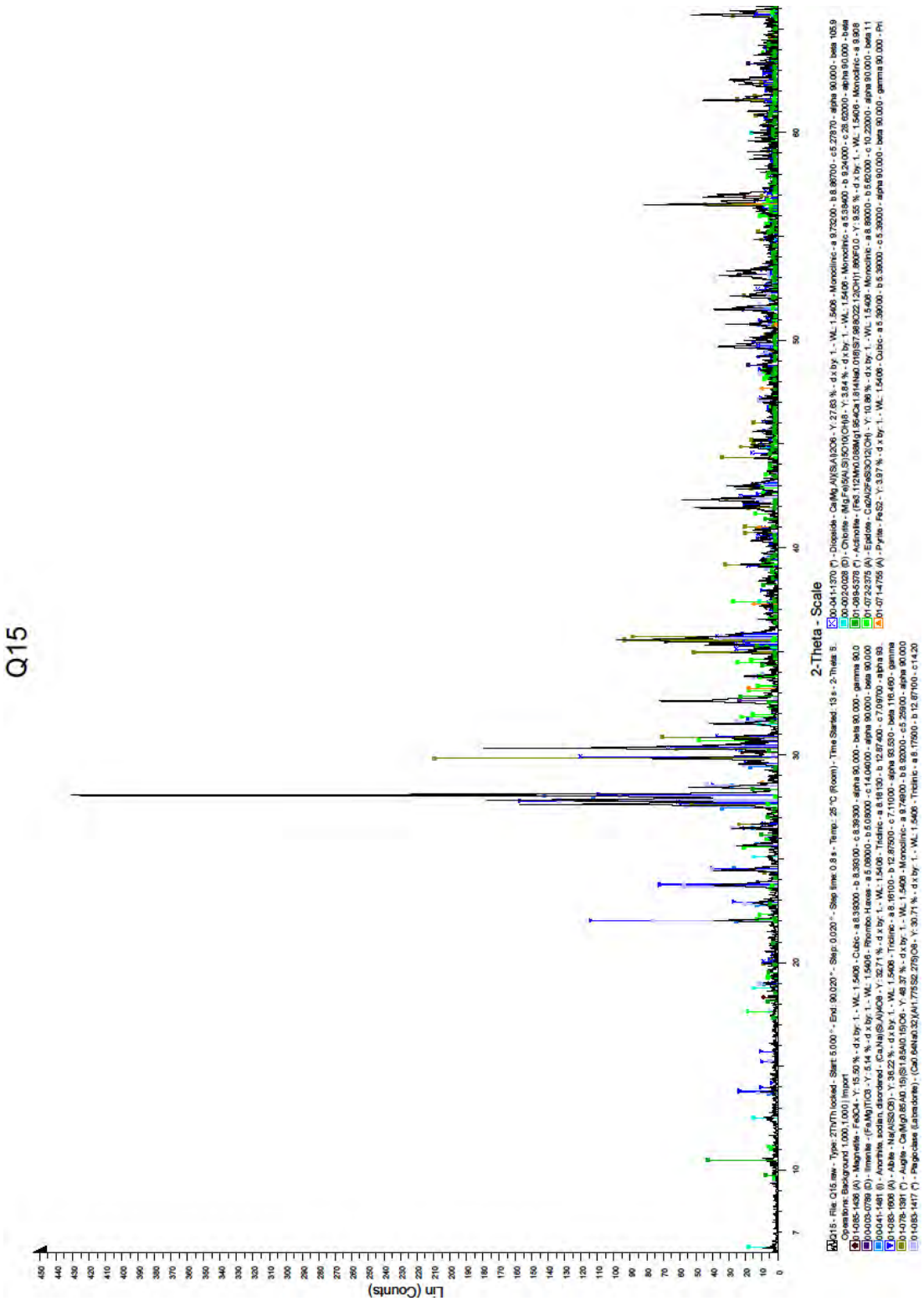

Plot of 2θ angle for sample Q15, *Pegmatoidal Gabbro*.

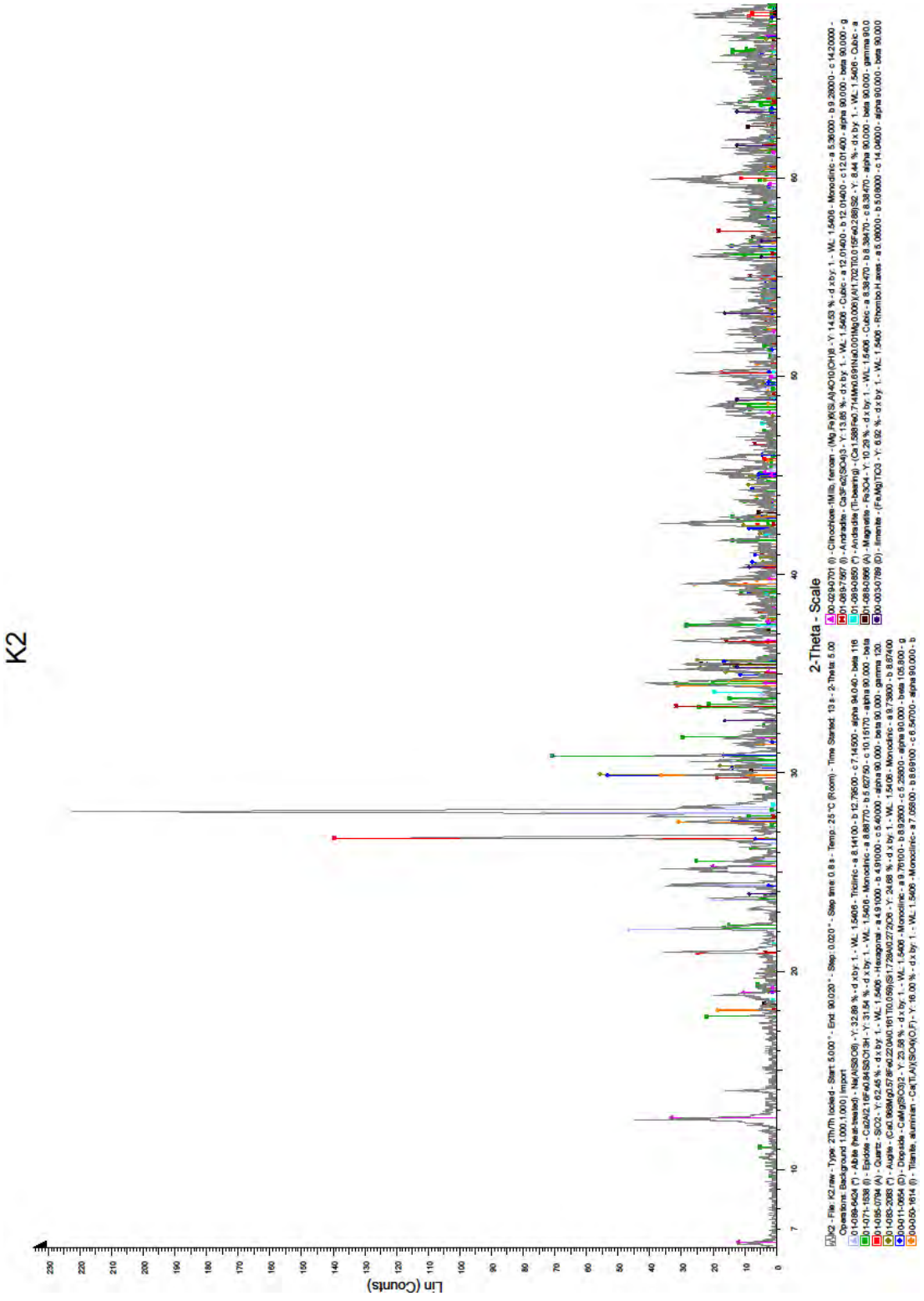

Plot of 2θ angle for sample K2, host basalt with intense alteration.

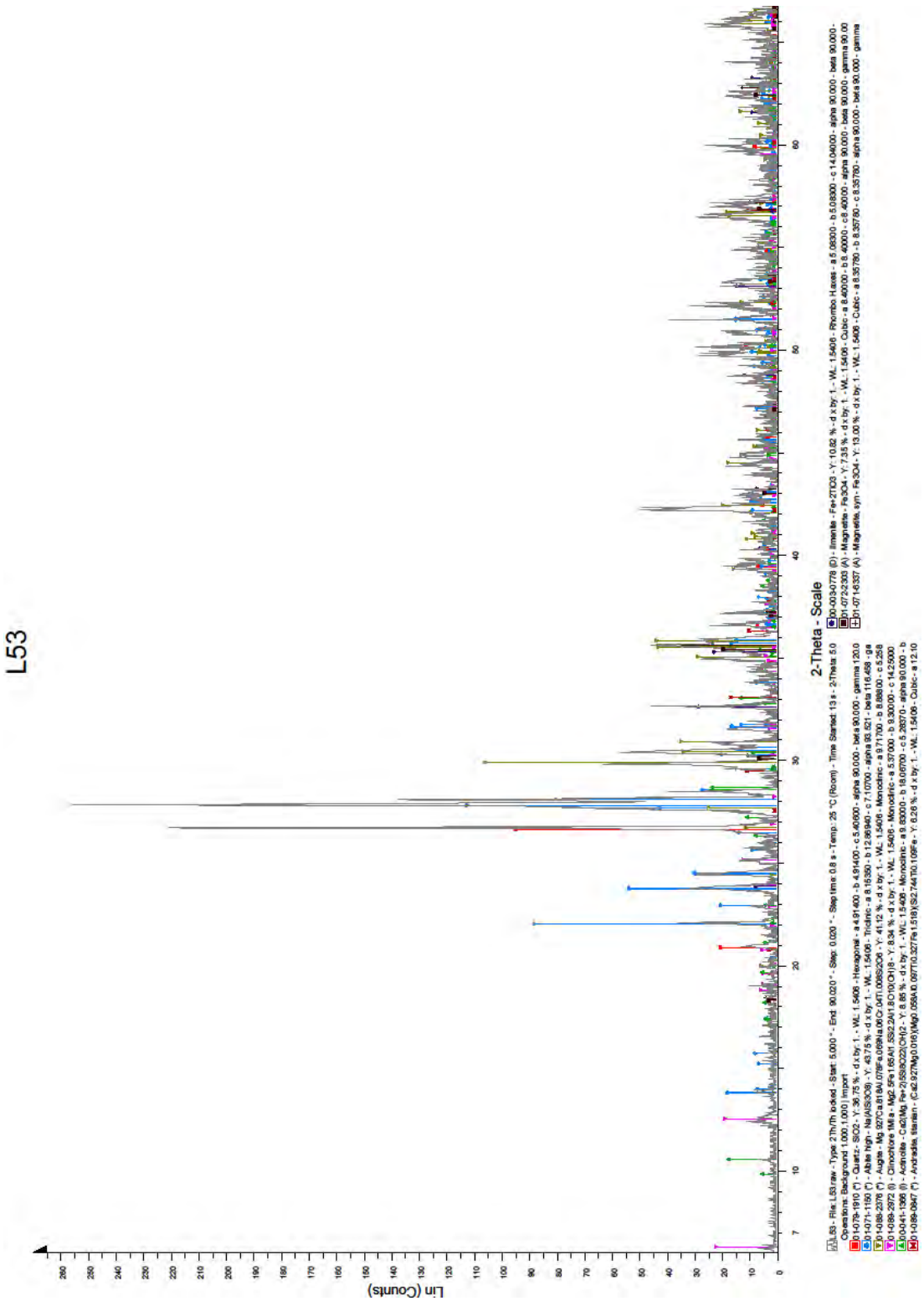

Plot of 2θ angle for sample L53, host basalt with weak alteration.

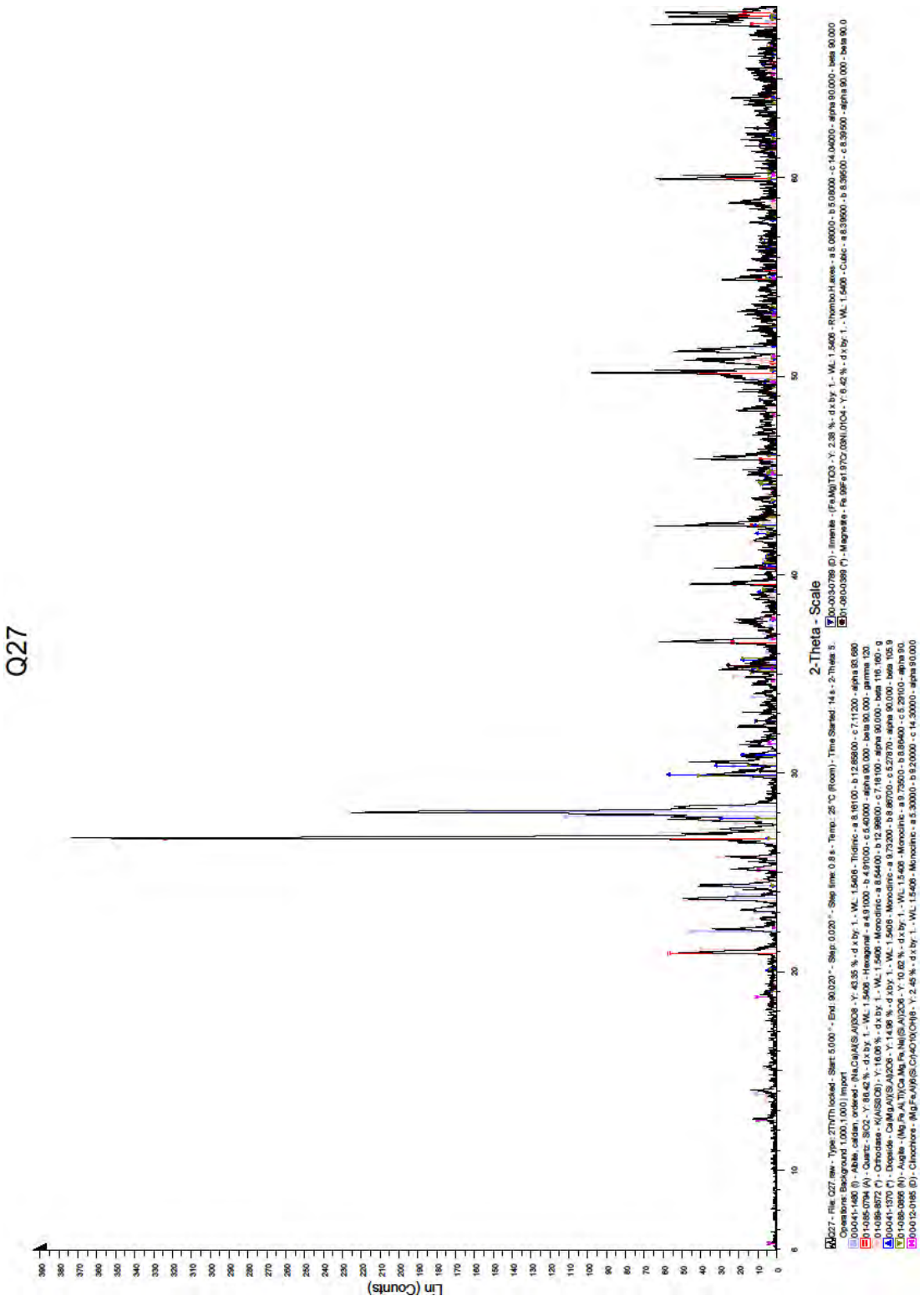

Plot of 2θ angle for sample Q27, White Acid rock.

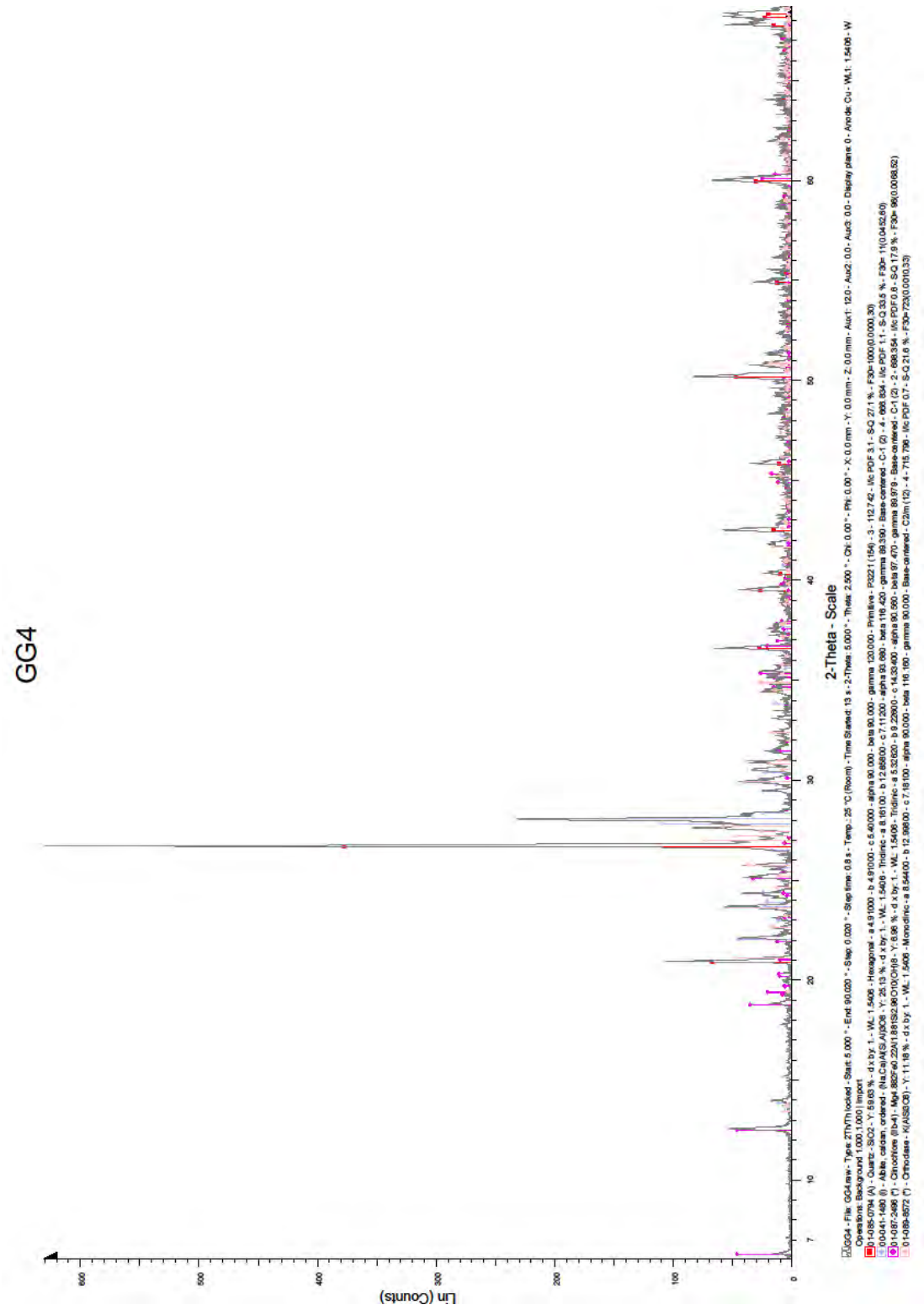

Plot of 2θ angle for sample GG4, *Granophyre*.

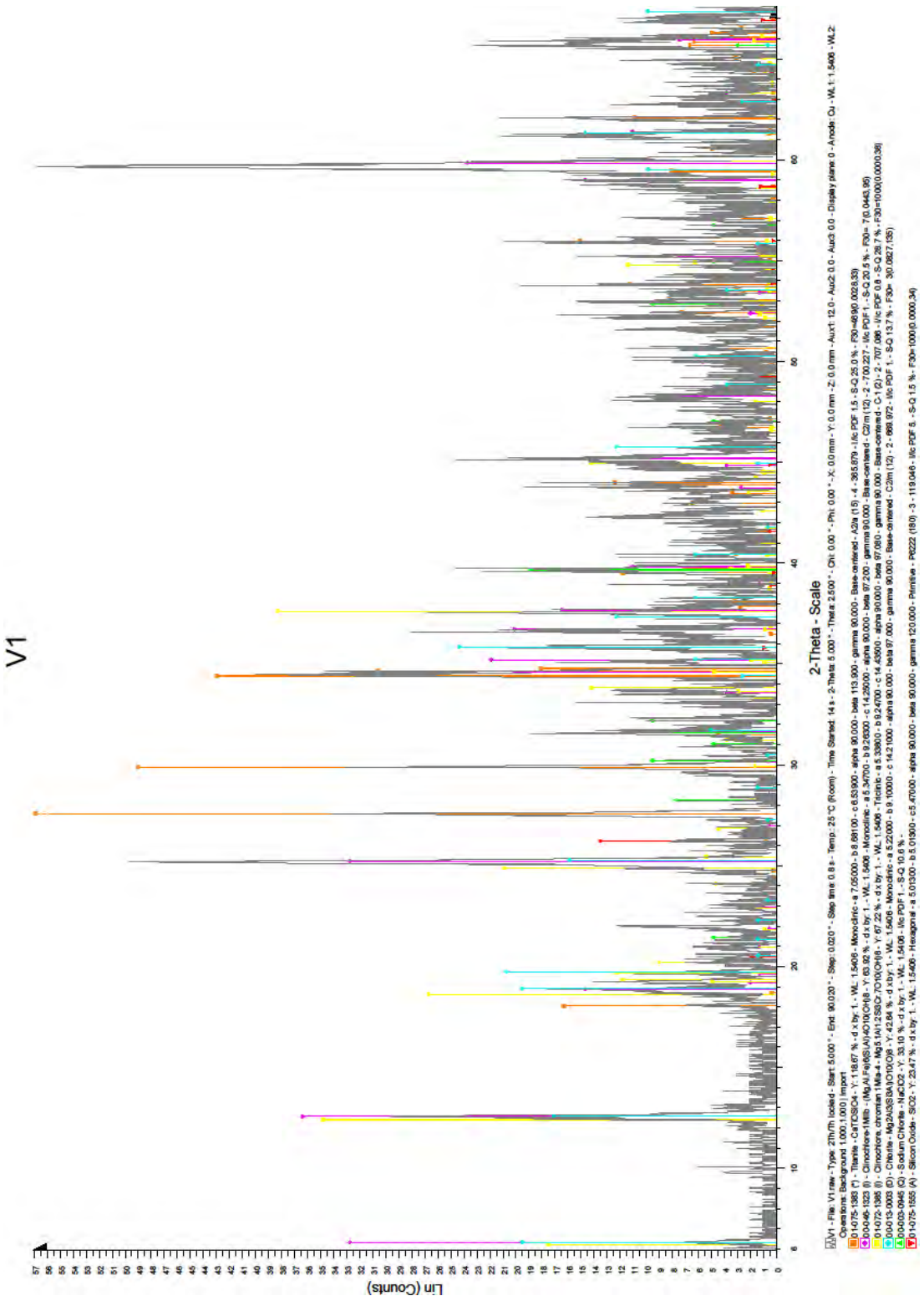

Plot of 2θ angle for sample V1, chlorite vein.

E. Map of magmatic structures at outcrop A

Legend

Magmatic features

- Pegmatite
- Pegmatite dykelet
- Diffuse zone with pegmatite and acid rock
- Acid dykelet
- Acid dykelet
- Aplite dykelet
- Aplite dykelet remnants
- Basalt dykelet

Landscape features

- Steep slope towards glacier
- Vegetation and gravel

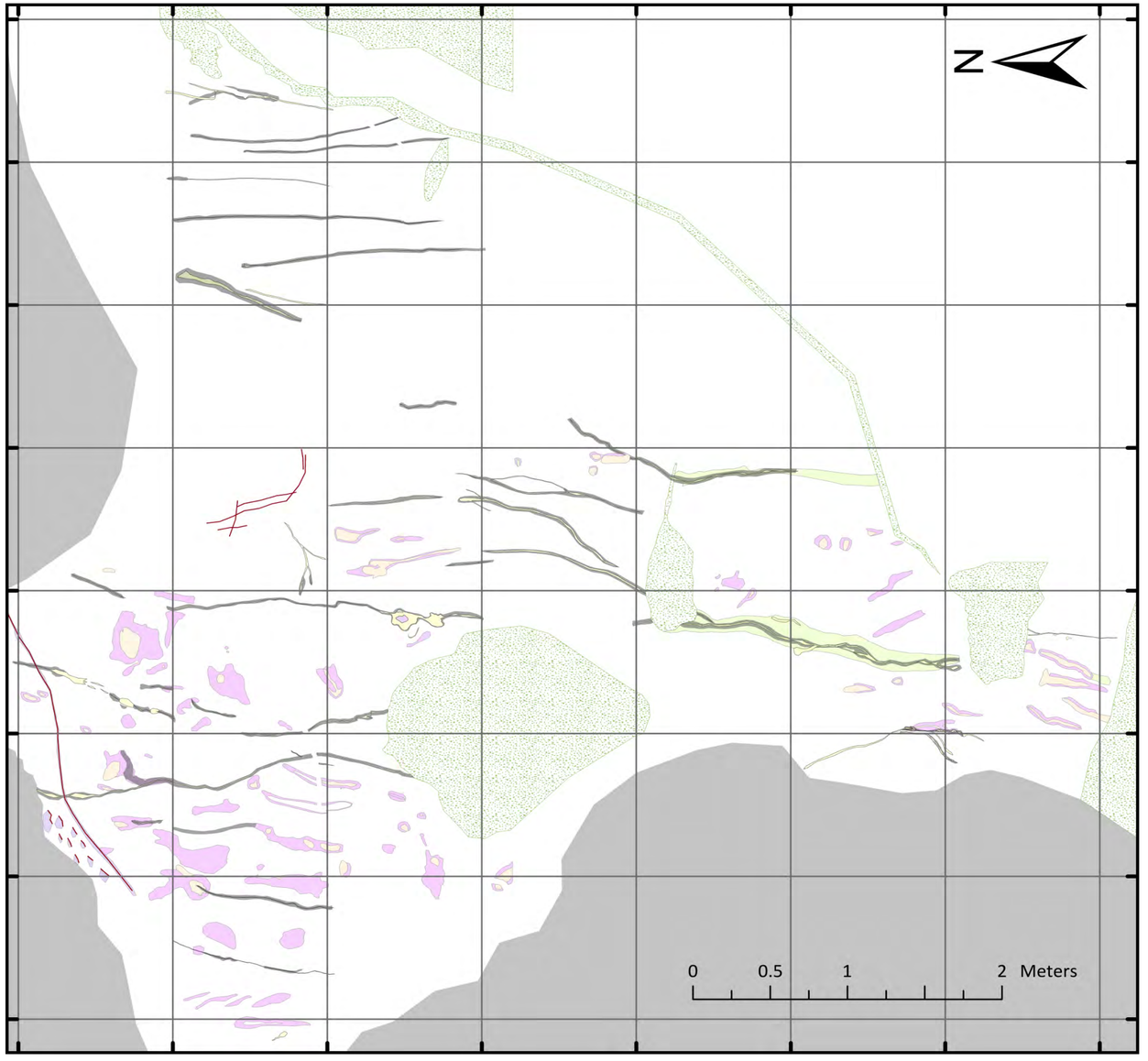

F. Map of hydrothermal veins at outcrop A

Legend

Magmatic features

- Pegmatite
- Pegmatite dykelet
- Diffuse zone with pegmatite and acid rock
- Acid dykelet
- Acid dykelet
- Aplite dykelet
- Aplite dykelet remnants
- Basalt dykelet

Hydrothermal features

- Actinolite vein
- Quartz vein
- Epidote vein
- Epidote vein halo
- Chlorite vein
- Zeolite vein
- Unknown vein

Landscape features

- Steep slope towards glacier
- Vegetation and gravel

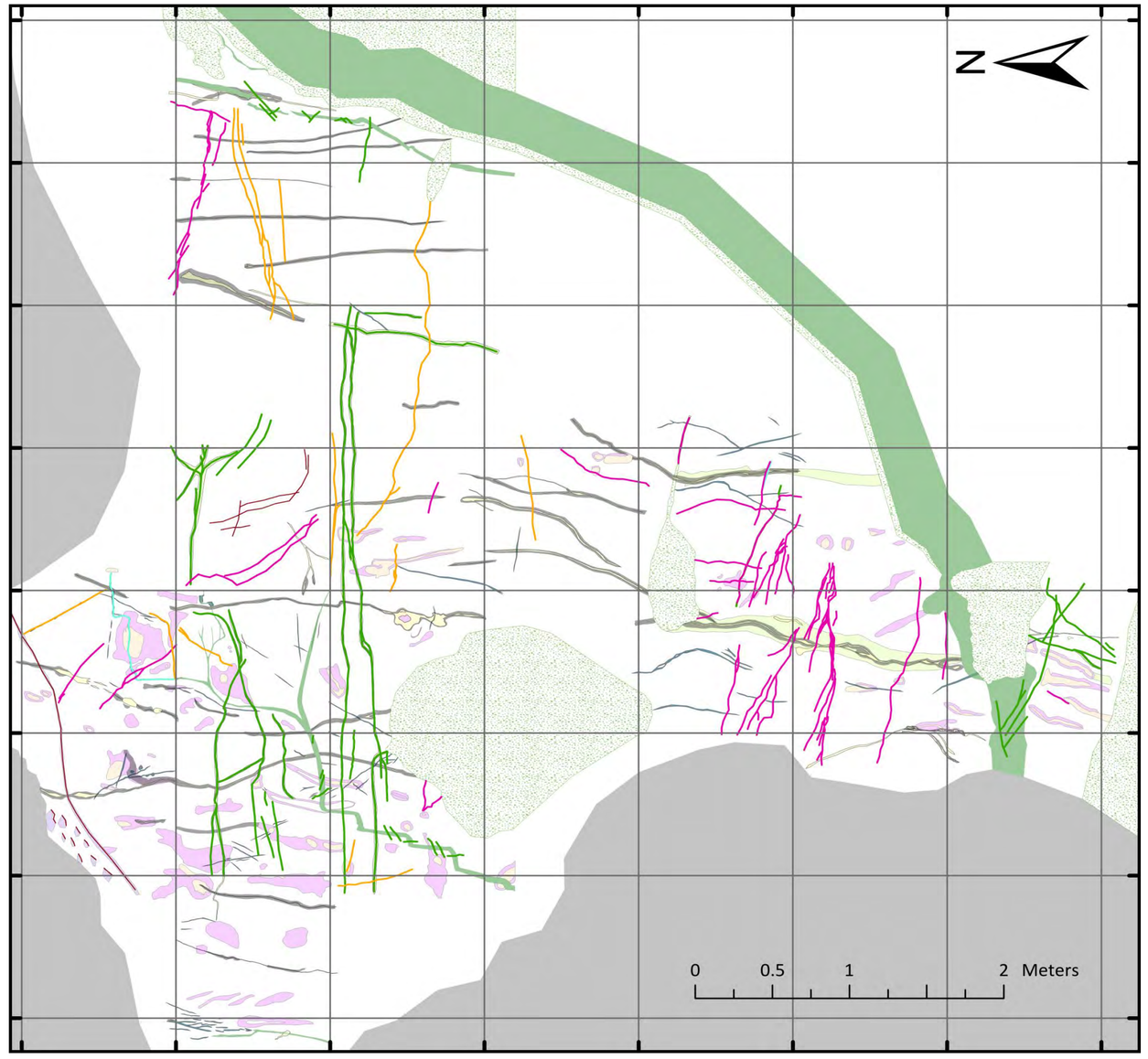

G. Geological map of Geitafell

Legend

- Drillholes (Friðleifson 2014)
- Geophysical profiles (Zürcher 2014)

Rock types mapped

- Basalt
- Unknown Dolerite
- Aphyric Dolerite
- Porphyric Dolerite
- Basalt Dyke
- Breccia Gabbro
- Breccia Host
- Hornfels
- Granophyre
- Fine Gabbro
- Gabbro
- Gabbro A
- Gabbro B
- Gabbro Xenolith
- Ophitic Gabbro
- Porphyric Gabbro

Dyke types

- vesicular Basalt
- Basalt
- Dolerite
- Porphyric Dolerite
- Aphyric Dolerite
- Rhyolite
- Unknown

Geological map

Rock types

- Basalt / Dyke
- Breccia
- Gabbro
- Alluvial
- Morain
- Lake

Geological boarders

- Well defined
- inferred